NUMERICAL STUDIES ON THE ZAKHAROV SYSTEM

SUN FANGFANG

(B.Sc., Jilin University)

A THESIS SUBMITTED

FOR THE DEGREE OF MASTER OF SCIENCE

DEPARTMENT OF COMPUTATIONAL SCIENCE

NATIONAL UNIVERSITY OF SINGAPORE

2003

Acknowledgments

I would like to thank my supervisor, Dr. Bao Weizhu, who gave me the opportunity to work on such an interesting research project, paid patient guidance to me, reviewed my thesis and gave me much invaluable help and constructive suggestion on it.

It is also my pleasure to express my appreciation and gratitude to A/P Wei Guowei, from whom I got effective training on programming, good ideas and experience, both of which are the foundation for my subsequent research project, and much valuable suggestion on my research project.

I would also wish to thank the National University of Singapore for her financial support by awarding me the Research Scholarship during the period of my MSc candidature.

My sincere thanks go to all my department-mates for their friendship and so much kind help. And special thanks go to Mr. Zhao Shan for his patient help whenever I encountered problems in my research.

I would like also to dedicate this work to my parents, who love me most in the world, for their unconditional love and support.

Sun Fangfang

June 2003

Contents

Acknowledgments **ii**

Summary **vii**

List of Symbols **ix**

List of Tables **xii**

List of Figures **xiii**

1 Introduction **1**

1.1 Physical background 1

1.2 The problem 2

1.3 Review of existing results 3

1.4 Our main results 3

2 The Zakharov system **6**

2.1 Derivation of the vector Zakharov system 6

2.2 Simplification and generalization 11

2.3 Relation to the nonlinear Schrödinger equation(NLS) 13
2.4 Conservation laws of the system 13
2.5 Well-posedness of the Zakharov system (ZS) 16
2.6 Plane wave and soliton wave solutions 17

3 Numerical Methods for the Zakharov System 19

3.1 Time-splitting spectral discretizations (TSSP) 20
3.1.1 The numerical method 20
3.1.2 For plane wave solution 23
3.1.3 Conservation and decay rate 25
3.2 Other numerical methods 28
3.2.1 Discrete singular convolution (DSC-RK4) 28
3.2.2 Fourier pseudospectral method (FPS-RK4) 31
3.2.3 Wavelet-Galerkin method (WG-RK4) 32
3.2.4 Finite difference method (FD) 33
3.3 Extension TSSP to Zakharov system for multi-component plasma . . 34
3.4 Extension TSSP to vector Zakharov system 35

4 Numerical Examples 38

4.1 Comparisons of different methods 38
4.2 Applications of TSSP 45
4.2.1 Plane-wave solution of the standard Zakharov system 45
4.2.2 Soliton-soliton collisions of the standard Zakharov system . . . 46
4.2.3 Solution of 2d standard Zakharov system 50
4.2.4 Soliton-soliton collisions of the generalized Zakharov system . 52
4.2.5 Solutions of the damped Zakharov system 56
4.2.6 Solutions of the Zakharov system for multi-component plasma 60

4.2.7 Dynamics of 3d vector Zakharov system 61

5 Conclusion **75**

Bibliography **77**

Summary

In this thesis, we present two numerical methods for studying solutions of the Zakharov system (ZS). We begin with the vector ZS derived from the two-fluid model, and simplify the vector ZS to get the standard ZS, then extend it for multicomponent plasma and finally get the generalized ZS. Furthermore, Conservation laws of the system are proven, relation to the nonlinear Schrödinger equation (NLS), plane wave and soliton wave solutions, as well as well-posedness of the ZS are reviewed. Then we proposed two numerical methods for the approximation of the generalized Zakharov system. The first one is the time-splitting spectral (TSSP) method, which is explicit, keeps the same decay rate of a standard variant as that in the generalized ZS, gives exact results for the plane-wave solution, and is of spectral-order accuracy in space and second-order accuracy in time. The second one is to use the discrete singular convolution (DSC) for spatial derivatives and the fourth-order Runge-Kutta (RK4) for time integration, which is of high (the same as spectral) order accuracy in space and can be applied to deal with general boundary conditions. Furthermore, extension of TSSP to the vector ZS as well as ZS for multi-component plasma are presented. In order to test accuracy and stability, we compare these two methods with other existing methods: Fourier pseudospectral method (FPS) and wavelet-Galerkin method (WG) for spatial derivatives combining with RK4 for time

integration, as well as the standard finite difference method (FD) for solving the ZS with a solitary-wave solution. Furthermore, extensive numerical tests are presented for plane waves, colliding solitary waves in 1d, a 2d problem as well as a damped problem of a generalized ZS.

The thesis is organized as follows: In Chapter 1, the physical background of the Zakharov system is introduced, and we review some existing results and report our main results. In Chapter 2, the Zakharov system are derived and their properties are analyzed. Chapter 3 is devoted to present the time-splitting spectral discretization and DSC algorithm of the generalized Zakharov system. In Chapter 4, we compare the accuracy and stability of different methods for the ZS with a solitary wave solution, as well as present numerical results for plane waves, soliton-soliton collisions in 1d, 2d problem, the generalized ZS with a damping term and ZS for multi-component plasma. Finally, some conclusions based on our findings and numerical results are drawn in Chapter 5.

List of Symbols

PARAMETERS AND VARIABLES

$\bar{}$	Denotes the conjugate of a variable when appearing over this variable
d	Dimension
$\mathbf{x}$	The spatial coordinate
x	Spatial coordinate in 1d
t	Time
$\mathbf{E}, E$	Complex electric field function
N	Real ion density function
γ	Damping parameter
ε	A parameter inversely proportional to the acoustic speed
α, λ, ν	Real parameters
$\mathbb{R}^d$	d dimensional real space
E^0	Initial function of E
N^0	Initial function of N
$N^{(1)}$	Initial function of N_t
e	The charge of the electrons
$-e$	The charge of the ions
m_e	Mass of the electrons

m_i	Mass of the ions
N_e	Number density of the electrons
N_i	Number density of the ions
$\mathbf{v}_e$	Velocity of the electrons
$\mathbf{v}_i$	Velocity of the ions
p_e	Pressure of the electrons
p_i	Pressure of the ions
γ_e	Specific heat ratios of the electrons
γ_i	Specific heat ratios of the ions
T_e	Temperature in energy units of the electrons
T_i	Temperature in energy units of the ions
$\mathcal{E}$	Electric field
$\mathcal{B}$	Magnetic field
ρ	Density of total charge
$\mathbf{j}$	Density of total current
$c.c.$	Stands for the complex conjugate
$\hat{\mathbf{E}}$	The mean complex amplitude
N_0	The unperturbed plasma density
$\tilde{N}_e$	Density fluctuation of the electrons
$\tilde{N}_i$	Density fluctuation of the ions
$\tilde{\mathbf{v}}_e$	Velocity oscillations of the electrons
$\tilde{\mathbf{v}}_i$	Velocity oscillations of the ions
ω_e	Electron plasma frequency
v_e	Electron thermal velocity
$\hat{\mathbf{v}}_e$	The mean electron velocity
$\hat{\mathbf{v}}_i$	The mean ion velocity
$\hat{\mathcal{E}}$	Leading contribution of the mean electron field
c_s	The speed of sound
ζ_d	Debye length

μ_m	The ratio of the electron to the ion masses
D	The wave energy
P	The momentum
H	The Hamiltonian
V	The flux
h	Spatial mesh size
k	Time step

List of Tables

4.1 Spatial discretization error analysis: e_1, e_2 at time t=2 under k = 0.00001. 40

4.2 Time discretization error analysis: e_1, e_2 at time t=2. 41

4.3 Conserved quantities analysis: $k = 0.001$ and $h = \frac{1}{8}$. 42

4.4 Stability analysis: time $t = 5.0$. 43

4.5 Parameter values for analytic solutions of the periodic Zakharov system. 46

List of Figures

4.1 Numerical solutions of the electric field $|E(x,t)|^2$ at $t = 1$ for Example 1 in the 'subsonic limit' regime by TSSP (3.17), (3.18). a). $\varepsilon = \frac{1}{8}$, $h = \frac{1}{2}$, $k = \frac{1}{50}$; b). $\varepsilon = \frac{1}{32}$, $h = \frac{1}{8}$, $k = \frac{1}{800}$; c). $\varepsilon = \frac{1}{128}$, $h = \frac{1}{32}$, $k = \frac{1}{12800}$ corresponding to $h = O(\varepsilon)$ and $k = O(\varepsilon h) = O(\varepsilon^2)$. 44

4.2 Numerical solutions at $t = 2$ ('left') and $t = 4$ ('right') in Example 1. '—': exact solution given in (4.6)-(4.7), '+ + +': numerical solution. a). Re$(E(x,t))$: real part of E, b). Im$(E(x,t))$: imaginary part of E, c). N. 47

4.3 Numerical solutions at different times in Example 3 for case I: Electric field $|E(x,t)|$. 49

4.4 Numerical solutions at different times in Example 3 for case II: Electric field $|E(x,t)|$. 51

4.5 Numerical solutions at different times in Example 3 for case III: Electric field $|E(x,t)|$. 53

4.6 Numerical solutions in Example 4. Surface-plot at time $t = 2.0$: a). Electric field $|E(x,y,2.0)|^2$, b). Ion density $N(x,y,2.0)$. 55

4.7 Contour-plots at different times. Left: Electric field $|E|^2$; Right: ion density N. 56

4.8 Evolution of the wave field $|E|^2$ in Example 5 for case 1. 57

4.9 Numerical solutions in Example 5 for case 2. a). Evolution of the wave field $|E|^2$; b). Evolution of the acoustic field N. 57

4.10 Numerical solutions in Example 5 for case 3. a). Evolution of the wave field $|E|^2$; b). Evolution of the acoustic field N. 58

4.11 Numerical solutions in Example 5 for case 4. a). Evolution of the wave field $|E|^2$; b). Evolution of the acoustic field N. 58

4.12 Numerical results in Example 6 for case 1. Surface-plot of the electric field $|E(x, y, t)|^2$ and ion density $N(x, y, t)$ with $\gamma = 0.8$ at different times: a). $t = 0$, b). $t = 0.5$, c). $t = 1.0$. 63

4.13 Numerical results in Example 6 for case 1. Surface-plot of the electric field $|E(x, y, t)|^2$ and ion density $N(x, y, t)$ with $\gamma = 0.1$ at different times: a). Before blow up (t=0.7), b). After blow up (t=1.333). . . . 64

4.14 Numerical results in Example 6 for case 1. Surface-plot of the electric field $|E(x, y, t)|^2$ and ion density $N(x, y, t)$ with $\gamma = 0$ at different times: a). Before blow up (t=0.5), b). After blow up (t=1.177). . . . 65

4.15 Numerical results in Example 6 for case 2. Surface-plot of the electric field $|E(x, y, t)|^2$ and ion density $N(x, y, t)$ with $\gamma = 0.8$ at different times: a). $t = 0$, b). $t = 0.5$, c). $t = 1.0$. 66

4.16 Numerical results in Example 6 for case 2. Surface-plot of the electric field $|E(x, y, t)|^2$ and ion density $N(x, y, t)$ with $\gamma = 0.1$ at different times: a). Before blow up (t=0.2), b). After blow up (t=0.473). . . . 67

4.17 Numerical results in Example 6 for case 2. Surface-plot of the electric field $|E(x, y, t)|^2$ and ion density $N(x, y, t)$ with $\gamma = 0$ at different times: a). Before blow up (t=0.2), b). After blow up (t=0.442). . . . 68

4.18 Numerical results in Example 6 for case 3. Surface-plot of the electric field $|E(x,y,t)|^2$ and ion density $N(x,y,t)$ with $\gamma = 0.8$ at different times: a). $t = 0$, b). $t = 0.5$, c). $t = 1.0$. 69

4.19 Numerical results in Example 6 for case 3. Surface-plot of the electric field $|E(x,y,t)|^2$ and ion density $N(x,y,t)$ with $\gamma = 0.1$ at different times: a). Before blow up (t=0.2), b). After blow up (t=0.4594). . . 70

4.20 Numerical results in Example 6 for case 3. Surface-plot of the electric field $|E(x,y,t)|^2$ and ion density $N(x,y,t)$ with $\gamma = 0$ at different times: a). Before blow up (t=0.2), b). After blow up (t=0.4316). . . 71

4.21 Numerical results in Example 6 for three cases: Energy, electric field and ion density as functions of time with $\gamma = 0.8$ (left: no blow up) , $\gamma = 0.1$ (center: blow up) and $\gamma = 0$ (right: blow up). a). Case 1, b). Case 2, c). Case 3. 72

4.22 Evolution of the wave field $|E|^2$ and the acoustic field N_1 in Example 7. a). Case 1, b). Case 2, c)&e). Case 3, d)&f). Case 4. 73

4.23 Evolution of the total wave energy $||\mathbf{E}(t)||_{l^2}^2$, and the wave energy of the three components of the electric field $||E_1(t)||_{l^2}^2$, $||E_2(t)||_{l^2}^2$, $||E_3(t)||_{l^2}^2$ in Example 8 for: a). Case I, b). Case II. 74

Chapter 1

Introduction

1.1 Physical background

Zakharov [52] derived the Zakharov system(ZS) governing the coupled dynamics of the electric-field amplitude and of the low-frequency density fluctuations of the ions. Later, it has become commonly accepted that ZS is a general model to govern interaction of dispersive and nondispersive waves. It has important applications in plasma physics (interaction between Langmuir and ion acoustic waves [52]), in the theory of molecular chains (interaction of the intramolecular vibrations forming Davydov solitons with the acoustic disturbances in the chain [17]), in hydrodynamics (interaction between short-wave and long-wave gravitational disturbances in the atmosphere [35]), and so on. In three spatial dimensions, ZS was also derived to model the collapse of caverns [52]. Since then a combined numerical and analytical attack has been launched on ZS. As is well known, ZS is not exactly integrable [37], so the numerical solution is very important.

1.2 The problem

The problem we will study numerically is the generalized Zakharov system(ZS), which describes the propagation of Langmuir waves in plasma:

$$i\,E_t + \Delta\,E - \alpha N\,E + \lambda|E|^2\,E + i\gamma\,E = 0, \qquad \mathbf{x}\in\mathbb{R}^d, \quad t>0, \tag{1.1}$$

$$\varepsilon^2 N_{tt} - \Delta N + \nu\Delta(|E|^2) = 0, \qquad \mathbf{x}\in\mathbb{R}^d, \quad t>0, \tag{1.2}$$

$$E(\mathbf{x},0) = E^0(\mathbf{x}),\ N(\mathbf{x},0) = N^0(\mathbf{x}),\ N_t(\mathbf{x},0) = N^{(1)}(\mathbf{x}), \quad \mathbf{x}\in\mathbb{R}^d; \tag{1.3}$$

where t is time , $\mathbf{x}$ is the spatial coordinate, the complex unknown function $E(\mathbf{x},t)$ is the slowly varying envelope of the highly oscillatory electric field, the real unknown function $N(\mathbf{x},t)$ is the deviation of the ion density from its equilibrium value, ε is a parameter inversely proportional to the acoustic speed, $\gamma \geq 0$ is a damping parameter, and α, λ, ν are all real constants.

The general form of (1.1) and (1.2) covers many different generalized Zakharov systems arising in various physical applications. For example: a) when $\varepsilon = 1$, $\nu = -1$, $\lambda = 0$, $\gamma = 0$ and $\alpha = 1$, the system of eqs. (1.1) and (1.2) reduces to the well-known Zakharov system, which has been first derived by Zakharov [52] to describe the interaction between Langmuir (dispersive) and ion acoustic (approximately nondispersive) waves in a plasma. Since then, it has become commonly accepted that the ZS is a general model governing the interaction of dispersive and nondispersive waves; b) when $\varepsilon = 1$, $\nu = -1$ and $\lambda \neq 0$, a cubic nonlinearity is added to the first equation (1.1); c) when $\gamma > 0$, a linear damping term is added to the ZS; d) when $\varepsilon \to 0$ (corresponding to infinite acoustic speed) in (1.2), one gets $N = \nu|E|^2$, which, together with (1.1), leads to the well-known nonlinear Schrödinger equation (NLS) without ($\gamma = 0$) or with ($\gamma > 0$) a linear damping term:

$$i\,E_t + \Delta\,E + (\lambda - \alpha\nu)|E|^2\,E + i\gamma\,E = 0, \qquad \mathbf{x}\in\mathbb{R}^d, \quad t>0.$$

1.3 Review of existing results

The global existence of a weak solution of the Zakharov equations in 1d is proven in [40], and the existence and uniqueness of the smooth solution for the equations are obtained under the ground that smooth initial data are prescribed. The well-posedness of the ZS was recently improved in [10] for $d = 1, 2, 3$, and extended for the case with generalized nonlinearity [15].

On the other hand, numerical methods for the standard Zakharov system, i.e. $\varepsilon = 1$, $\nu = -1$, $\lambda = 0$, $\gamma = 0$ in (1.1) and (1.2), were studied in the last two decades. Payne et al. [31] proposed a Fourier spectral method for the 1d Zakharov system. They used only two-thirds of the Fourier components for a particular mesh in the fast Fourier transform in order to suppress the aliasing errors in their algorithm [31]. Of course, this is not an optimal way to use spectral method. In [19, 20], Glassey presented an energy-preserving implicit finite difference scheme for the system and proved its convergence. Later, Chang et al. [12] considered an implicit or semiexplicit conservative finite difference scheme for the ZS, proved its convergence, and extended their method for the generalized Zakharov system [13]. More numerical study of soliton-soliton collisions for a (generalized) Zakharov system can be found in [29, 24, 25].

1.4 Our main results

In this thesis, we propose a time-splitting spectral (TSSP) approximation and a discrete singular convolution (DSC) algorithm for the generalized Zakharov system. TSSP is explicit, easy to extend to high dimension, and gives exact results for plane-wave solutions of the ZS. For stability, TSSP requires $k = O(h)$. In fact, the spectral method has showed greatly success in solving problems arising from many areas [4, 11, 21] and the split-step procedure was presented for differential

equations [39] and applied to Schrödinger equation [18, 27, 42] and KDV equation [43]. Recently, the time-splitting spectral approximation was studied and used for nonlinear Schrödinger equation in the semiclassical regimes in [7] and applied to the numerical study of the dynamics of Bose-Einstein condensation [8] as well. Very promising numerical results were obtained due to its exponentially high order accuracy in space. The approach for the ZS is based on a time splitting for (1.1) which keeps the same decay rate in time of $\int_{\mathbb{R}^d} |E(x,t)|^2 \, dx$ as that in (1.1) and (1.2).

Another method we will present for ZS is the discrete singular convolution(DSC) method which was recently proposed by Wei [45] as a potential approach for the numerical discretization of spatial derivatives. The main merit of the DSC method is that it is of high (the same as spectral) order accuracy in space and can be applied to deal with complex geometries and general boundary conditions. So far this method has been successfully applied to solve many problems in science and engineering, such as eigenvalue problems of both quantum [47] and classical [48] origins, analysis of stochastic process [45, 46], simulation of fluid flow in simple [49] and complex geometries, and nanoscale pattern formation in a circular domain [23]. DSC method has the theory of distribution as its mathematical foundation [38]. And numerical analysis indicates that the DSC method has spectral convergence for approximating appropriate functions [3, 4]. The accuracy and stability of TSSP and DSC will be compared with other existing methods like finite difference method. The numerical results demonstrate the high accuracy and efficiency of these two proposed methods for the ZS.

This thesis consists of four Chapters arranged as following. Chapter 1 introduce the physical background of the Zakharov system, and we also review some existing results and report our main results. In Chapter 2, the Zakharov system, which governs the coupled dynamics of the electric-field amplitude and of the low-frequency density fluctuations of the ions, is derived and its properties are analyzed. Chapter 3 is devoted to present the time-splitting spectral discretization and DSC algorithm for

the generalized Zakharov system and some other existing methods are introduced, too. Furthermore, extension TSSP to ZS for multi-component and vector ZS. In Chapter 4, we will compare the accuracy and stability of different methods for the ZS with a solitary wave solution, and also present the numerical results for plane waves, soliton-soliton collisions in 1d, 2d problems and the generalized ZS with a damping term. Finally, some conclusions based on our findings and numerical results are drawn in Chapter 5.

Chapter 2

The Zakharov system

In this Chapter, We firstly review the derivation of the vector ZS from the two-fluid model [41], and simplify the vector ZS to get the standard ZS, then extend it in a multicomponent plasma and finally get the generalized ZS with a damping term. Furthermore, Conservation laws of the system are proved and relation to the nonlinear Schrödinger equation(NLS), plane wave and soliton wave solutions, as well as well-posedness of the ZS are reviewed.

2.1 Derivation of the vector Zakharov system

This section is devoted to derive the Zakharov system from the two-fluid model [41]. Here we will use a more formal approach based on the multiple-scale modulation analysis. Following from [41], we will consider a plasma as two interpenetrating fluids, an electron fluid and an ion fluid, and denote the mass, number density (number of particles per unit volume) and velocity of the electrons (respectively of the ions), by m_e, $N_e(\mathbf{x},t)$ and $\mathbf{v}_e(\mathbf{x},t)$ (respectively m_i, $N_i(\mathbf{x},t)$ and $\mathbf{v}_i(\mathbf{x},t)$). The continuity equations for these fluids read

$$\partial_t N_e + \nabla\cdot(N_e\mathbf{v}_e) = 0, \tag{2.1}$$

$$\partial_t N_i + \nabla\cdot(N_i\mathbf{v}_i) = 0, \tag{2.2}$$

and the momentum equations read

$$m_e\, N_e(\partial_t \mathbf{v}_e + \mathbf{v}_e \cdot \nabla \mathbf{v}_e) = -\nabla p_e - e\, N_e \left(\mathcal{E} + \frac{1}{c}\mathbf{v}_e \times \mathcal{B}\right), \tag{2.3}$$

$$m_i\, N_i(\partial_t \mathbf{v}_i + \mathbf{v}_i \cdot \nabla \mathbf{v}_i) = -\nabla p_i + e\, N_i \left(\mathcal{E} + \frac{1}{c}\mathbf{v}_i \times \mathcal{B}\right), \tag{2.4}$$

where $-e$ and e represent the charge of the electron and the ions assumed to reduce to protons, respectively; p_e and p_i are the pressure. For small fluctuations, we write $\nabla p_e = \gamma_e\, T_e\, \nabla N_e$ and $\nabla p_i = \gamma_i\, T_i\, \nabla N_i$, where γ_e and γ_i denote the specific heat ratios of the electrons and the ions and T_e and T_i their respective temperatures in energy units. The electric field $\mathcal{E}$ and magnetic field $\mathcal{B}$ are provided by the Maxwell equations

$$\nabla \cdot \mathcal{E} = 4\pi\rho, \tag{2.5}$$

$$\nabla \cdot \mathcal{B} = 0, \tag{2.6}$$

$$\nabla \times \mathcal{E} = -\frac{1}{c}\partial_t \mathcal{B}, \tag{2.7}$$

$$\nabla \times \mathcal{B} = \frac{4\pi}{c}\mathbf{j} + \frac{1}{c}\,\partial_t \mathcal{E}, \tag{2.8}$$

where $\rho = -e(N_e - N_i)$ and $\mathbf{j} = -e(N_e\mathbf{v}_e - N_i\mathbf{v}_i)$ are the densities of total charge and total current, respectively.

Equations (2.7) and (2.8) yield

$$\frac{1}{c^2}\partial_{tt}\mathcal{E} + \nabla \times (\nabla \times \mathcal{E}) + \frac{4\pi}{c^2}\partial_t \mathbf{j} = 0, \tag{2.9}$$

and using equations (2.1)-(2.4), we have

$$\begin{aligned}\partial_t \mathbf{j} = \; & e(\nabla \cdot (N_e\mathbf{v}_e)\mathbf{v}_e + N_e\mathbf{v}_e \cdot \nabla \mathbf{v}_e + \tfrac{1}{m_e}\nabla p_e + \tfrac{eN_e}{m_e}(\mathcal{E} + \tfrac{1}{c}\mathbf{v}_e \times \mathcal{B})) \\ & -e(\nabla \cdot (N_i\mathbf{v}_i)\mathbf{v}_i + N_i\mathbf{v}_i \cdot \nabla \mathbf{v}_i + \tfrac{1}{m_i}\nabla p_i + \tfrac{eN_i}{m_i}(\mathcal{E} + \tfrac{1}{c}\mathbf{v}_i \times \mathcal{B})).\end{aligned} \tag{2.10}$$

In order to get the vector Zakharov system from the two-fluid model just mentioned, as in [41], we consider a long-wavelength small-amplitude Langmuir oscillation of the form

$$\mathcal{E} = \frac{\varepsilon}{2}(\mathbf{E}(\mathbf{X}, T)e^{-i\omega_e t} + c.c.) + \varepsilon^2 \hat{\mathbf{E}}(\mathbf{X}, T) + \cdots, \tag{2.11}$$

where the complex amplitude $\mathbf{E}$ depends on the slow variables $\mathbf{X} = \varepsilon\mathbf{x}$ and $T = \varepsilon^2 t$, the notation *c.c.* stands for the complex conjugate and $\hat{\mathbf{E}}(\mathbf{X}, T)$ denotes the mean complex amplitude. It induces fluctuations for the density and velocity of the electrons and of the ions whose dynamical time will be seen to be $\tau = \varepsilon t$, thus shorter than T. We write

$$N_e = N_0 + \frac{\varepsilon^2}{2}(\tilde{N}_e(\mathbf{X},\tau)e^{-i\omega_e t} + c.c.) + \varepsilon^2 \hat{N}_e(\mathbf{X},\tau) + \cdots, \tag{2.12}$$

$$N_i = N_0 + \frac{\varepsilon^2}{2}(\tilde{N}_i(\mathbf{X},\tau)e^{-i\omega_e t} + c.c.) + \varepsilon^2 \hat{N}_i(\mathbf{X},\tau) + \cdots, \tag{2.13}$$

$$\mathbf{v}_e = \frac{\varepsilon}{2}(\tilde{\mathbf{v}}_e(\mathbf{X},\tau)e^{-i\omega_e t} + c.c.) + \varepsilon^2 \hat{\mathbf{v}}_e(\mathbf{X},\tau) + \cdots, \tag{2.14}$$

$$\mathbf{v}_i = \frac{\varepsilon}{2}(\tilde{\mathbf{v}}_i(\mathbf{X},\tau)e^{-i\omega_e t} + c.c.) + \varepsilon^2 \hat{\mathbf{v}}_i(\mathbf{X},\tau) + \cdots, \tag{2.15}$$

where N_0 is the unperturbed plasma density.

From the momentum equation (2.3), considering the leading order and noting that the magnetic field $\mathcal{B}$ is of order ε^2, we can easily get

$$m_e\, N_e \left(i\omega_e \tilde{\mathbf{v}}_e \frac{\varepsilon}{2} e^{-i\omega_e t}\right) = e\, N_e \left(\mathbf{E}\frac{\varepsilon}{2} e^{-i\omega_e t}\right),$$

thus the amplitude of the electron velocity oscillations is given by

$$\tilde{\mathbf{v}}_e = -\frac{ie}{m_e\omega_e}\mathbf{E}. \tag{2.16}$$

Neglecting the velocity oscillations of the ions due to their large mass, we take

$$\tilde{\mathbf{v}}_i = 0. \tag{2.17}$$

Applying (2.16) and (2.17) into the continuity equations (2.1) and (2.2), at the order of ε^2, we have

$$-i\omega_e \tilde{N}_e \frac{\varepsilon^2}{2} e^{-i\omega_e t} + N_0 \nabla\cdot\tilde{\mathbf{v}}_e \frac{\varepsilon^2}{2} e^{-i\omega_e t} = 0,$$

thus the density fluctuations are obtained as

$$\tilde{N}_e = -i\frac{N_0}{\omega_e}\nabla\cdot\tilde{\mathbf{v}}_e = -\frac{eN_0}{m_e\omega_e^2}\nabla\cdot\mathbf{E}, \tag{2.18}$$

$$\tilde{N}_i = 0. \tag{2.19}$$

At leading order, the equation for the electric field (2.9) with $\mathbf{j} = -e(N_e\mathbf{v}_e - N_i\mathbf{v}_i)$ becomes

$$-\frac{1}{c^2}\omega_e^2\mathbf{E}\frac{\varepsilon}{2}e^{-i\omega_e t} + \frac{4\pi}{c^2}i\omega_e e N_0\tilde{\mathbf{v}}_e\frac{\varepsilon}{2}e^{-i\omega_e t} = 0,$$

from which, with (2.16), we finally get the electron plasma frequency

$$\omega_e = \sqrt{\frac{4\pi e^2 N_0}{m_e}}. \tag{2.20}$$

At the order of ε^3, if no large-scale magnetic field is generated, then the equation (2.9) with (2.10) implies that

$$\begin{aligned}&-2i\frac{\omega_e}{c^2}\partial_T\mathbf{E}\frac{\varepsilon^3}{2}e^{-i\omega_e t} + \nabla\times(\nabla\times\mathbf{E})\frac{\varepsilon^3}{2}e^{-i\omega_e t}\\ &-\frac{4\pi e^2 N_0\gamma_e T_e}{c^2 m_e^2\omega_e^2}\nabla(\nabla\cdot\mathbf{E})\frac{\varepsilon^3}{2}e^{-i\omega_e t} + \frac{4\pi e^2\hat{N}_e\mathbf{E}}{c^2 m_e}\frac{\varepsilon^3}{2}e^{-i\omega_e t} = 0,\end{aligned}$$

and thus

$$-2i\frac{\omega_e}{c^2}\partial_T\mathbf{E} + \nabla\times(\nabla\times\mathbf{E}) - \frac{\gamma_e T_e}{m_e c^2}\nabla(\nabla\cdot\mathbf{E}) + \frac{4\pi e^2}{c^2 m_e}\hat{N}_e\mathbf{E} = 0, \tag{2.21}$$

where, resulting from (2.17) and (2.19), the contribution of the ions is negligible.

We rewrite the amplitude equation (2.21) as

$$i\partial_T\mathbf{E} - \frac{c^2}{2\omega_e}\nabla\times(\nabla\times\mathbf{E}) + \frac{3v_e^2}{2\omega_e}\nabla(\nabla\cdot\mathbf{E}) = \frac{\omega_e}{2}\frac{\hat{N}_e}{N_0}\mathbf{E}, \tag{2.22}$$

where the electron thermal velocity v_e is defined by

$$v_e = \sqrt{\frac{T_e}{m_e}} \tag{2.23}$$

and γ_e is taken to be 3 [41, 30, 44].

It is seen from (2.3), (2.4) and (2.17) that the mean electron velocity $\hat{\mathbf{v}}_e$ and the mean ion velocity $\hat{\mathbf{v}}_i$ satisfy

$$m_e\left(\partial_\tau\hat{\mathbf{v}}_e + \frac{1}{4}(\tilde{\mathbf{v}}_e\cdot\nabla\overline{\tilde{\mathbf{v}}_e} + \overline{\tilde{\mathbf{v}}_e}\cdot\nabla\tilde{\mathbf{v}}_e)\right) = -\frac{\gamma_e T_e}{N_0}\nabla\hat{N}_e - e\hat{\mathcal{E}}, \tag{2.24}$$

$$m_i\partial_\tau\hat{\mathbf{v}}_i = -\frac{\gamma_i T_i}{N_0}\nabla\hat{N}_i + e\hat{\mathcal{E}}, \tag{2.25}$$

where

$$\frac{1}{4}(\tilde{\mathbf{v}}_e \cdot \nabla\overline{\tilde{\mathbf{v}}_e} + \overline{\tilde{\mathbf{v}}_e} \cdot \nabla\tilde{\mathbf{v}}_e) = \frac{e^2}{4m_e^2\omega_e^2}\nabla|\mathbf{E}|^2, \tag{2.26}$$

and $\overline{\tilde{\mathbf{v}}_e}$ denotes the conjugate of $\tilde{\mathbf{v}}_e$ and $m_e\partial_\tau\hat{\mathbf{v}}_e$ is negligible because of the small mass of the electron. Furthermore, $\hat{\mathcal{E}}$ denotes the leading contribution (of order ε^3) of the mean electron field. We thus replace (2.24) by

$$\frac{e^2}{4m_e\omega_e^2}\nabla|\mathbf{E}|^2 = -\frac{\gamma_e T_e}{N_0}\nabla\hat{N}_e - e\hat{\mathcal{E}}. \tag{2.27}$$

The system is closed by using the quasi-neutrality of the plasma in the form

$$\hat{N}_e = \hat{N}_i, \tag{2.28}$$

$$\hat{\mathbf{v}}_e = \hat{\mathbf{v}}_i, \tag{2.29}$$

which we denote by N and $\mathbf{v}$, respectively. Then from the continuity equations, one gets

$$\partial_\tau N + N_0\nabla\cdot\mathbf{v} = 0. \tag{2.30}$$

Adding (2.27) to (2.25) and noting (2.30), we have

$$\partial_\tau\mathbf{v} = -\frac{c_s^2}{N_0}\nabla N - \frac{1}{16\pi m_i N_0}\nabla|\mathbf{E}|^2, \tag{2.31}$$

with the speed of sound c_s,

$$c_s^2 = \eta\frac{T_e}{m_i}, \qquad \eta = \frac{\gamma_e T_e + \gamma_i T_i}{T_e}. \tag{2.32}$$

Finally, we obtain the vector Zakharov equations [28, 44, 30, 53] from equations (2.22), (2.30) and (2.31) as

$$i\partial_T\mathbf{E} - \frac{c^2}{2\omega_e}\nabla\times(\nabla\times\mathbf{E}) + \frac{3v_e^2}{2\omega_e}\nabla(\nabla\cdot\mathbf{E}) = \frac{\omega_e}{2}\frac{N}{N_0}\mathbf{E}, \tag{2.33}$$

$$\varepsilon^2\partial_{TT}N - c_s^2\Delta N = \frac{1}{16\pi m_i}\Delta|\mathbf{E}|^2. \tag{2.34}$$

This Zakharov system governs the coupled dynamics of the electric-field amplitude and of the low-frequency density fluctuations of the ions and describes the dynamics of the complex envelope of the electric field oscillations near the electron plasma frequency and the slow variations of the density perturbations.

In order to obtain a dimensionless form of the system (2.33)-(2.34), we define the normalized variables

$$t' = \frac{2\eta}{3}\mu_m\,\omega_e\,T, \qquad \mathbf{x}' = \frac{2}{3}\,(\eta\mu_m)^{1/2}\,\frac{\mathbf{X}}{\zeta_d}, \tag{2.35}$$

$$N' = \frac{3}{4\eta}\frac{1}{\mu_m}\frac{N}{N_0}, \qquad \mathbf{E}' = \frac{1}{\eta}\frac{1}{\mu_m^{1/2}}\left(\frac{3}{64\pi N_0 T_e}\right)^{1/2}\mathbf{E}. \tag{2.36}$$

with

$$\zeta_d = \sqrt{\frac{T_e}{4\pi e^2 N_0}}, \qquad \mu_m = \frac{m_e}{m_i}, \tag{2.37}$$

where ζ_d is the Debye length and μ_m is the ratio of the electron to the ion masses. Then defining

$$a = \frac{c^2}{3v_e^2} = \frac{c^2}{3\omega_e^2\zeta_d^2} \tag{2.38}$$

and plugging (2.35)-(2.36) into (2.33)-(2.34), and then removing all primes, we get the following dimensionless vector Zakharov system in three dimension

$$i\partial_t\mathbf{E} - a\nabla\times(\nabla\times\mathbf{E}) + \nabla(\nabla\cdot\mathbf{E}) = N\mathbf{E}, \tag{2.39}$$

$$\varepsilon^2\partial_{tt}N - \Delta N = \Delta|\mathbf{E}|^2. \tag{2.40}$$

2.2 Simplification and generalization

When we choose $a = 1$ in (2.39), the system (2.39)-(2.40) collapses to the standard vector Zakharov system

$$i\partial_t\mathbf{E} + \Delta\mathbf{E} = N\mathbf{E}, \tag{2.41}$$

$$\varepsilon^2\partial_{tt}N - \Delta N = \Delta|\mathbf{E}|^2. \tag{2.42}$$

If $\mathbf{E} = (E_1, E_2, E_3)$, it can be written as following:

$$i\partial_t E_1 + \Delta E_1 = NE_1, \tag{2.43}$$

$$i\partial_t E_2 + \Delta E_2 = NE_2, \tag{2.44}$$

$$i\partial_t E_3 + \Delta E_3 = NE_3, \tag{2.45}$$

$$\varepsilon^2 \partial_{tt} N - \Delta N = \Delta(|E_1|^2 + |E_2|^2 + |E_3|^2). \tag{2.46}$$

In the case when $E_2 = E_3 = 0$, the system (2.43)-(2.46) leads to scalar case, or the standard ZS:

$$i\partial_t E + \Delta E = NE, \tag{2.47}$$

$$\varepsilon^2 \partial_{tt} N - \Delta N = \Delta |E|^2. \tag{2.48}$$

Let us consider a physical situation when the dispersive waves interact with two different acoustic modes (e.g., in a multicomponent plasma), which may be described by the following generalization of ZS:

$$i\partial_t E + \Delta E + 2(N_1 + N_2)E = 0, \tag{2.49}$$

$$\varepsilon_1^2 \partial_{tt} N_1 - \Delta N_1 + \nu_1 \Delta |E|^2 = 0, \tag{2.50}$$

$$\varepsilon_2^2 \partial_{tt} N_2 - \Delta N_2 + \nu_2 \Delta |E|^2 = 0, \tag{2.51}$$

and assume that $1/\varepsilon_2^2 \gg 1/\varepsilon_1^2$, so the fast nondispersive component N_2 can be excluded by means of the relation $N_2 = \nu_2 |E|^2$, and the system (2.49)-(2.51) turns into the system

$$i\partial_t E + \Delta E + 2\lambda |E|^2 E + 2NE = 0, \tag{2.52}$$

$$\varepsilon^2 \partial_{tt} N - \Delta N + \nu \Delta |E|^2 = 0 \tag{2.53}$$

with $\lambda = \nu_2$, $\varepsilon = \varepsilon_1$, $\nu = \nu_1$. Mathematically, When $\varepsilon \to 0$, $\lambda > 0$, the system (2.52)-(2.53) will be blowup, therefore in practice, if a linear damping term is added to arrest blow up, one arrives at the generalized ZS (1.1)-(1.2).

2.3 Relation to the nonlinear Schrödinger equation(NLS)

Note that in the "subsonic limit", where the density fluctuations are assumed to follow adiabatically the modulation of the Langmuir wave. Letting $\varepsilon \to 0$ in (2.40), one gets $N = -|\mathbf{E}|^2$. Plugging into (2.39), the vector ZS collapses to the vector NLS equation

$$i\partial_t \mathbf{E} - a\nabla \times (\nabla \times \mathbf{E}) + \nabla(\nabla \cdot \mathbf{E}) + |\mathbf{E}|^2 \mathbf{E} = 0. \tag{2.54}$$

For the generalized ZS (1.1)- (1.2), in the case of $\varepsilon \to 0$ (corresponding to infinite acoustic speed), one gets $N = \nu|E|^2$, which, together with (1.1), leads to the well-known nonlinear Schrödinger equation(NLS) without ($\gamma = 0$) or with ($\gamma > 0$) a linear damping term:

$$i\ E_t + \Delta\ E + (\lambda - \alpha\nu)|E|^2\ E + i\gamma\ E = 0.$$

2.4 Conservation laws of the system

There are at least three conservation laws in the generalized ZS (1.1)-(1.2) without damping ($\gamma = 0$) describing the propagation of Langmuir waves in plasma.

Theorem 2.4.1. The generalized Zakharov system (ZS) (1.1)-(1.2) without damping term ($\gamma = 0$) preserves the conserved quantities. They are the wave energy

$$D = \int_{\mathbb{R}^d} |E(\mathbf{x}, t)|^2\ d\mathbf{x} \tag{2.55}$$

the momentum

$$\mathbf{P} = \int_{\mathbb{R}^d} \left[\frac{i}{2} \left(E\overline{\nabla E} - \overline{E}\nabla E \right) - \frac{\varepsilon^2 \alpha}{\nu} N\mathbf{V} \right]\ d\mathbf{x}, \tag{2.56}$$

and the Hamiltonian

$$H = \int_{\mathbb{R}^d} \left[|\nabla E|^2 + \alpha N|E|^2 - \frac{\lambda}{2}|E|^4 - \frac{\alpha}{2\nu}N^2 - \frac{\alpha\varepsilon^2}{2\nu}|\mathbf{V}|^2 \right] d\mathbf{x}, \tag{2.57}$$

where the flux $\mathbf{V}$ is introduced through the equations

$$N_t = -\nabla \cdot \mathbf{V}, \tag{2.58}$$

$$\mathbf{V}_t = -\frac{1}{\varepsilon^2}\nabla(N - \nu|E|^2). \tag{2.59}$$

Proof. Multiplying (1.1) by $\overline{E}$, the conjugate of E, we get

$$iE_t\overline{E} + \overline{E}\Delta E - \alpha N|E|^2 + \lambda|E|^4 = 0. \tag{2.60}$$

Then calculating the conjugate of (1.1) and multiplying it by E, one finds

$$-i\overline{E}_t E + E\Delta\overline{E} - \alpha N|E|^2 + \lambda|E|^4 = 0. \tag{2.61}$$

Subtracting (2.61) from (2.60) and then multiplying both sides by $-i$, one gets

$$E_t\overline{E} + \overline{E}_t E + i(E\Delta\overline{E} - \overline{E}\Delta E) = 0. \tag{2.62}$$

Integrating over $\mathbb{R}^d$, integration by parts, (2.62) leads to the conservation of the wave energy

$$D'(t) = \frac{d}{dt}\int_{\mathbb{R}^d} |E(\mathbf{x},t)|^2 \, d\mathbf{x} = 0.$$

From (1.1), noting (2.58), (2.59), one has the conservation of the momentum

$$\begin{aligned}
\frac{d}{dt}\mathbf{P} &= \frac{i}{2}\int_{\mathbb{R}^d} (E_t\overline{\nabla E} + E\overline{\nabla E_t} - \overline{E}\nabla E_t - \overline{E_t}\nabla E)\, d\mathbf{x} - \frac{\varepsilon^2\alpha}{\nu}\int_{\mathbb{R}^d} (N_t\mathbf{V} + N\mathbf{V}_t)\, d\mathbf{x} \\
&= i\int_{\mathbb{R}^d} (E_t\overline{\nabla E} - \overline{E_t}\nabla E)\, d\mathbf{x} - \frac{\varepsilon^2\alpha}{\nu}\int_{\mathbb{R}^d} (N_t\mathbf{V} + N\mathbf{V}_t)\, d\mathbf{x} \\
&= i\int_{\mathbb{R}^d} \left[\overline{\nabla E}(i\Delta E - i\alpha N E + i\lambda|E|^2 E) - \nabla E(-i\overline{\Delta E} + i\alpha N\overline{E} - i\lambda|E|^2\overline{E})\right] d\mathbf{x} \\
&\quad -\frac{\varepsilon^2\alpha}{\nu}\int_{\mathbb{R}^d} (N_t\mathbf{V} + N\mathbf{V}_t)\, d\mathbf{x} \\
&= \alpha\int_{\mathbb{R}^d} N\nabla|E|^2\, d\mathbf{x} + \frac{\varepsilon^2\alpha}{\nu}\int_{\mathbb{R}^d} \mathbf{V}\nabla\cdot\mathbf{V}\, d\mathbf{x} + \frac{\alpha}{\nu}\int_{\mathbb{R}^d} \nabla(N - \nu|E|^2)N\, d\mathbf{x} \\
&= 0.
\end{aligned}$$

Noting (2.58), (2.59) and multiplying (1.1) by $\overline{E_t}$, the conjugate of E_t, we write it

$$\mathcal{T} = \int_{\mathbb{R}^d} \left[i|E_t|^2 + \overline{E_t}\Delta E - \alpha N E\overline{E_t} + \lambda|E|^2 E\overline{E_t} \right] \, d\mathbf{x} = 0. \tag{2.63}$$

Then the real part of $\mathcal{T}$ is

$$\begin{aligned}
0 = Re(\mathcal{T}) &= Re\int_{\mathbb{R}^d} \left[\overline{E_t}\Delta E - \alpha N E\overline{E_t} + \lambda|E|^2 E\overline{E_t} \right] \, d\mathbf{x} \\
&= Re\int_{\mathbb{R}^d} \left[-\nabla E\overline{\nabla E_t} - \frac{\alpha}{2}(N|E|^2)_t + \frac{\alpha}{2}N_t|E|^2 + \frac{\lambda}{4}|E|_t^4 \right] \, d\mathbf{x} \\
&= -\frac{1}{2}\int_{\mathbb{R}^d} \left[(|\nabla E|^2 + \alpha N|E|^2 - \frac{\lambda}{2}|E|^4)_t + \frac{\alpha}{2}N_t|E|^2 \right] \, d\mathbf{x} \\
&= -\frac{1}{2}\int_{\mathbb{R}^d} \left[(|\nabla E|^2 + \alpha N|E|^2 - \frac{\lambda}{2}|E|^4)_t - \frac{\alpha}{2}|E|^2\nabla\cdot\mathbf{V} \right] \, d\mathbf{x} \\
&= -\frac{1}{2}\int_{\mathbb{R}^d} \left[(|\nabla E|^2 + \alpha N|E|^2 - \frac{\lambda}{2}|E|^4)_t + \frac{\alpha}{2}\nabla|E|^2\cdot\mathbf{V} \right] \, d\mathbf{x} \\
&= -\frac{1}{2}\int_{\mathbb{R}^d} \left[(|\nabla E|^2 + \alpha N|E|^2 - \frac{\lambda}{2}|E|^4)_t + \frac{\alpha}{2}(\frac{\varepsilon^2}{\nu}\mathbf{V}_t + \frac{1}{\nu}\nabla N)\cdot\mathbf{V} \right] \, d\mathbf{x} \\
&= -\frac{1}{2}\int_{\mathbb{R}^d} \left(|\nabla E|^2 + \alpha N|E|^2 - \frac{\lambda}{2}|E|^4 \right)_t \, d\mathbf{x} \\
&\quad + \frac{\alpha\varepsilon^2}{2\nu}\int_{\mathbb{R}^d} (\frac{1}{2}|\mathbf{V}|^2)_t \, d\mathbf{x} - \frac{\alpha}{2\nu}\int_{\mathbb{R}^d} N\nabla\cdot\mathbf{V} \, d\mathbf{x} \\
&= -\frac{1}{2}\int_{\mathbb{R}^d} \left(|\nabla E|^2 + \alpha N|E|^2 - \frac{\lambda}{2}|E|^4 \right)_t \, d\mathbf{x} \\
&\quad + \frac{\alpha\varepsilon^2}{2\nu}\int_{\mathbb{R}^d} (\frac{1}{2}|\mathbf{V}|^2)_t \, d\mathbf{x} + \frac{\alpha}{2\nu}\int_{\mathbb{R}^d} NN_t \, d\mathbf{x} \\
&= -\frac{1}{2}\int_{\mathbb{R}^d} \left(|\nabla E|^2 + \alpha N|E|^2 - \frac{\lambda}{2}|E|^4 - \frac{\alpha}{2\nu}N^2 - \frac{\alpha\varepsilon^2}{2\nu}|\mathbf{V}|^2) \right)_t \, d\mathbf{x},
\end{aligned}$$

which implies the conservation of Hamiltonian

$$\frac{d}{dt}H = 0.$$

□

For the standard ZS ($\varepsilon = 1$, $\nu = -1$, $\lambda = 0$, $\gamma = 0$ and $\alpha = 1$), the conserved

quantities collapse

$$D = \int_{\mathbb{R}^d} |E(\mathbf{x},t|^2\, d\mathbf{x}, \tag{2.64}$$

$$\mathbf{P} = \int_{\mathbb{R}^d} \left[\frac{i}{2}\left(E\overline{\nabla E} - \overline{E}\nabla E\right) + N\mathbf{V}\right]\, d\mathbf{x}, \tag{2.65}$$

$$H = \int_{\mathbb{R}^d} \left[|\nabla E|^2 + N|E|^2 + \frac{1}{2}N^2 + \frac{1}{2}|\mathbf{V}|^2\right]\, d\mathbf{x}, \tag{2.66}$$

where the flux $\mathbf{V}$ is introduced through the equations

$$N_t = -\nabla\cdot\mathbf{V}, \tag{2.67}$$

$$\mathbf{V}_t = -\nabla(N+|E|^2). \tag{2.68}$$

In the one-dimensional case the conserved quantities become

$$D = \int_{-\infty}^{\infty} |E(x,t)|^2\, dx, \tag{2.69}$$

$$P = \int_{-\infty}^{\infty} \left[\frac{i}{2}(E(x,t)\overline{E_x(x,t)} - \overline{E(x,t)}E_x(x,t)) - \frac{\varepsilon^2\alpha}{\nu}NV(x,t)\right]\, dx, \tag{2.70}$$

$$H = \int_{-\infty}^{\infty} \left[|E_x(x,t)|^2 + \alpha N|E|^2 - \frac{\lambda}{2}|E|^4 - \frac{\alpha}{2\nu}N^2 - \frac{\alpha\varepsilon^2}{2\nu}V(x,t)^2\right]\, dx, \tag{2.71}$$

where the flux V is introduced through the equations

$$N_t = -V_x, \tag{2.72}$$

$$V_t = -(N+|E|^2)_x. \tag{2.73}$$

Similar to the derivation of the conservation of the wave energy in Theorem 2.4.1. one gets the decay rate of the wave energy D when $\gamma \neq 0$,

$$D(t) = \int_a^b |E(x,t)|^2\, dx = e^{-2\gamma t}\int_a^b |E^0(x)|^2\, dx = e^{-2\gamma t}D(0), \qquad t \geq 0.$$

2.5 Well-posedness of the Zakharov system (ZS)

Based on the conservation laws, C.Sulem and P.L.Sulem [40] prove the wellposedness for the standard ZS (2.47)-(2.48).

Theorem 2.5.1. In one dimension, for initial conditions, $E^0 \in H^p(\mathbb{R})$, $N^0 \in H^{p-1}(\mathbb{R})$, and $N^{(1)} \in H^{p-2}(\mathbb{R})$ with $p \leq 3$, there exists a unique solution $E \in L^\infty(\mathbb{R}^+, H^p(\mathbb{R}))$, $N \in L^\infty(\mathbb{R}^+, H^{p-1}(\mathbb{R}))$ for (2.47)-(2.48).

Theorem 2.5.2. In dimensions 2 and 3, for initial conditions $E^0 \in H^p(\mathbb{R}^d)$, $N^0 \in H^{p-1}(\mathbb{R}^d)$, and $N^{(1)} \in H^{p-2}(\mathbb{R}^d)$ with $p \leq 3$, there exists a unique solution $E \in L^\infty([0,T^*), H^p(\mathbb{R}^d))$, $N \in L^\infty([0,T^*), H^{p-1}(\mathbb{R}^d))$ for (2.47)-(2.48), where time T^* depends on the initial conditions.

2.6 Plane wave and soliton wave solutions

In one spatial dimension, the generalized ZS (1.1)- (1.2) collapses to

$$i\,E_t + E_{xx} - \alpha N\,E + \lambda|E|^2\,E + i\gamma\,E = 0, \qquad a < x < b, \quad t > 0, \tag{2.74}$$

$$\varepsilon^2 N_{tt} - N_{xx} + \nu(|E|^2)_{xx} = 0, \qquad a < x < b, \quad t > 0, \tag{2.75}$$

which admits plane wave and soliton wave solutions.

Firstly, it is instructive to examine some explicit solutions to (2.74) and (2.75). The well-known plane wave solutions [29] can be given in the following form:

$$N(x,t) = d, \qquad a < x < b, \quad t \geq 0, \tag{2.76}$$

$$E(x,t) = \begin{cases} c\,e^{i\left(\frac{2\pi r x}{b-a} - \omega t\right)}, & \omega = \alpha d + \frac{4\pi^2 r^2}{(b-a)^2} - \lambda c^2, \quad \gamma = 0, \\ c\,e^{-\gamma t} e^{i\left(\frac{2\pi r x}{b-a} - \omega t - \frac{\lambda c^2}{2\gamma}(e^{-2\gamma t}-1)\right)}, & \omega = \alpha d + \frac{4\pi^2 r^2}{(b-a)^2}, \quad \gamma \neq 0, \end{cases} \tag{2.77}$$

where r is an integer and c, d are constants.

Secondly, as is well known, the standard ZS is not exactly integrable. Therefore the generalized ZS cannot be exactly integrable, either. However, it has exact one-soliton solutions to (2.74) and (2.75) for $\gamma = 0$ [24, 25]:

$$E_s(x,t;\eta,V,\varepsilon,\nu) = \left[\frac{\lambda}{2} - \frac{\alpha\nu}{2\varepsilon^2}(1/\varepsilon^2 - V^2)^{-1}\right]^{-1/2} U_s, \quad x \in \mathbb{R},\ t \geq 0, \tag{2.78}$$

$$U_s \equiv 2i\eta\,\mathrm{sech}[2\eta(x - Vt)]\,\exp\left[iVx/2 + i(4\eta^2 - V^2/4)t + i\Phi_0\right], \tag{2.79}$$

$$N_s(x,t;\eta,V,\varepsilon,\nu) = \frac{\nu}{\varepsilon^2}(1/\varepsilon^2 - V^2)^{-1}|E_s|^2, \tag{2.80}$$

where η and V are the soliton's amplitude and velocity, respectively, and Φ_0 is a trivial phase constant.

Finally, we will consider the periodic soliton solution with a period L in 1d of the standard ZS, that is, $d = 1$, $\varepsilon = 1$, $\alpha = 1$, $\lambda = 0$, $\gamma = 0$ and $\nu = -1$ in (1.1)-(1.2). The analytic solution of the ZS (2.74)-(2.75) was derived in [26] and used to test different numerical methods for the ZS in [31, 19, 12]. The solution can be written as

$$E_s(x,t;v,E_{\max}) = F(x-vt)\exp[i\phi(x-ut)], \tag{2.81}$$

$$N_s(x,t;v,E_{\max}) = G(x-vt), \tag{2.82}$$

where

$$F(x-vt) = E_{\max}\cdot dn(w,q), \quad G(x-vt) = \frac{|F(x-vt)|^2}{v^2-1} + N_0,$$

$$w = \frac{E_{\max}}{\sqrt{(2(1-v^2))}}\cdot(x-vt), \quad q = \frac{\sqrt{(E_{\max}^2 - E_{\min}^2)}}{E_{\max}},$$

$$\phi = v/2, \qquad \frac{v}{2}L = 2\pi m, \quad m = 1,2,3\cdots, \quad u = \frac{v}{2} + \frac{2N_0}{v} - \frac{E_{\max}^2 + E_{\min}^2}{v(1-v^2)},$$

$$L = \frac{2\sqrt{2(1-v^2)}}{E_{\max}}K(q) = \frac{2\sqrt{2(1-v^2)}}{E_{\max}}K'\left(\frac{E_{\min}}{E_{\max}}\right),$$

with $dn(w,q)$ a Jacobian elliptic function [22, 1], L the period of the Jacobian elliptic functions, K and K' the complete elliptic integrals of the first kind [22, 1] satisfying $K(q) = K'\left(\sqrt{1-q^2}\right)$, and N_0 chosen such that $\langle N_s\rangle = \frac{1}{L}\int_0^L N_s(x,t)\,dx = 0$.

In Chapter 4, we will present some numerical examples with one of these three solutions as exact solution: plane waves, solitary wave and periodic soliton solution, to demonstrate the efficiency of our proposed methods for the ZS.

Chapter 3

Numerical Methods for the Zakharov System

In this chapter we present the time-splitting spectral discretizations and DSC algorithm for the generalized ZS (1.1), (1.2) and (1.3) with periodic boundary conditions. For simplicity of notation we shall introduce the method in one spatial dimension ($d = 1$). Generalizations to $d > 1$ are straightforward by tensor product grids and the results remain valid without modifications. For $d = 1$, the problem becomes

$$i\,E_t + E_{xx} - \alpha N\,E + \lambda|E|^2\,E + i\gamma\,E = 0, \qquad a < x < b, \quad t > 0, \tag{3.1}$$

$$\varepsilon^2 N_{tt} - N_{xx} + \nu(|E|^2)_{xx} = 0, \qquad a < x < b, \quad t > 0, \tag{3.2}$$

$$E(x,0) = E^0(x),\ N(x,0) = N^0(x),\ N_t(x,0) = N^{(1)}(x), \quad a \le x \le b, \tag{3.3}$$

$$E(a,t) = E(b,t), \qquad E_x(a,t) = E_x(b,t), \qquad t \ge 0, \tag{3.4}$$

$$N(a,t) = N(b,t), \qquad N_x(a,t) = N_x(b,t), \qquad t \ge 0. \tag{3.5}$$

Furthermore, we supplement (3.1)-(3.5) by imposing the compatibility condition

$$E^0(a) = E^0(b), \quad N^0(a) = N^0(b), \quad N^{(1)}(a) = N^{(1)}(b), \quad \int_a^b N^{(1)}(x)\,dx = 0. \tag{3.6}$$

As is known in Chapter 2, the generalized ZS has the property

$$D(t) = \int_a^b |E(x,t)|^2\,dx = e^{-2\gamma t}\int_a^b |E^0(x)|^2\,dx = e^{-2\gamma t}D(0), \qquad t \ge 0. \tag{3.7}$$

When $\gamma = 0$, $D(t) \equiv D(0)$, i.e., it is an invariant of the ZS [12]. Moreover, the ZS also has the following properties

$$\int_a^b N_t(x,t)\,dx = 0, \qquad \int_a^b N(x,t)\,dx = \int_a^b N^0(x)\,dx = \text{const.}, \qquad t \geq 0. \quad (3.8)$$

In some cases, the boundary conditions (3.4) and (3.5) may be replaced by

$$E(a,t) = E(b,t) = 0, \qquad N(a,t) = N(b,t) = 0, \qquad t \geq 0. \quad (3.9)$$

We choose the spatial mesh size $h = \Delta x > 0$ with $h = (b-a)/M$ for M being an even positive integer, the time step being $k = \Delta t > 0$ and let the grid points and the time step be

$$x_j := a + jh, \qquad j = 0, 1, \cdots, M; \qquad t_m := mk, \qquad m = 0, 1, 2, \cdots.$$

Let E_j^m and N_j^m be the approximations of $E(x_j, t_m)$ and $N(x_j, t_m)$, respectively. Furthermore, let E^m and N^m be the solution vectors at time $t = t_m = mk$ with components E_j^m and N_j^m, respectively.

3.1 Time-splitting spectral discretizations (TSSP)

3.1.1 The numerical method

By TSSP from time $t = t_m$ to $t = t_{m+1}$, equation (3.2) in the generalized ZS is discretized by Fourier spectral method in space and second-order central difference scheme in time, and equation (3.1) is solved in two splitting steps. One solves first

$$iE_t + E_{xx} = 0, \quad (3.10)$$

for the time step of length k, and then

$$iE_t = \alpha N\, E - \lambda |E|^2\, E - i\gamma\, E, \quad (3.11)$$

for the same time step. Equation (3.10) will be discretized in space by the Fourier spectral method and integrated in time *exactly*. For $t \in [t_m, t_{m+1}]$, multiplying (3.11) by $\overline{E}$, the conjugate of E, we get

$$iE_t\overline{E} = \alpha N|E|^2 - \lambda|E|^4 - i\gamma|E|^2. \tag{3.12}$$

Then calculating the conjugate of the ODE (3.11) and multiplying it by E, one finds

$$-i\overline{E}_t E = \alpha N|E|^2 - \lambda|E|^4 + i\gamma|E|^2. \tag{3.13}$$

Subtracting (3.13) from (3.12) and then multiplying both sides by $-i$, one gets

$$\frac{d}{dt}\left(|E(x,t)|^2\right) = E_t(x,t)\overline{E(x,t)} + \overline{E_t(x,t)}E(x,t) = -2\gamma|E(x,t)|^2 \tag{3.14}$$

and hence

$$|E(x,t)|^2 = e^{-2\gamma(t-t_m)}|E(x,t_m)|^2, \quad t_m \le t \le t_{m+1}. \tag{3.15}$$

Substituting (3.15) into (3.11), we obtain

$$iE_t(x,t) = \alpha N(x,t)\ E(x,t) - \lambda e^{-2\gamma(t-t_m)}|E(x,t_m)|^2\ E(x,t) - i\gamma\ E(x,t). \tag{3.16}$$

Integrating (3.16) from t_m to t_{m+1}, and then approximating the integral of N on $[t_m, t_{m+1}]$ via the trapezoidal rule, one obtains

$$\begin{aligned} E(x,t_{m+1}) &= e^{-i\int_{t_m}^{t_{m+1}}[\alpha N(x,\tau)-\lambda e^{-2\gamma(\tau-t_m)}|E(x,t_m)|^2-i\gamma]\,d\tau}\ E(x,t_m) \\ &\approx \begin{cases} e^{-ik[\alpha(N(x,t_m)+N(x,t_{m+1}))/2-\lambda|E(x,t_m)|^2]}\ E(x,t_m), & \gamma = 0, \\ e^{-\gamma k - i[k\alpha(N(x,t_m)+N(x,t_{m+1}))/2+\lambda|E(x,t_m)|^2(e^{-2\gamma k}-1)/2\gamma]}\ E(x,t_m), & \gamma \neq 0. \end{cases} \end{aligned}$$

From time $t = t_m$ to $t = t_{m+1}$, we combine the splitting steps via the standard Strang splitting:

$$\varepsilon^2\frac{N_j^{m+1} - 2N_j^m + N_j^{m-1}}{k^2} - \left(D_{xx}^f N^m - \nu D_{xx}^f|E^m|^2\right)\big|_{x=x_j} = 0, \tag{3.17}$$

$$E_j^* = \sum_{l=-M/2}^{M/2-1} e^{-ik\mu_l^2/2}(\widehat{E^m})_l\ e^{i\mu_l(x_j-a)},$$

$$E_j^{**} = \begin{cases} e^{-ik[\alpha(N_j^m+N_j^{m+1})/2-\lambda|E_j^*|^2]}\ E_j^*, & \gamma = 0, \\ e^{-\gamma k - i[k\alpha(N_j^m+N_j^{m+1})/2+\lambda|E_j^*|^2(e^{-2\gamma k}-1)/2\gamma]}\ E_j^*, & \gamma \neq 0, \end{cases}$$

$$E_j^{m+1} = \sum_{l=-M/2}^{M/2-1} e^{-ik\mu_l^2/2}(\widehat{E^{**}})_l\ e^{i\mu_l(x_j-a)}, 0 \le j \le M-1, m = 0, 1, \cdots; \tag{3.18}$$

where $(\widehat{U})_l$, the Fourier coefficient of a vector $U = (U_0, U_1, U_2, \ldots, U_M)^T$ with $U_0 = U_M$, is defined as

$$(\widehat{U})_l = \frac{1}{M}\sum_{j=0}^{M-1} U_j\, e^{-i\mu_l(x_j-a)}, \qquad \mu_l = \frac{2\pi l}{b-a}, \qquad l = -\frac{M}{2}, \ldots, \frac{M}{2}-1, \tag{3.19}$$

and D_{xx}^f, a spectral differential operator approximation of ∂_{xx}, is defined as

$$D_{xx}^f U\big|_{x=x_j} = -\sum_{l=-M/2}^{M/2-1} \mu_l^2 (\widehat{U})_l\, e^{i\mu_l(x_j-a)}. \tag{3.20}$$

The initial conditions (3.3) are discretized as

$$E_j^0 = E^0(x_j),\ N_j^0 = N^0(x_j),\ \frac{N_j^1 - N_j^{-1}}{2k} = N_j^{(1)}, \quad j = 0, 1, 2, \cdots, M-1, \tag{3.21}$$

where

$$N_j^{(1)} = \begin{cases} N^{(1)}(x_j), & 0 \le j \le M-2, \\ -\sum_{l=0}^{M-2} N^{(1)}(x_l), & j = M-1. \end{cases} \tag{3.22}$$

This type of discretization for the initial condition (3.3) is equivalent to the use of the trapezoidal rule for the periodic function $N^{(1)}$. The discretization error converges to 0 exponentially fast as the mesh size h goes to 0.

Note that the spatial discretization error of this method is of spectral-order accuracy in h and time discretization error is of second-order accuracy in k, which will be demonstrated in Chapter 4 by our numerical results.

Note that a main advantage of the time-splitting spectral method is that if a constant r is added to the initial data $N^0(x)$ in (3.3), then the discrete function N_j^{m+1} obtained from (3.17) gets added by r and E_j^{m+1} obtained from (3.18) gets multiplied by the phase factor $e^{-ir(m+1)k}$, which leaves the discrete function $|E_j^{m+1}|^2$ unchanged. This property also holds for the exact solution of the ZS, but does not hold for the finite difference schemes proposed in [19, 12] and the spectral method proposed in [31], in contrast.

Remark 3.1.1. If the periodic boundary conditions (3.4) and (3.5) are replaced by (3.9), then the Fourier basis used in the above algorithm can be replaced by the sine basis. In fact, the generalized Zakharov system (3.1) and (3.2) with the homogeneous periodic boundary condition (3.9) and initial condition (3.3) can be discretized by

$$\varepsilon^2\frac{N_j^{m+1}-2N_j^m+N_j^{m-1}}{k^2}-\left(D_{xx}^s N^m-\nu D_{xx}^s|E^m|^2\right)\big|_{x=x_j}=0, \tag{3.23}$$

$$E_j^*=\sum_{l=1}^{M-1} e^{-ik\eta_l^2/2}\widetilde{(E^m)}_l\ \sin(\eta_l(x_j-a)),$$

$$E_j^{**}=\begin{cases} e^{-ik[\alpha(N_j^m+N_j^{m+1})/2-\lambda|E_j^*|^2]}\ E_j^*, & \gamma=0,\\ e^{-\gamma k-i[k\alpha(N_j^m+N_j^{m+1})/2+\lambda|E_j^*|^2(e^{-2\gamma k}-1)/2\gamma]}\ E_j^*, & \gamma\neq 0,\end{cases}$$

$$E_j^{m+1}=\sum_{l=1}^{M-1} e^{-ik\eta_l^2/2}\widetilde{(E^{**})}_l\ \sin(\eta_l(x_j-a)), 1\le j\le M-1, m=0,1,\cdots, \tag{3.24}$$

where $(\widetilde{U})_l$, the sine-transform coefficients of a vector $U=(U_0,U_1,U_2,\cdots,U_M)^T$ with $U_0=U_M=0$, are defined as

$$\eta_l=\frac{\pi l}{b-a},\qquad \widetilde{U}_l=\frac{2}{M}\sum_{j=1}^{M-1}U_j\ \sin(\eta_l(x_j-a)),\qquad l=1,2,\cdots,M-1, \tag{3.25}$$

and D_{xx}^s, a spectral differential operator approximating ∂_{xx} based on sine-basis, is defined as

$$D_{xx}^s U|_{x=x_j}=-\sum_{l=1}^{M-1}\eta_l^2(\widetilde{U})_l\ \sin(\eta_l(x_j-a)). \tag{3.26}$$

3.1.2 For plane wave solution

Choose the initial data in (3.4)-(3.5) as

$$N^0(x) = d,\quad N^{(1)}(x)=0,\qquad a<x<b, \tag{3.27}$$

$$E^0(x) = c\,e^{i\frac{2\pi r x}{b-a}},\qquad a<x<b, \tag{3.28}$$

then 1d generalized ZS (2.74)-(2.75) admits the plane wave solution (2.76)-(2.77). In this case, our numerical method TSSP gives exact solution provided $M\ge 2(|r|+1)$.

Plugging (3.27)-(3.28) into (3.21)-(3.22), we get

$$N_j^{-1} = N_j^1, \tag{3.29}$$

$$E_j^0 = c\, e^{i\frac{2\pi r x_j}{b-a}}, \qquad j = 0, 1, 2, \cdots, M-1, \tag{3.30}$$

and note (3.19), we also get

$$(\widehat{E^0})_l = c\, e^{i\mu_r a}\, \delta_{lr}, \qquad l = -\frac{M}{2}, \ldots, \frac{M}{2} - 1, \tag{3.31}$$

with

$$\delta_{lr} = \begin{cases} 0, & l \neq r, \\ 1, & l = r, \end{cases} \qquad \mu_r = \frac{2\pi r}{b-a}.$$

Plugging (3.29), (3.30) and (3.31) into (3.17)-(3.18) with $m = 1$, we have

$$N_j^1 = N_j^0 = d, \tag{3.32}$$

$$E_j^* = c\, e^{i\mu_r x_j}\, e^{-ik\mu_r^2/2}, \tag{3.33}$$

and

$$E_j^{**} = \begin{cases} c\, e^{i\mu_r x_j}\, e^{-ik[\alpha d - \lambda c^2 + \mu_r^2/2]}, & \gamma = 0, \\ c\, e^{i\mu_r x_j}\, e^{-ik\mu_r^2/2}\, e^{-i\frac{\lambda c^2}{2\gamma}(e^{-2\gamma k}-1) - \gamma k - ik\alpha d} & \gamma \neq 0. \end{cases} \tag{3.34}$$

Then we obtain

$$E_j^1 = \begin{cases} c\, e^{i(\mu_r x_j - \omega k)}, \quad \omega = \alpha d + \frac{4\pi^2 r^2}{(b-a)^2} - \lambda c^2, & \gamma = 0, \\ c\, e^{-\gamma k} e^{i\left(\mu_r x_j - \omega k - \frac{\lambda c^2}{2\gamma}(e^{-2\gamma k}-1)\right)}, \quad \omega = \alpha d + \frac{4\pi^2 r^2}{(b-a)^2}, & \gamma \neq 0. \end{cases} \tag{3.35}$$

By induction, we get

$$N_j^{m+1} = d, \tag{3.36}$$

$$E_j^{m+1} = \begin{cases} c\, e^{i(\mu_r x_j - \omega t)}, \quad \omega = \alpha d + \frac{4\pi^2 r^2}{(b-a)^2} - \lambda c^2, & \gamma = 0, \\ c\, e^{-\gamma t} e^{i\left(\mu_r x_j - \omega t - \frac{\lambda c^2}{2\gamma}(e^{-2\gamma t}-1)\right)}, \quad \omega = \alpha d + \frac{4\pi^2 r^2}{(b-a)^2}, & \gamma \neq 0, \end{cases} \tag{3.37}$$

with

$$t = t_{m+1} = (m+1)k, \qquad m = 1, 2, \cdots.$$

Here we use the identity

$$\sum_{j=0}^{M-1} e^{i2\pi(r-l)j/M} = \begin{cases} 0, & r-l \neq nM, \\ M, & r-l = nM. \end{cases} \quad \text{for} \quad n \text{ integer} \tag{3.38}$$

Thus in this case our numerical method TSSP really gives exact results provided that the number of grid points $M \geq 2(|r|+1)$.

3.1.3 Conservation and decay rate

Let $U = (U_0, U_1, \cdots, U_M)^T$ with $U_0 = U_M$, $f(x)$ a periodic function on the interval $[a, b]$, and let $\|\cdot\|_{l^2}$ be the usual discrete l^2-norm on the interval (a, b), i.e.,

$$\|U\|_{l^2} = \sqrt{\frac{b-a}{M}\sum_{j=0}^{M-1}|U_j|^2}, \qquad \|f\|_{l^2} = \sqrt{\frac{b-a}{M}\sum_{j=0}^{M-1}|f(x_j)|^2}. \tag{3.39}$$

Then we have

Theorem 3.1.1. The time-splitting spectral discretization TSSP (3.17), (3.18) of the generalized ZS possesses the following properties (in fact, they are the discretized version of (3.7) and (3.8)):

$$\|E^m\|_{l^2}^2 = e^{-2\gamma t_m}\|E^0\|_{l^2}^2, \qquad m = 0, 1, 2, \cdots, \tag{3.40}$$

$$\frac{b-a}{M}\sum_{j=0}^{M-1}\frac{N_j^{m+1}-N_j^m}{k} = 0, \qquad m = 0, 1, 2, \cdots. \tag{3.41}$$

and

$$\frac{b-a}{M}\sum_{j=0}^{M-1} N_j^m = \frac{b-a}{M}\sum_{j=0}^{M-1} N_j^0 = \frac{b-a}{M}\sum_{j=0}^{M-1} N^0(x_j), \qquad m = 0, 1, 2, \cdots \tag{3.42}$$

Proof. From (3.18) in the scheme of TSSP, noting (3.39), (3.19), one has

$$\begin{aligned}
\frac{M}{b-a}\|E^{m+1}\|_{l^2}^2 &= \sum_{j=0}^{M-1}\left|E_j^{m+1}\right|^2 = \sum_{j=0}^{M-1}\left|\sum_{l=-M/2}^{M/2-1} e^{-ik\mu_l^2/2}(\widehat{E^{**}})_l\ e^{i\mu_l(x_j-a)}\right|^2 \\
&= M\sum_{l=-M/2}^{M/2-1}\left|e^{-ik\mu_l^2/2}\ (\widehat{E^{**}})_l\right|^2 = M\sum_{l=-M/2}^{M/2-1}\left|(\widehat{E^{**}})_l\right|^2 \\
&= \frac{1}{M}\sum_{l=-M/2}^{M/2-1}\left|\sum_{j=0}^{M-1} E_j^{**}\ e^{-i\mu_l(x_j-a)}\right|^2 = \sum_{j=0}^{M-1}\left|E_j^{**}\right|^2 \\
&= \begin{cases} \displaystyle\sum_{j=0}^{M-1}\left|e^{-ik[\alpha(N_j^m+N_j^{m+1})/2-\lambda|E_j^*|^2]}\ E_j^*\right|^2, & \gamma=0, \\ \displaystyle\sum_{j=0}^{M-1}\left|e^{-\gamma k-i[k\alpha(N_j^m+N_j^{m+1})/2+\lambda|E_j^*|^2(e^{-2\gamma k}-1)/2\gamma]}\ E_j^*\right|^2, & \gamma\neq 0, \end{cases} \\
&= e^{-2\gamma k}\sum_{j=0}^{M-1}\left|E_j^*\right|^2 = e^{-2\gamma k}\sum_{j=0}^{M-1}\left|\sum_{l=-M/2}^{M/2-1} e^{-ik\mu_l^2/2}(\widehat{E^m})_l\ e^{i\mu_l(x_j-a)}\right|^2 \\
&= e^{-2\gamma k}M\sum_{l=-M/2}^{M/2-1}\left|e^{-ik\mu_l^2/2}(\widehat{E^m})_l\right|^2 = e^{-2\gamma k}M\sum_{l=-M/2}^{M/2-1}\left|(\widehat{E^m})_l\right|^2 \\
&= \frac{e^{-2\gamma k}}{M}\sum_{l=-M/2}^{M/2-1}\left|\sum_{j=0}^{M-1} E_j^m e^{-i\mu_l(x_j-a)}\right|^2 = e^{-2\gamma k}\sum_{j=0}^{M-1}\left|E_j^m\right|^2 \\
&= \frac{Me^{-2\gamma k}}{b-a}\|E^m\|_{l^2}^2 = \cdots = \frac{Me^{-2\gamma t_{m+1}}}{b-a}\|E^0\|_{l^2}^2, \quad m\geq 1. \qquad (3.43)
\end{aligned}$$

Thus the equality (3.40) is proved. Here we use the identities (3.38) and

$$\sum_{l=-M/2}^{M/2-1} e^{i2\pi(k-j)l/M} = \begin{cases} 0, & k-j\neq nM, \\ M, & k-j=nM, \end{cases} \quad \text{for} \quad n \text{ integer}. \qquad (3.44)$$

From the equality (3.17), it follows that

$$\frac{N_j^{m+1}-N_j^m}{k} - \frac{N_j^m-N_j^{m-1}}{k} = \frac{k}{\varepsilon^2}\ \left(D_{xx}^f N^m - \nu D_{xx}^f|E^m|^2\right)\big|_{x=x_j}, \quad 0\leq j<M. \qquad (3.45)$$

Summing the above equality for j from 0 to $M-1$, noting (3.20), (3.19) and (3.38),

we obtain

$$\begin{aligned}
&\sum_{j=0}^{M-1}\frac{N_j^{m+1}-N_j^m}{k}-\sum_{j=0}^{M-1}\frac{N_j^m-N_j^{m-1}}{k}\\
&= \frac{k}{\varepsilon^2}\sum_{j=0}^{M-1}\left(D_{xx}^f N^m-\nu D_{xx}^f|E^m|^2\right)\big|_{x=x_j}\\
&= -\frac{k}{\varepsilon^2}\sum_{j=0}^{M-1}\sum_{l=-M/2}^{M/2-1}\mu_l^2\left[(\widehat{N^m})_l-\nu(\widehat{|E^m|^2})_l\right]\,e^{i\mu_l(x_j-a)}\\
&= -\frac{k}{\varepsilon^2}\sum_{j=0}^{M-1}\sum_{l=-M/2}^{M/2-1}\mu_l^2\left[(\widehat{N^m})_l-\nu(\widehat{|E^m|^2})_l\right]\,e^{i2\pi lj/M}\\
&= -\frac{k}{\varepsilon^2}\sum_{l=-M/2}^{M/2-1}\mu_l^2\left[(\widehat{N^m})_l-\nu(\widehat{|E^m|^2})_l\right]\,\sum_{j=0}^{M-1}e^{i2\pi lj/M}\\
&= 0,\qquad m=1,2,\cdots. \qquad (3.46)
\end{aligned}$$

By induction, we get

$$\sum_{j=0}^{M-1}\frac{N_j^{m+1}-N_j^m}{k}=\sum_{j=0}^{M-1}\frac{N_j^1-N_j^0}{k},\qquad m=1,2,\cdots. \qquad (3.47)$$

Applying (3.21) to (3.17) with $m=1$, we have

$$\frac{N_j^1-N_j^0}{k}=N_j^{(1)}+\frac{k}{2\varepsilon^2}\left(D_{xx}^f N^0-\nu D_{xx}^f|E^0|^2\right)\big|_{x=x_j},\qquad j=0,1,2,\cdots,M. \qquad (3.48)$$

Summing (3.48) with respect to j from 0 to $M-1$, noting (3.22) and proceeding analogously to (3.46), we get

$$\sum_{j=0}^{M-1}\frac{N_j^1-N_j^0}{k}=\sum_{j=0}^{M-1}N_j^{(1)}+\sum_{j=0}^{M-1}\frac{k}{2\varepsilon^2}\left(D_{xx}^f N^0-\nu D_{xx}^f|E^0|^2\right)\big|_{x=x_j}=0+0=0. \qquad (3.49)$$

Obviously equality (3.41) is a combination of (3.47) and (3.49). Combining (3.49) and (3.21), we obtain

$$\sum_{j=0}^{M-1}N_j^1=\sum_{j=0}^{M-1}N_j^0=\sum_{j=0}^{M-1}N^0(x_j). \qquad (3.50)$$

Thus equality (3.42) follows from (3.41) and (3.50) by induction. □

3.2 Other numerical methods

We present in this section discrete singular convolution (DSC) method proposed in [45], and in order to compare the accuracy and stability, we also consider the Fourier pseudospectral (FPS) method proposed in [36] and wavelet-Galerkin (WG) method proposed in [32] and [2] for spatial derivatives, both of which use RK4 for time discretization, as well as the finite difference (FD) method proposed in [12] for Zakharov system. We rewrite (3.1), (3.2) into the following form:

$$E_t = iE_{xx} - i\alpha NE + i\lambda|E|^2E - \gamma E, \tag{3.51}$$

$$N_t = F, \tag{3.52}$$

$$F_t = \frac{1}{\varepsilon^2}[N_{xx} - \nu(|E|^2)_{xx}]. \tag{3.53}$$

3.2.1 Discrete singular convolution (DSC-RK4)

Discrete singular convolution (DSC) method, proposed in [45], provides a general approach for numerical realization of singular integrations. It has been successfully applied to many areas such as signal processing and numerical solutions to differential equations and so on. By an appropriate approximation to a singular kernel, the discrete singular convolution can be an extremely efficient, accurate and reliable algorithm for practical applications.

From the distribution theory, the singular convolution means

$$\Phi(x) = \int_R T(x-y)\varphi(y)dy, \tag{3.54}$$

where $T(x)$ is a singular kernel. Here we mainly consider Dirac delta function $\delta(x)$, or called delta distribution. First of all, delta distribution has the sifting property

$$\varphi(0) = \int_R \delta(y)\varphi(y)dy, \tag{3.55}$$

for any continuous function. And subsequently we can show that it has the property of reproducing kernel, that is,

$$\varphi(x) = \int_R \delta(x-y)\varphi(y)dy, \tag{3.56}$$

for any continuous function. Obviously if delta distribution could be discretized, the singular integral (3.56) would be discretized and thus $\varphi(x)$ be approximated in terms of delta distribution and the sampling values of φ. Unfortunately, however, it is not true because delta distribution has strong singularity and it cannot be discretized directly as a result. Therefore some regularization and approximation of delta distribution are necessary in order to utilize its reproducing property. This is the reason why we will have to choose a good classical approximation to it.

Suppose that $T_\alpha(x)$ is a classical smooth approximation of delta distribution, then the singular convolution (3.56) can be regularized as

$$\varphi(x) \approx \int_R T_\alpha(x-y)\varphi(y)dy. \tag{3.57}$$

Note that $T_\alpha(x)$ is classical and can be discretized and hence

$$\varphi(x) \approx \sum_{i=-\infty}^{\infty} T_\alpha(x-x_i)\varphi(x_i)\Delta x_i. \tag{3.58}$$

After truncation, we obtain the formulae of DSC algorithm

$$\varphi(x) \approx \sum_{i=-W}^{W} T_\alpha(x-x_i)\varphi(x_i)\Delta x_i, \tag{3.59}$$

where $2W+1$ is the computational bandwidth, or effective kernel support, which is usually smaller than the whole computational domain, x_j is sampling point or grid point, $\Delta x_i = x_i - x_{i-1}$.

For more details about DSC method, please refer to [45].

Actually there are many delta sequences which can be generated by dilation of some functions including Shannon kernel $\frac{\sin \pi x}{\pi x}$, Gaussian e^{-x^2}, etc. Nevertheless, a good choice in numerical computation is regularized Shannon kernel(RSK) $\frac{\sin \pi x}{\pi x} e^{-\frac{x^2}{2\sigma^2}}$.

With RSK kernel, DSC method has been testified as a robust method for solving differential equation numerically. Furthermore, it has been proved in [3] that DSC method with RSK kernel has spectral convergence for bandlimited functions.

Now we will review how to discretize the second order spatial derivative of a function u(x) by using RSK kernel [45, 50]

$$u_{xx}(x) \approx \sum_{j=-W}^{W} \delta_{h,\sigma}^{(2)}(x - x_j)u(x_j) \tag{3.60}$$

and

$$\delta_{h,\sigma}(x) = \frac{\sin \frac{\pi}{h}x}{\frac{\pi}{h}x} \exp(-\frac{x^2}{2\sigma^2}) \tag{3.61}$$

is the regularized Shannon's kernel dilated by $\frac{1}{h}$, $\delta_{h,\sigma}^{(2)}$ is a symbol for the second order derivative of $\delta_{h,\sigma}(x)$ with respect to x. The detailed expression for $\delta_{h,\sigma}^{(2)}(x)$ can be easily given as:

$$\delta_{h,\sigma}^{(2)}(x) = \begin{cases} \frac{-\frac{\pi}{h}\sin(\frac{\pi x}{h})\exp(-\frac{x^2}{2\sigma^2})}{x} - 2\frac{\cos(\frac{\pi x}{h})\exp(-\frac{x^2}{2\sigma^2})}{x^2} \\ -2\frac{\cos(\frac{\pi x}{h})\exp(-\frac{x^2}{2\sigma^2})}{\sigma^2} + 2\frac{\sin(\frac{\pi x}{h})\exp(-\frac{x^2}{2\sigma^2})}{\pi x^3/h} \\ +\frac{\sin(\frac{\pi x}{h})\exp(-\frac{x^2}{2\sigma^2})}{\pi\sigma^2 x/h} + \frac{x\sin(\frac{\pi x}{h})\exp(-\frac{x^2}{2\sigma^2})}{\pi\sigma^4/h}, & (x \neq 0), \\ -\frac{3+\pi^2\sigma^2/h^2}{3\sigma^2}, & (x = 0). \end{cases} \tag{3.62}$$

In our computations, we choose W=50 and $\sigma = 5h$.

Therefore, the second-order derivative of a function $u(x)$ at the grid point $x = x_j$ is approximated by

$$u_{xx}|_{x=x_j} = \sum_{l=-W}^{W} \delta_{h,\sigma}^{(2)}(lh)u_{j+l}, \tag{3.63}$$

and thus we get an ordinary differential system of (3.1) and (3.2), then the classical fourth-order Runge-Kutta method (RK4)[33] is used to evaluate E and N at each time step for the time integration.

3.2.2 Fourier pseudospectral method (FPS-RK4)

In general, spectral methods refer to all those global methods that can be interpreted as projection methods over a finite-dimensional space of polynomials with respect to an appropriate inner product. Three most important spectral formulations are the Galerkin, tau, and collocation methods. The spectral method employed in the present work is the collocation scheme with the discrete Fourier basis as the trial functions and is referred as the Fourier pseudospectral (FPS) method. In general, the Fourier pseudospectral method is implemented with the use of the periodic boundary conditions.

We still consider eqs. (3.51)-(3.53). As reviewed in [21], the discrete Fourier transform (DFT) of a function $u(x,t)$ is defined as

$$(\widehat{u})_l = \sum_{j=0}^{M-1} u_j \; e^{-i\mu_l(x_j-a)}, \quad \mu_l = \frac{2\pi l}{b-a}, \quad l = -\frac{M}{2}, \cdots, \frac{M}{2}-1,$$

and its inverse discrete Fourier transform is given by

$$u_j = \frac{1}{M} \sum_{l=-M/2}^{M/2-1} (\widehat{u})_l \; e^{i\mu_l(x_j-a)}, \quad j = 0, 1, \cdots, M-1.$$

For the use of the fast Fourier transform(FFT) for the DFT and its inverse, M has to be chosen as the powers of 2.

If $u(x)$ is a sufficiently smooth function of its variables, its spatial derivatives can be evaluated as

$$\left.\frac{d^n u}{dx^n}\right|_{x=x_j} = \sum_{l=-M/2}^{M/2-1} (i\mu_l)^n (\widehat{u})_l \; e^{i\mu_l(x_j-a)}, \tag{3.64}$$

where $(\widehat{u})_l$ is defined as (3.19). This expression constitutes the basis of the Fourier pseudospectral (FPS) method. For the time integration, the classical fourth-order Runge-Kutta method (RK4) is used to evaluate E and N at each time step. Some detail of FPS-RK4 can also be found in [51].

3.2.3 Wavelet-Galerkin method (WG-RK4)

We also try to use the wavelet-Galerkin method to evaluate the spatial derivatives u_{xx}. The wavelet-Galerkin solution of the periodic problem is slightly more complicated than the finite difference solution, since the solution procedure consists of solving a set of simultaneous equations in wavelet space and not in physical space. This means that we have to transform u_{xx} into wavelet space, solve the set of simultaneous equations to get the solution in wavelet space, and then transform the solution from wavelet space back into physical space. Using the idea of [32] and [2], the wavelet-Galerkin method entails representing the function u and u_{xx} as expansions of scaling functions at a particular scale J:

$$u(x) = \sum_k \tilde{c}_k 2^{\frac{J}{2}} \phi(2^J x - k), \tag{3.65}$$

$$u_{xx}(x) = \sum_k \tilde{g}_k 2^{\frac{J}{2}} \phi(2^J x - k); \tag{3.66}$$

where $\tilde{c}_k$ and $\tilde{g}_k$ are the wavelet coefficients of u and u_{xx}, respectively, i.e., they define the function in the wavelet space, and the scaling function ϕ is defined by a dilation equation of the form

$$\phi(x) = \sum a_k \phi(2x - k). \tag{3.67}$$

Compactly supported scaling functions, such as those belonging to the Daubechies family of wavelets [16], have a finite number of nonzero filter coefficients a_k. We denote the number of nonzero filter coefficients by L.

By transformation of variable

$$y = 2^J x,$$

we can get

$$U(y) = u(x) = \sum_k c_k \phi(y - k), \qquad c_k = 2^{\frac{J}{2}} \tilde{c}_k, \tag{3.68}$$

$$F(y) = u_{xx}(x) = \sum_k g_k \phi(y - k), \qquad g_k = 2^{\frac{J}{2}} \tilde{g}_k. \tag{3.69}$$

Refer to [2], we have

$$\mathcal{F}_k(U) = \mathcal{F}_k(F)/\mathcal{F}_k(K_\Omega). \tag{3.70}$$

The notation $\mathcal{F}_k$ is used for the coefficient in the Fourier space, the convolution kernel $K_\Omega = 2^{2J} \cdot(\Omega_0, \Omega_1, \cdots, \Omega_{L-2}, 0, \cdots, 0, \Omega_{2-L}, \cdots, \Omega_{-1})$, where

$$\Omega_l = \int \phi''(y)\phi(y-l)\, dy$$

is the connection coefficient. The method for computing these coefficients was presented in [9]. Conversely, one gets

$$\mathcal{F}_k(F) = \mathcal{F}_k(U) \cdot \mathcal{F}_k(K_\Omega). \tag{3.71}$$

Therefore, in eqs. (3.51)-(3.53), the spatial derivatives can be evaluated by (3.71) with $h = \frac{1}{2^J}$. For the time integration, we again use the classical fourth-order Runge-Kutta method (RK4). In our computations, we use DAUB12 wavelet basis [9, 16], i.e., L=12.

3.2.4 Finite difference method (FD)

Finite difference (FD) method is the oldest method for numerical solution of partial differential equations, and was already in use by Euler in 1768. It is one of the dominant approaches for solving problems in science and engineering, e.g., in electromagnetic wave simulations. Here we review the finite difference method proposed for the standard ZS [12], i.e., in (3.1)-(3.2) with $\varepsilon = 1$, $\nu = -1$, $\alpha = 1$, $\lambda = 0$ and $\gamma = 0$:

$$i\frac{E_j^{m+1}-E_j^m}{k}+\frac{1}{2}\left(\frac{E_{j+1}^{m+1}-2E_j^{m+1}+E_{j-1}^{m+1}}{h^2}+\frac{E_{j+1}^m-2E_j^m+E_{j-1}^m}{h^2}\right)$$
$$=\frac{1}{4}(N_j^m+N_j^{m+1})(E_j^{m+1}+E_j^m), \tag{3.72}$$

$$\frac{N_j^{m+1}-2N_j^m+N_j^{m-1}}{k^2}-(1-2\theta)\frac{N_{j+1}^m-2N_j^m+N_{j-1}^m}{h^2}$$
$$-\theta\left(\frac{N_{j+1}^{m+1}-2N_j^{m+1}+N_{j-1}^{m+1}}{h^2}+\frac{N_{j+1}^{m-1}-2N_j^{m-1}+N_{j-1}^{m-1}}{h^2}\right)$$
$$=\frac{|E_{j+1}^m|^2-2|E_j^m|^2+|E_{j-1}^m|^2}{h^2}. \tag{3.73}$$

In computations, E_j^0, N_j^0 and N_j^1 are obtained from initial data

$$E_j^0 = E^0(x_j), \qquad N_j^0=N^0(x_j), \tag{3.74}$$
$$N_j^1 = N_j^0+kN^1(x_j)+\frac{k^2}{2}(\frac{N_{j+1}^0-2N_j^0+N_{j-1}^0}{h^2}$$
$$+\frac{|E_{j+1}^0|^2-2|E_j^0|^2+|E_{j-1}^0|^2}{h^2}). \tag{3.75}$$

In our computation, we choose $\theta=0.5$.

3.3 Extension TSSP to Zakharov system for multi-component plasma

For $d=1$, ZS for multi-component plasma (2.49)-(2.51) with periodic boundary conditions can be written as

$$i\partial_t E+E_{xx}+2\sum_J N_J E=0, \tag{3.76}$$
$$\varepsilon_J^2\partial_{tt}N_J-(N_J)_{xx}+\nu_J(|E|^2)_{xx}=0, \quad J=1,2, \tag{3.77}$$
$$E(x,0)=E^0(x),\ N_J(x,0)=N_J^0(x),\ (N_J)_t(x,0)=N_J^{(1)}(x), \quad a\le x\le b, \tag{3.78}$$
$$E(a,t)=E(b,t), \qquad E_x(a,t)=E_x(b,t), \qquad t\ge 0, \tag{3.79}$$
$$N_J(a,t)=N_J(b,t), \qquad (N_J)_x(a,t)=(N_J)_x(b,t), \qquad t\ge 0. \tag{3.80}$$

The idea to construct the TSSP for the ZS (3.1)-(3.5) can be easily extended to the ZS for multi-component plasma (3.76)-(3.80). the detail scheme is following:

$$\varepsilon_J^2\frac{(N_J)_j^{m+1}-2(N_J)_j^m+(N_J)_j^{m-1}}{k^2}-\left(D_{xx}^f N_J^m-\nu_J D_{xx}^f|E^m|^2\right)\big|_{x=x_j}=0, \quad (3.81)$$

$$E_j^*=\sum_{l=-M/2}^{M/2-1} e^{-ik\mu_l^2/2}(\widehat{E^m})_l\, e^{i\mu_l(x_j-a)},$$

$$E_j^{**}=e^{ik\sum_J\left((N_J)_j^m+(N_J)_j^{m+1}\right)}\, E_j^*, \qquad J=1,2$$

$$E_j^{m+1}=\sum_{l=-M/2}^{M/2-1} e^{-ik\mu_l^2/2}(\widehat{E^{**}})_l\, e^{i\mu_l(x_j-a)}, 0\le j\le M-1, m=0,1,\cdots. \quad (3.82)$$

The initial conditions (3.78) are discretized as

$$E_j^0=E^0(x_j),\ (N_J)_j^0=N_J^0(x_j), \quad J=1,2 \quad (3.83)$$

$$\frac{(N_J)_j^1-(N_J)_j^{-1}}{2k}=N_J^{(1)}(x_j), \quad j=0,1,2,\cdots,M-1, \quad (3.84)$$

where

$$N_J^{(1)}(x_j)=\begin{cases} N_J^{(1)}(x_j), & 0\le j\le M-2,\\ -\sum_{l=0}^{M-2} N_J^{(1)}(x_l), & j=M-1. \end{cases} \quad (3.85)$$

3.4 Extension TSSP to vector Zakharov system

The idea to construct the TSSP for ZS (3.1)-(3.5) can be easily extended to the vector ZS (2.39)-(2.40). Consider vector ZS (2.39)-(2.40) with periodic boundary condition for $\mathbf{E}$ and N as following:

$$i\partial_t\mathbf{E}-a\nabla\times(\nabla\times\mathbf{E})+\nabla(\nabla\cdot\mathbf{E})=N\mathbf{E}, \quad (3.86)$$

$$\varepsilon^2\partial_{tt}N-\Delta N=\Delta|\mathbf{E}|^2, \quad \mathbf{x}\in[a_1,b_1]\times[a_2,b_2]\times[a_3,b_3], \quad (3.87)$$

$$\mathbf{E}(\mathbf{x},0)=\mathbf{E}^0(\mathbf{x}),\ N(\mathbf{x},0)=N^0(\mathbf{x}),\ N_t(\mathbf{x},0)=N^{(1)}(\mathbf{x}), \quad (3.88)$$

where $\mathbf{x}=(x,y,z)$. Denote $h_1=\frac{b_1-a_1}{M_1}$ and $h_2=\frac{b_2-a_2}{M_2}$, $h_3=\frac{b_3-a_3}{M_3}$ as the mesh sizes in x, y, z direction, respectively, and choose M_1, M_2, M_3 as even positive integers, and time step $k=\Delta t>0$, the grid points and time step as

$$x_j := a_1 + jh_1, \qquad j = 0, 1, \cdots, M_1; \qquad y_p := a_2 + ph_2, \qquad p = 0, 1, \cdots, M_2;$$

$$z_s := a_3 + sh_3, \qquad s = 0, 1, \cdots, M_3; \qquad t_m := mk, \qquad m = 0, 1, 2, \cdots.$$

Let $\mathbf{E}^m_{j,p,s}$ and $N^m_{j,p,s}$ be the approximations of $\mathbf{E}(x_j, y_p, z_s, t_m)$ and $N(x_j, y_p, z_s, t_m)$, respectively.

Following the idea to construct the TSSP for the ZS (3.1)-(3.5), from time $t = t_m$ to $t = t_{m+1}$, we extend the splitting steps via the standard Strang splitting to vector ZS (3.86)-(3.88) [5]:

$$\varepsilon^2 \frac{N^{m+1}_{j,p,s} - 2N^m_{j,p,s} + N^{m-1}_{j,p,s}}{k^2} - \left(D^f N^m + D^f(|\mathbf{E}^m|^2)\right)\Big|_{\mathbf{x}=(x_j,y_p,z_s)} = 0, \tag{3.89}$$

$$\begin{aligned}
\mathbf{E}^*_{j,p,s} &= \sum_{l=-M_1/2}^{M_1/2-1} \sum_{g=-M_2/2}^{M_2/2-1} \sum_{r=-M_3/2}^{M_3/2-1} B_{l,g,r}(k/2)\ (\widehat{\mathbf{E}^m})_{l,g,r}\ e^{i\left(\frac{2lj\pi}{M_1}+\frac{2pg\pi}{M_2}+\frac{2sr\pi}{M_3}\right)}, \\
\mathbf{E}^{**}_{j,p,s} &= e^{-ik(N^m_{j,p,s}+N^{m+1}_{j,p,s})/2}\ \mathbf{E}^*_{j,p,s}, \\
\mathbf{E}^{m+1}_{j,p,s} &= \sum_{l=-M_1/2}^{M_1/2-1} \sum_{g=-M_2/2}^{M_2/2-1} \sum_{r=-M_3/2}^{M_3/2-1} B_{l,g,r}(k/2)\ (\widehat{\mathbf{E}^{**}})_{l,g,r}\ e^{i\left(\frac{2lj\pi}{M_1}+\frac{2pg\pi}{M_2}+\frac{2sr\pi}{M_3}\right)},
\end{aligned} \tag{3.90}$$

where

$$B_{l,g,r}(t-t_m) = \begin{cases} I_3, & l = g = r = 0, \\ \left(I_3 + \dfrac{e^{-i(1-a)(t-t_m)R^2_{l,g,r}} - 1}{R^2_{l,g,r}} A_{l,g,r}\right) e^{-ia(t-t_m)R^2_{l,g,r}}, & \text{otherwise}, \end{cases}$$

with

$$R^2_{l,g,r} = \mu_l^2 + \zeta_g^2 + \eta_r^2, \qquad A_{l,g,r} = \begin{pmatrix} \mu_l^2 & \mu_l\zeta_g & \mu_l\eta_r \\ \mu_l\zeta_g & \zeta_g^2 & \zeta_g\eta_r \\ \mu_l\eta_r & \zeta_g\eta_r & \eta_r^2 \end{pmatrix} = \begin{pmatrix} \mu_l \\ \zeta_g \\ \eta_r \end{pmatrix} \begin{pmatrix} \mu_l & \zeta_g & \eta_r \end{pmatrix}.$$

This is due to $A^2_{l,g,r} = R^2_{l,g,r} A_{l,g,r}$, which leads to

$$\begin{aligned}
e^{A_{l,g,r}} &= \sum_{n=0}^{\infty} \frac{A^n_{l,g,r}}{n!} = I_3 + \sum_{n=1}^{\infty} \frac{A^n_{l,g,r}}{n!} = I_3 + \sum_{n=1}^{\infty} \frac{R^{2(n-1)}_{l,g,r}}{n!} A_{l,g,r} \\
&= I_3 + \sum_{n=1}^{\infty} \frac{R^{2n}_{l,g,r}}{R^2 n!} A_{l,g,r} = I_3 + \frac{e^{R^2_{l,g,r}} - 1}{R^2} A_{l,g,r},
\end{aligned}$$

where I_3 is the 3×3 identity matrix. Where $(\widehat{\mathbf{U}})_{l,g,r}$ is defined as

$$(\widehat{\mathbf{U}})_{l,g,r} = \frac{1}{M_1}\frac{1}{M_2}\frac{1}{M_3}\sum_{j=0}^{M_1-1}\sum_{p=0}^{M_2-1}\sum_{s=0}^{M_3-1}\mathbf{U}_{j,p,s}\, e^{-i\left(\frac{2lj\pi}{M_1}+\frac{2pg\pi}{M_2}+\frac{2sr\pi}{M_3}\right)}, \tag{3.91}$$

with

$$\begin{aligned}
\mu_l &= \frac{2\pi l}{b_1-a_1}, \qquad l = -\frac{M_1}{2},\ldots,\frac{M_1}{2}-1,\\
\zeta_g &= \frac{2\pi g}{b_2-a_2}, \qquad g = -\frac{M_2}{2},\ldots,\frac{M_2}{2}-1,\\
\eta_r &= \frac{2\pi r}{b_3-a_3}, \qquad r = -\frac{M_3}{2},\ldots,\frac{M_3}{2}-1,
\end{aligned} \tag{3.92}$$

and D^f, a spectral differential operator approximation of $\Delta = \partial_{xx}+\partial_{yy}+\partial_{zz}$, is defined as

$$\begin{aligned}
&D^f\mathbf{U}\big|_{\mathbf{x}=(x_j,y_p,z_s)}\\
&= -\sum_{l=-\frac{M_1}{2}}^{\frac{M_1}{2}-1}\sum_{g=-\frac{M_2}{2}}^{\frac{M_2}{2}-1}\sum_{r=-\frac{M_3}{2}}^{\frac{M_3}{2}-1}(\mu_l^2+\zeta_g^2+\eta_r^2)(\widehat{\mathbf{U}})_{l,g,r}\, e^{i\left(\frac{2lj\pi}{M_1}+\frac{2pg\pi}{M_2}+\frac{2sr\pi}{M_3}\right)}.
\end{aligned} \tag{3.93}$$

The initial conditions (3.88) are discretized as

$$\begin{aligned}
&\mathbf{E}^0_{j,p,s} = \mathbf{E}^0(x_j,y_p,z_s), \qquad N^0_{j,p,s} = N^0(x_j,y_p,z_s),\\
&\frac{N^1_{j,p,s}-N^{-1}_{j,p,s}}{2k} = N^{(1)}_{j,p,s}, \qquad j=0,\cdots,M_1,\ p=0,\cdots,M_2,\ s=0,\cdots,M_3,
\end{aligned}$$

with

$$N^{(1)}_{j,p,s} = N^{(1)}(x_j,y_p,z_s), \quad j\neq M_1-1 \& p\neq M_2-1 \& s\neq M_3-1$$

and $N^{(1)}_{M_1-1,M_2-1,M_3-1}$ is chosen such that

$$\sum_{l=0}^{M_1-1}\sum_{g=0}^{M_2-1}\sum_{r=0}^{M_3-1}N^{(1)}_{j,p,s} = 0,$$

which implies that

$$N^{(1)}_{M_1-1,M_2-1,M_3-1} = N^{(1)}(x_{M_1-1},y_{M_2-1},z_{M_3-1}) - \sum_{l=0}^{M_1-1}\sum_{g=0}^{M_2-1}\sum_{r=0}^{M_3-1}N^{(1)}(x_l,y_g,z_r).$$

This type of discretization for the initial condition (3.88) is equivalent to the use of the trapezoidal rule for the periodic function $N^{(1)}$ and such that the properties (3.8) is satisfied in the discretized level. The discretization error converges to 0 exponentially fast as the mesh size $h = \max\{h_1,h_2,h_3\}$ goes to 0.

Chapter 4

Numerical Examples

In this chapter, we present numerical results of the ZS with a solitary wave solution in 1d to compare the accuracy and stability of different methods described in Chapter 3. We also present numerical examples including plane waves, soliton-soliton collisions in 1d, as well as a 2d problem and damped problem of the ZS to demonstrate the efficiency and spectral accuracy of the time-splitting spectral method (TSSP) and discrete singular convolution method (DSC-RK4) for the generalized Zakharov system.

In the examples 1, 3 and 4, 6, 8, the initial conditions for (1.3) are always chosen such that $|E^0|$, N^0 and $N^{(1)}$ decay to zero sufficiently fast as $|\mathbf{x}| \to \infty$. We always compute on a domain, which is large enough such that the periodic boundary conditions (3.4)-(3.5) do not introduce a significant aliasing error relative to the problem in the whole space.

4.1 Comparisons of different methods

Example 1 The standard ZS with a solitary-wave solution, i.e., we choose $d = 1$, $\varepsilon = 1$, $\alpha = 1$, $\lambda = 0$, $\gamma = 0$ and $\nu = -1$ in (1.1)-(1.3). The well-known solitary-wave

solution of the ZS (1.1)-(1.3) in this case is given in [29, 25]

$$E(x,t) = \sqrt{2B^2(1-C^2)}\,\mathrm{sech}(B(x-Ct))\; e^{i[(C/2)x-((C/2)^2-B^2)t]}, \tag{4.1}$$

$$N(x,t) = -2B^2\,\mathrm{sech}^2(B(x-Ct)), \quad -\infty < x < \infty, \quad t \geq 0, \tag{4.2}$$

where B, C are constants. The initial condition is taken as

$$E^0(x) = E(x,0), \quad N^0(x) = N(x,0), \quad N^{(1)}(x,0) = N_t(x,0), \qquad -\infty < x < \infty, \tag{4.3}$$

where $E(x,0)$, $N(x,0)$ and $N_t(x,0)$ are obtained from (4.1), (4.2) by setting $t = 0$. We present computations for two different regimes of the acoustic speed, i.e. $1/\varepsilon$:

Case I. $O(1)$-acoustic speed, i.e. we choose $\varepsilon = 1$, $B = 1$, $C = 0.5$ in (4.1), (4.2). Here we test the spatial and temporal discretization errors, conservation of the conserved quantities as well as the stability constraint of different numerical methods. We solve the problem on the interval [-32, 32], i.e., $a = -32$ and $b = 32$ with periodic boundary conditions. Let $E_{h,k}$ and $N_{h,k}$ be the numerical solution of (1.1), (1.2) in 1d with the initial condition (4.3) by using a numerical method with mesh size h and time step k. To quantify the numerical methods, we define the error functions as

$$e_1 = \|E(\cdot,t) - E_{h,k}(t)\|_{l^2}, \qquad e_2 = \|N(\cdot,t) - N_{h,k}(t)\|_{l^2},$$
$$e = \frac{\|E(\cdot,t) - E_{h,k}(t)\|_{l^2}}{\|E(\cdot,t)\|_{l^2}} + \frac{\|N(\cdot,t) - N_{h,k}(t)\|_{l^2}}{\|N(\cdot,t)\|_{l^2}} = \frac{e_1}{\|E(\cdot,t)\|_{l^2}} + \frac{e_2}{\|N(\cdot,t)\|_{l^2}}$$

and evaluate the conserved quantities by using the numerical solution (i.e., replacing E and N by their numerical counterparts $E_{h,k}$ and $N_{h,k}$, respectively) as

$$D = \int_{-\infty}^{\infty} |E(x,t)|^2\, dx,$$
$$P = \int_{-\infty}^{\infty} \left[\frac{i}{2}(E(x,t)\overline{E_x(x,t)} - \overline{E(x,t)}E_x(x,t)) + N(x,t)V(x,t)\right] dx,$$
$$H = \int_{-\infty}^{\infty} \left[|E_x(x,t)|^2 + N|E|^2 + \frac{1}{2}N^2 + \frac{1}{2}V(x,t)^2\right] dx,$$

where V is the flux and its value is determined from the continuity equation

$$N_t + V_x = 0. \tag{4.4}$$

First, we test the discretization error in space. In order to do this, we choose a very small time step, e.g., $k = 0.00001$ such that the error from time discretization is negligible comparing to the spatial discretization error, and solve the ZS with different methods under different mesh sizes h. Table 4.1 lists the numerical errors of e_1 and e_2 at $t = 2.0$ with different mesh sizes h for different numerical methods.

	Mesh	$h = 1.0$	$h = \frac{1}{2}$	$h = \frac{1}{4}$
TSSP	e_1	9.810E-2	1.500E-4	2.286E-9
	e_2	0.143	1.168E-3	2.201E-8
DSC-RK4	e_1	0.151	1.955E-4	3.452E-9
	e_2	0.243	2.347E-3	4.692E-8
WG-RK4	e_1	0.697	1.866E-2	1.403E-5
	e_2	0.968	3.651E-2	5.677E-5
FD	e_1	0.491	0.120	2.818E-2
	e_2	0.889	0.209	4.726E-2

Table 4.1: Spatial discretization error analysis: e_1, e_2 at time t=2 under $k = 0.00001$.

Secondly, we test the discretization error in time. Table 4.2 shows the numerical errors of e_1 and e_2 at $t = 2.0$ under different time steps k and mesh sizes h for different numerical methods. For the FD method, due to its second-order convergence rate in space, we list errors for larger time steps k in order to view the convergence rate in time.

Thirdly, we test the conservation of conserved quantities. Table 4.3 presents the quantities and numerical errors at different times with mesh size $h = \frac{1}{8}$ and time step $k = 0.001$ for different numerical methods.

	h	Error	$k = 0.01$	$k = 0.0025$	$k = 0.000625$	$k = 0.00015625$
TSSP	$\frac{1}{4}$	e_1	4.631E-5	2.894E-6	1.809E-7	1.148E-8
		e_2	1.029E-4	6.429E-6	4.024E-7	3.338E-8
	$\frac{1}{8}$	e_1	4.631E-5	2.894E-6	1.809E-7	1.129E-8
		e_2	1.029E-4	6.429E-6	4.018E-7	2.513E-8
DSC-RK4	$\frac{1}{4}$	e_1	2.822E-9	3.442E-9	3.452E-9	3.452E-9
		e_2	4.693E-8	4.692E-8	4.692E-8	4.692E-8
	$\frac{1}{8}$	e_1	—	4.338E-12	3.756E-13	3.765E-13
		e_2	—	3.789E-12	6.194E-14	6.276E-14
FPS-Rk4	$\frac{1}{4}$	e_1	2.078E-9	2.185E-9	2.192E-9	2.192E-9
		e_2	5.990E-8	5.989E-8	5.989E-8	5.989E-8
	$\frac{1}{8}$	e_1	—	4.342E-12	7.369E-14	7.218E-14
		e_2	—	3.762E-12	1.467E-14	4.899E-15
WG-RK4	$\frac{1}{4}$	e_1	1.399E-5	1.403E-5	1.403E-5	1.403E-5
		e_2	5.677E-5	5.677E-5	5.677E-5	5.677E-5
	$\frac{1}{8}$	e_1	8.172E-9	8.506E-9	8.508E-9	8.508E-9
		e_2	4.239E-8	4.221E-8	4.221E-8	4.221E-8
	h	Error	$k = 0.8$	$k = 0.2$	$k = 0.05$	$k = 0.0125$
FD	$\frac{1}{4}$	e_1	0.802	3.480E-2	2.855E-2	2.820E-2
		e_2	0.674	9.012E-2	5.005E-2	4.743E-2
	$\frac{1}{8}$	e_1	0.809	1.753E-2	7.363E-3	6.961E-3
		e_2	0.656	5.491E-2	1.427E-2	1.167E-2

Table 4.2: Time discretization error analysis: e_1, e_2 at time t=2.

Fourthly, we compare the stability constraint for different numerical methods and list the results in Table 4.4. There the error e is computed at time $t = 5.0$.

	Time	e	D	P	H
TSSP	1.0	5.323E-7	3.0000000000	3.397277646	0.519446033
	2.0	7.127E-7	3.0000000000	3.397277653	0.519446032
DSC-RK4	1.0	1.966E-13	3.0000000000	3.397343618	0.519445999
	2.0	2.813E-13	3.0000000000	3.397343618	0.519445999
FPS-RK4	1.0	9.631E-14	3.0000000000	3.397343618	0.519445999
	2.0	1.184E-13	3.0000000000	3.397343618	0.519445999
WG-RK4	1.0	3.064E-8	3.0000000000	3.397343618	0.51944599
	2.0	2.319E-8	3.0000000000	3.397343618	0.51944599
FD	1.0	4.745E-3	3.0000000000	3.394829741	0.510115589
	2.0	8.983E-3	3.0000000000	3.394791238	0.510076710

Table 4.3: Conserved quantities analysis: $k = 0.001$ and $h = \frac{1}{8}$.

Case II: 'Subsonic limit' regime, i.e. we choose $\varepsilon \ll 1$, $B = 1$ and $C = 1/2\varepsilon$ in (4.1), (4.2). Here we test the ε-resolution of different numerical methods. We solve the problem on the interval [-8, 120], i.e., $a = -8$ and $b = 120$ with periodic boundary conditions. Figure 4.1 shows the numerical results of TSSP at $t = 1$ when we choose the meshing strategy: $\varepsilon = \frac{1}{8}$, $h = \frac{1}{2}$, $k = \frac{1}{50}$; $\varepsilon = \frac{1}{32}$, $h = \frac{1}{8}$, $k = \frac{1}{800}$; $\varepsilon = \frac{1}{128}$, $h = \frac{1}{32}$, $k = \frac{1}{12800}$ corresponding to $h = O(\varepsilon)$ and $k = O(\varepsilon h) = O(\varepsilon^2)$. FPS-RK4 gives similar results at the same meshing strategy.

From Tables 4.1-4.4 and Figure 4.1, we can draw the following observations:

h		DSC-RK4	TSSP	FPS-RK4	WG-RK4	FD ($\theta = \frac{1}{2}$)	FD($\theta = 0$)
$\frac{1}{2}$	k	$\frac{1}{16}$	$\frac{1}{4}$	$\frac{1}{16}$	$\frac{1}{8}$	$\frac{1}{2}$	$\frac{1}{2}$
	e	1.125E-3	0.101	1.645E-3	4.388E-2	0.702	0.207
$\frac{1}{4}$	k	$\frac{1}{64}$	$\frac{1}{8}$	$\frac{1}{64}$	$\frac{1}{32}$	$\frac{1}{4}$	$\frac{1}{4}$
	e	2.458E-8	1.466E-2	3.526E-8	4.815E-5	0.167	4.194E-2
$\frac{1}{8}$	k	$\frac{1}{256}$	$\frac{1}{16}$	$\frac{1}{256}$	$\frac{1}{128}$	$\frac{1}{8}$	$\frac{1}{8}$
	e	2.465E-11	3.163E-3	4.936E-11	2.552E-8	3.937E-2	1.009E-2
$\frac{1}{16}$	k	$\frac{1}{1024}$	$\frac{1}{32}$	$\frac{1}{1024}$	$\frac{1}{512}$	$\frac{1}{16}$	$\frac{1}{16}$
	e	2.869E-13	7.812E-4	2.659E-13	9.147E-12	9.758E-3	2.499E-3

Table 4.4: Stability analysis: time $t = 5.0$.

(1) For TSSP, the spatial discretization error is of spectral order accuracy and the time discretization error is of second-order accuracy. TSSP conserves D exactly and P, H very well (up to 8 digits). The stability constraint of TSSP is weaker, it requires $k = O(h)$ for $\varepsilon = O(1)$. Furthermore, it is explicit, easy to program, less memory requirement, easy to extend to 2d and 3d cases and keeps more properties of the generalized ZS in the discretized level. Of course, the finite difference method is easy to program.

(2) DSC-RK4 can also obtain the exponentially high order accuracy in space. Table 4.3 shows that DSC-RK4 can conserve D, P and H very well. The stability constraint of DSC-RK4 is $k = O(h^2)$ for $\varepsilon = O(1)$. Furthermore, DSC-RK4 is explicit and can be applied to deal with complex geometry and more general boundary conditions.

(3) FD, FPS-RK4 and WG-RK4 give good approximations of the standard ZS with the solitary-wave solution. FPS-RK4 and WG-RK4 are explicit and of spectral order accuracy and high order accuracy in space, respectively. The stability constraint of these two methods is $k = O(h^2)$ for $\varepsilon = O(1)$. FD is implicit, time reversible and

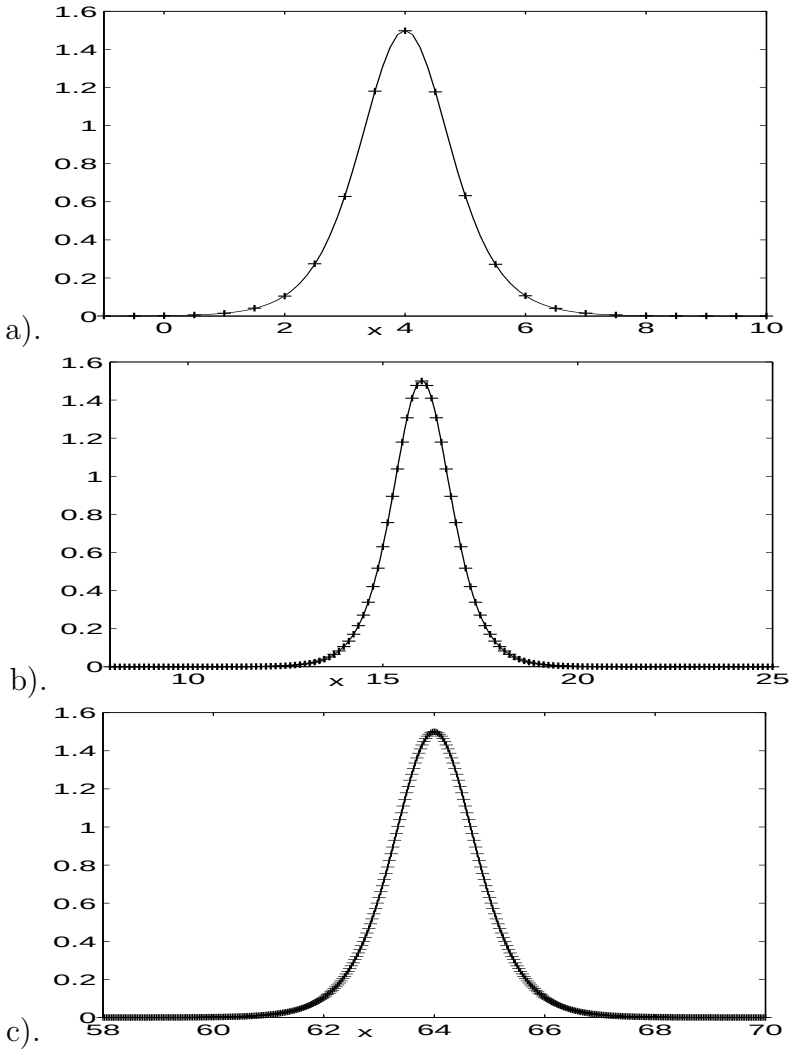

Figure 4.1: Numerical solutions of the electric field $|E(x,t)|^2$ at $t = 1$ for Example 1 in the 'subsonic limit' regime by TSSP (3.17), (3.18). a). $\varepsilon = \frac{1}{8}$, $h = \frac{1}{2}$, $k = \frac{1}{50}$; b). $\varepsilon = \frac{1}{32}$, $h = \frac{1}{8}$, $k = \frac{1}{800}$; c). $\varepsilon = \frac{1}{128}$, $h = \frac{1}{32}$, $k = \frac{1}{12800}$ corresponding to $h = O(\varepsilon)$ and $k = O(\varepsilon h) = O(\varepsilon^2)$.

of second order accuracy in both space and time. The stability constraint of FD is $k = O(h)$ for $\varepsilon = O(1)$.

(4) In the 'subsonic limit' regime, i.e. $0 < \varepsilon \ll 1$, the ε-resolution is: For TSSP, $h = O(\varepsilon)$ and $k = O(\varepsilon h)$; for DSC-RK4, $h = o(\varepsilon)$ and $k = O(\varepsilon h)$ when the bandwidth w in (3.60) is fixed and $h = O(\varepsilon)$ and $k = O(\varepsilon h)$ when $w = O(1/\varepsilon)$; for

FPS-RK4, $h = O(\varepsilon)$ and $k = O(\varepsilon h)$; for WG-RK4 and FD: $h = o(\varepsilon)$ and $k = O(\varepsilon h)$.

In general, the numerical study on the standard ZS with periodic boundary condition suggests that TSSP, DSC-RK4 and FPS-RK4 have much better spatial resolution than FD and WG-RK4. It is obvious that TSSP is easy to program and less memory requirement, keeps more properties of the generalized ZS in discretized level and its stability constraint is weaker, where DSC-RK4 algorithm can be applied for complex geometry and general boundary conditions. For more comprehensive comparisons between the DSC-RK4 and FPS-RK4 for PDEs, we refer to [51]. In summary, for generalized ZS with periodic boundary conditions or in the whole space with initial data decaying to zero sufficiently fast as $|\mathbf{x}| \to \infty$ which can be approximated in a bounded domain with periodic boundary conditions, we recommend to use TSSP; for generalized ZS in a complex geometry or with non-periodic boundary conditions, we recommend to use DSC-RK4.

4.2 Applications of TSSP

4.2.1 Plane-wave solution of the standard Zakharov system

Example 2 The standard ZS with a plane-wave solution, i.e., we choose $d = 1$, $\varepsilon = 1$, $\alpha = 1$, $\lambda = 0$, $\gamma = 0$ and $\nu = -1$ in (1.1)-(1.3) and consider the problem on the interval $[a, b]$ with $a = 0$ and $b = 2\pi$. The initial condition is taken as

$$E(x,0) = E^0(x) = e^{i7x},\ N(x,0) = N^0(x) = 1,\ N_t(x,0) = N^{(1)}(x) = 0,\ 0 \le x \le 2\pi. \tag{4.5}$$

It is easy to see that the ZS (3.1), (3.2) with the periodic boundary conditions (3.4), (3.5), and initial condition (4.5) admits the plane wave solution [29]

$$E(x,t) = e^{i(7x-\omega t)}, \qquad \text{with} \quad \omega = 7^2 + 1 = 50, \tag{4.6}$$

$$N(x,t) = 1, \qquad a \le x \le b, \quad t \ge 0. \tag{4.7}$$

We solve this problem by using the time-splitting spectral method (TSSP) on the interval $[0, 2\pi]$ with mesh size $h = \frac{\pi}{8}$ (i.e., 17 grid points in the interval $[0, 2\pi]$) and time step $k = 0.01$. Figure 4.2 shows the numerical results at $t = 2$ and $t = 4$.

From Figure 4.2, we can see that the time-splitting spectral method really provides the exact plane-wave solution of the Zakharov system.

4.2.2 Soliton-soliton collisions of the standard Zakharov system

Example 3 Soliton-soliton collisions in 1d of the standard ZS, i.e., we choose $d = 1$, $\varepsilon = 1$, $\alpha = 1$, $\lambda = 0$, $\gamma = 0$ and $\nu = -1$ in (1.1)-(1.3). Here we use this solution (2.81)-(2.82) to test our method TSSP and DSC-RK4. The values of the various parameters used in our computations are given in Table 4.5.

Parameter set	L	$E_{\max}$	$E_{\min}$	v	u	N_0
A	160	1.0	1.0535×10^{-31}	0.628319	2.24323	0.0227232
B	160	0.5	1.0535×10^{-18}	0.628319	-0.27094	0.0227232
C	160	1.0	1.0535×10^{-38}	0.314159	-3.22992	0.0227232

Table 4.5: Parameter values for analytic solutions of the periodic Zakharov system.

In the following we will study soliton-soliton collisions using the time-splitting spectral method. The initial data is chosen as

$$\begin{aligned} E(x,0) &= E_s(x+p,0,v_1,E^1_{\max}) + E_s(x-p,0,v_2,E^2_{\max}),\\ N(x,0) &= N_s(x+p,0,v_1,E^1_{\max}) + N_s(x-p,0,v_2,E^2_{\max}),\\ N_t(x,0) &= \frac{\partial N_s(x+p,0,v_1,E^1_{\max})}{\partial t} + \frac{\partial N_s(x-p,0,v_2,E^2_{\max})}{\partial t}, \end{aligned}$$

where $x = \mp p$ are initial locations of the two solitons. We present computations for three cases:

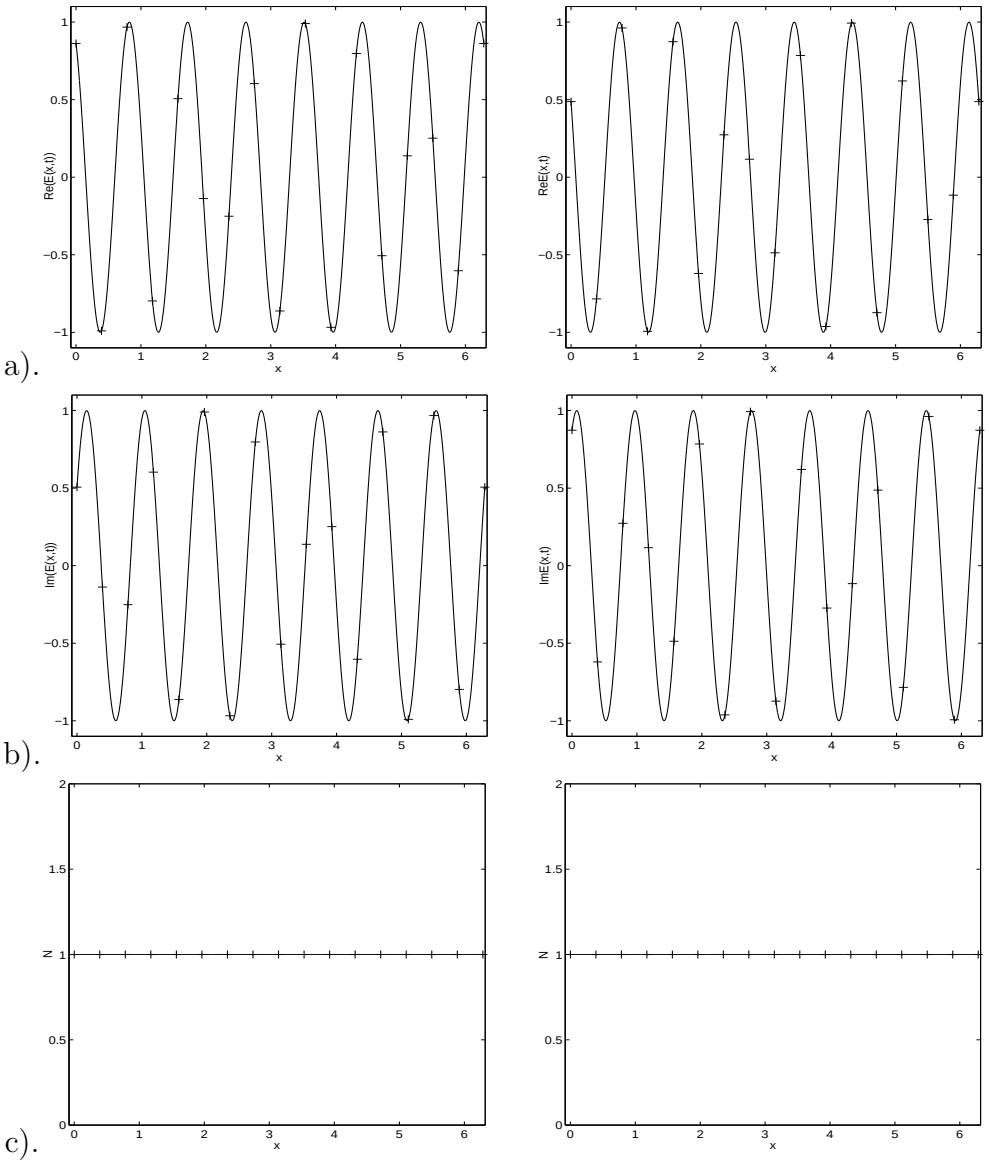

Figure 4.2: Numerical solutions at $t = 2$ ('left') and $t = 4$ ('right') in Example 1. '— ': exact solution given in (4.6)-(4.7), '+ + +': numerical solution. a). $\mathrm{Re}(E(x,t))$: real part of E, b). $\mathrm{Im}(E(x,t))$: imaginary part of E, c). N.

I. Collision of two solutions with equal amplitudes and opposite velocities.

$$E^1_{\max} = E^2_{\max} = E_{\max} = 1.0, \qquad v_1 = -v_2 = v = 0.628319, \qquad \text{(parameter set A)}.$$

II. Collision of two solutions with different amplitudes and opposite velocities.

$$E^1_{\max} = 0.5, \quad v_1 = 0.628319, \qquad \text{(parameter values set B)},$$
$$E^2_{\max} = 1.0, \quad v_2 = -0.628319, \qquad \text{(parameter values set A)}.$$

III. Collision of two solutions with equal amplitudes and opposite velocities but different speeds.

$$E^1_{\max} = 1.0, \quad v_1 = 0.314159, \qquad \text{(parameter value set C)},$$
$$E^2_{\max} = 1.0, \quad v_2 = -0.628319, \qquad \text{(parameter value set A)}.$$

We solve the problem in the interval $[-80, 80]$, i.e., $a = -80$ and $b = 80$ with mesh size $h = \frac{5}{16}$ and time step $k = 0.01$. We take $p = 10$. Figure 4.3 shows the values of $|E(x,t)|$ and $N(x,t)$ at various times for case I, Figure 4.4 for case II and Figure 4.5 for case III.

Case I which was already used in [31, 12, 19] to test their numerical methods corresponds to collision of two solutions with equal amplitudes and opposite velocities. In this case, the time $t = 15.9$ corresponds to the time when the two solutions are at the same position and the time $t = 31.8$ corresponds to a time when the collision is nearing completion (cf. Figure 4.3). From the figure we can see that during the collision waves are emitted, and that after the collision the two solutions have a reduced value of $E_{\max}$. Comparison of our graphical results (under mesh size $h = \frac{5}{16}$) with those (under mesh size $h = \frac{1}{20}$) of [31, 19, 12] shows excellent qualitative agreement. This also demonstrates that the time-splitting spectral method TSSP has a better resolution than the finite difference method proposed in [19, 12]. Case II corresponds to the collision of a right-going soliton with a smaller peak value of $E^1_{\max}$ and a left-going soliton with a larger value of $E^2_{\max}$. They have equal speeds. In this case, during the collision waves are emitted and exchanged, and that after the collision the peak value of the left-going soliton becomes bigger than its value before

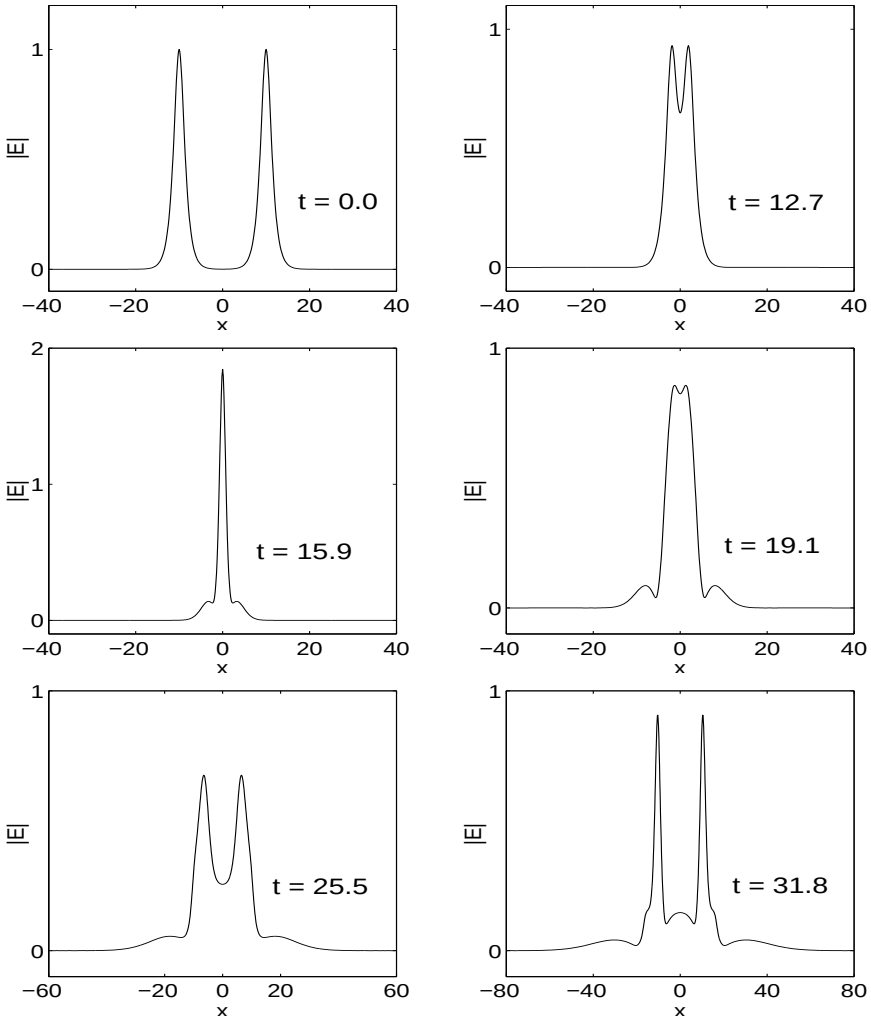

Figure 4.3: Numerical solutions at different times in Example 3 for case I: Electric field $|E(x,t)|$.

collision and the peak of the other becomes much smaller (cf. Figure 4.4). This means that the soliton with larger peak value will absorb part of the other wave during their collision. Case III corresponds to a collision of a right-going soliton with a smaller speed $|v_1|$ and a left-going soliton with a larger speed $|v_2|$. They have equal amplitudes. Again, waves are emitted and exchanged during collision. After the collision, the peak value of the left-going soliton becomes larger than its value before collision and the peak of the other becomes much smaller (cf. Figure 4.5). This means that the soliton with larger speed will absorb part of the other wave

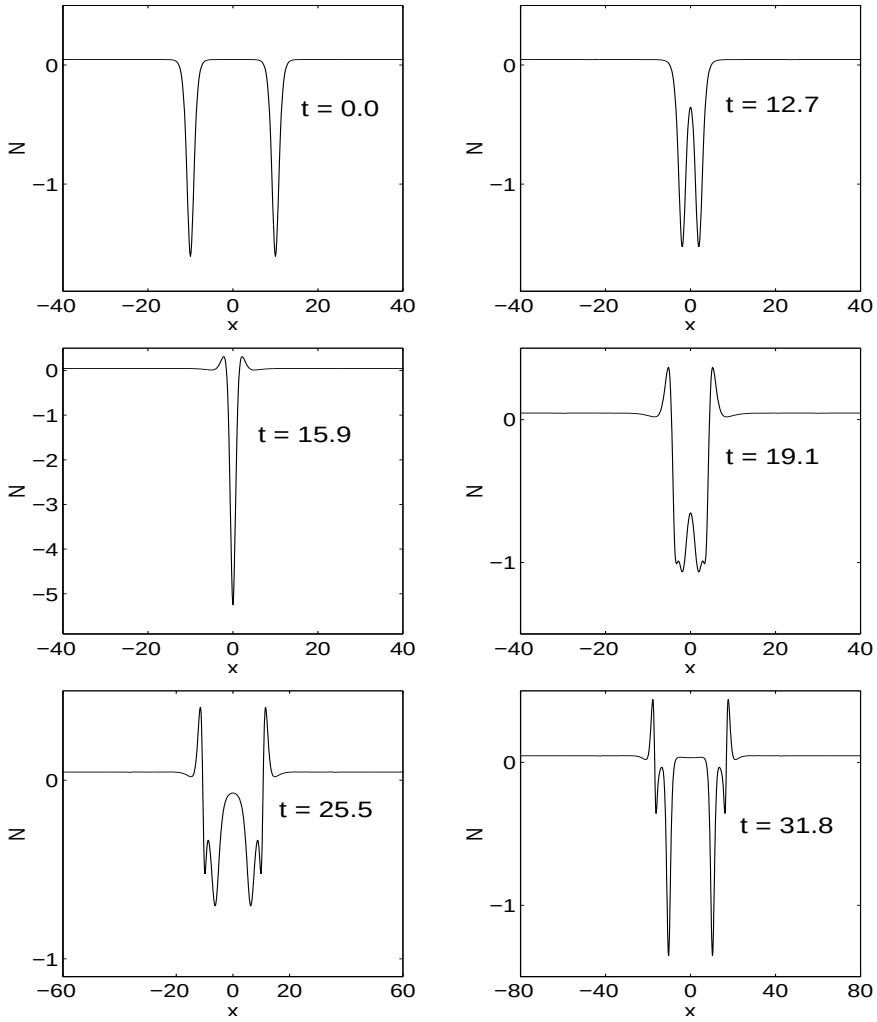

Figure 4.3 (cont'd): Ion density $N(x,t)$.

during their collision.

The same results can also be obtained by the DSC-RK4 with mesh size $h = \frac{5}{16}$ and time step $k = 0.01$.

4.2.3 Solution of 2d standard Zakharov system

Example 4 A 2d problem of the standard ZS, i.e., we choose $d = 2$, $\varepsilon = 1$, $\alpha = 1$,

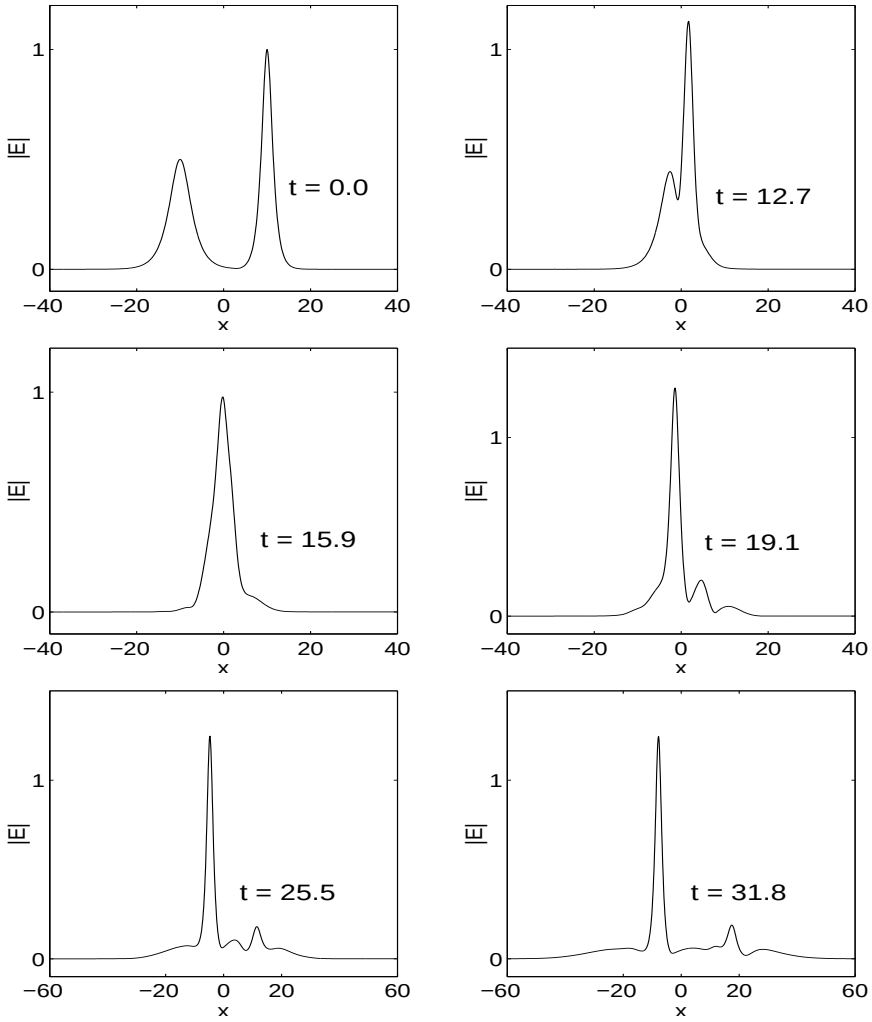

Figure 4.4: Numerical solutions at different times in Example 3 for case II: Electric field $|E(x,t)|$.

$\lambda = 0$, $\gamma = 0$ and $\nu = -1$ in (1.1)-(1.3). The initial condition is taken as

$$E(x,y,0) = \frac{2}{e^{x^2+2y^2} + e^{-(x^2+2y^2)}}\, e^{i5/\cosh(\sqrt{4x^2+y^2})},$$
$$N(x,y,0) = e^{-(x^2+y^2)}, \qquad N_t(x,y,0) = 0.$$

We solve the problem on the rectangle $[-64,64]^2$ with mesh size $h = \frac{1}{4}$ and time step $k = 0.01$. Figure 4.6 shows the surface plots of $|E|^2$ and N at time $t = 2.0$, Figure 4.7 shows the contour plots of $|E|^2$ and N at different times.

From Figure 4.6-4.7, we can see that the time-splitting spectral method can really

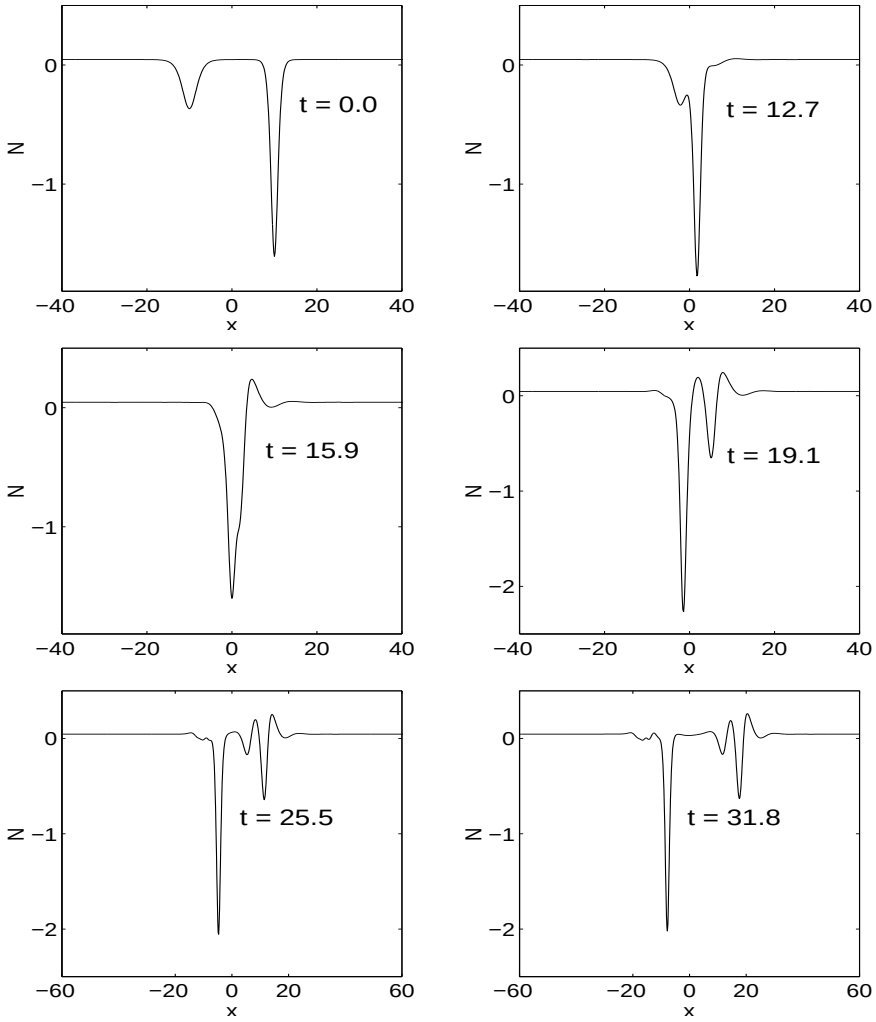

Figure 4.4 (cont'd): Ion density $N(x,t)$.

be applied to solve 2d Zakharov system.

4.2.4 Soliton-soliton collisions of the generalized Zakharov system

Example 5 Soliton-soliton collisions in 1d of the generalized ZS, i.e., we choose $d = 1$, $\varepsilon = 1$, $\alpha = -2$ and $\gamma = 0$ in (1.1)-(1.3). We use the family of one-soliton solutions (2.78)-(2.80) to test our methods TSSP and DSC-RK4. The initial data

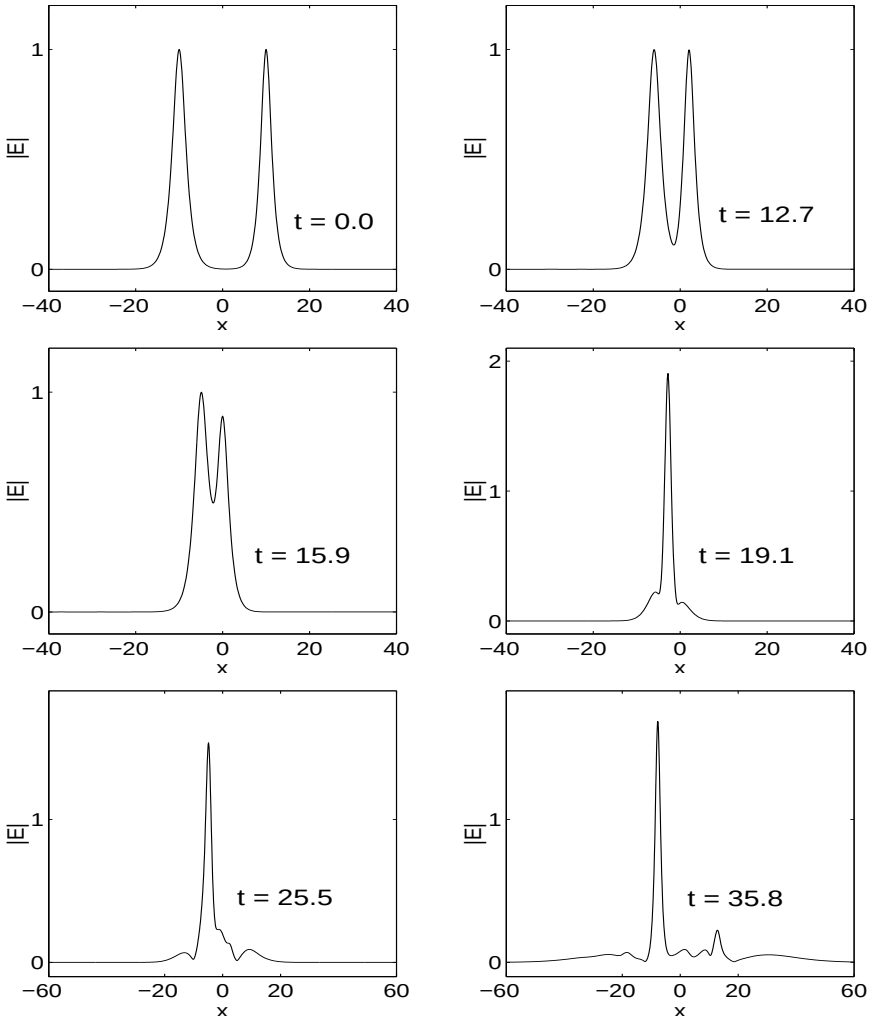

Figure 4.5: Numerical solutions at different times in Example 3 for case III: Electric field $|E(x,t)|$.

is chosen as

$$E(x,0) = E_s(x+p,0,\eta_1,V_1,\varepsilon,\nu) + E_s(x-p,0,\eta_2,V_2,\varepsilon,\nu),$$
$$N(x,0) = N_s(x+p,0,\eta_1,V_1,\varepsilon,\nu) + N_s(x-p,0,\eta_2,V_2,\varepsilon,\nu),$$
$$N_t(x,0) = \frac{\partial N_s(x+p,0,\eta_1,V_1,\varepsilon,\nu)}{\partial t} + \frac{\partial N_s(x-p,0,\eta_2,V_2,\varepsilon,\nu)}{\partial t},$$

where $x = \mp p$ are initial locations of the two solitons.

In all the numerical simulations reported in this example, we set $\lambda = 2$, and $\Phi_0 = 0$. We only simulated the symmetric collisions, i.e., the collisions of solitons with equal

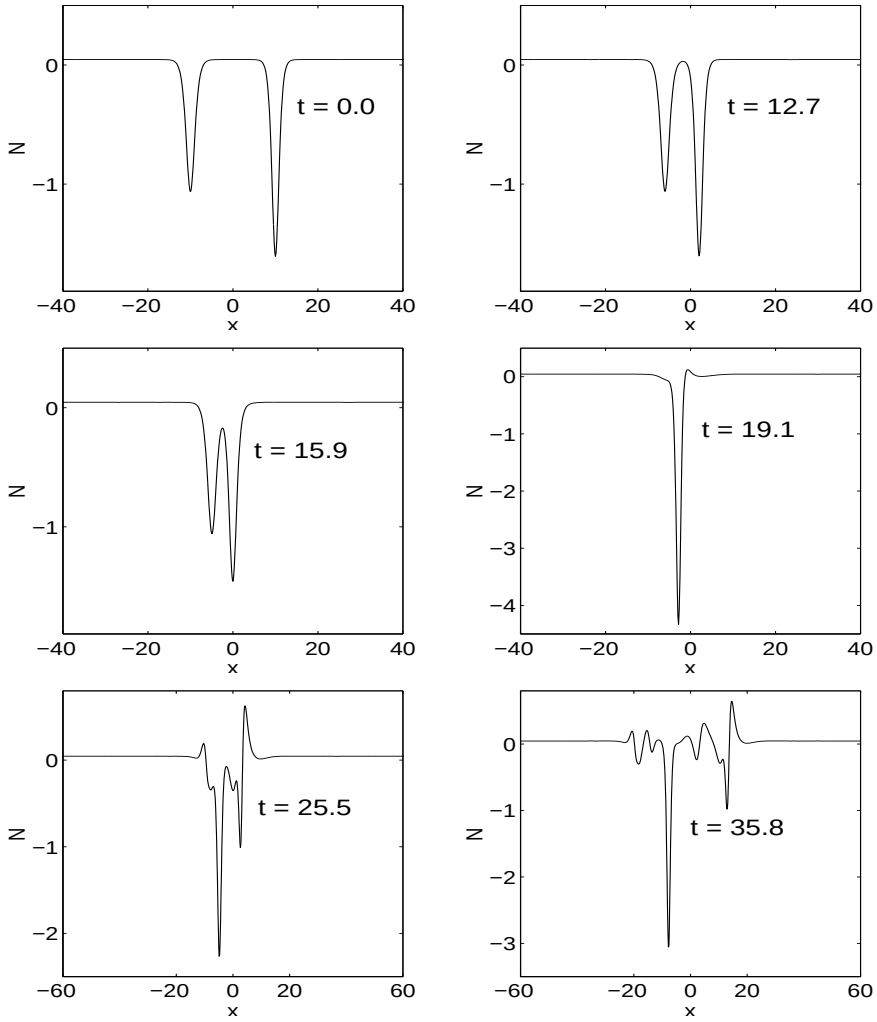

Figure 4.5 (cont'd): Ion density $N(x,t)$.

amplitudes $\eta_1 = \eta_2 = \eta$ and opposite velocities $V_1 = -V_2 \equiv V$. Here, we present computations for four cases:

I. Collision between solitons moving with the subsonic velocities, $V < 1/\varepsilon = 1$.

$$\text{Case 1:} \quad \nu = 0.2, \quad \eta = 0.3, \quad V = 0.5;$$

$$\text{Case 2:} \quad \nu = 2, \quad \eta = 0.3, \quad V = 0.045;$$

$$\text{Case 3:} \quad \nu = 2, \quad \eta = 0.3, \quad V = 0.45.$$

II. Collision between solitons in the transonic regime, $V > 1/\varepsilon = 1$.

$$\text{Case 4:} \quad \nu = 2.0, \quad \eta = 0.3, \quad V = 3.0.$$

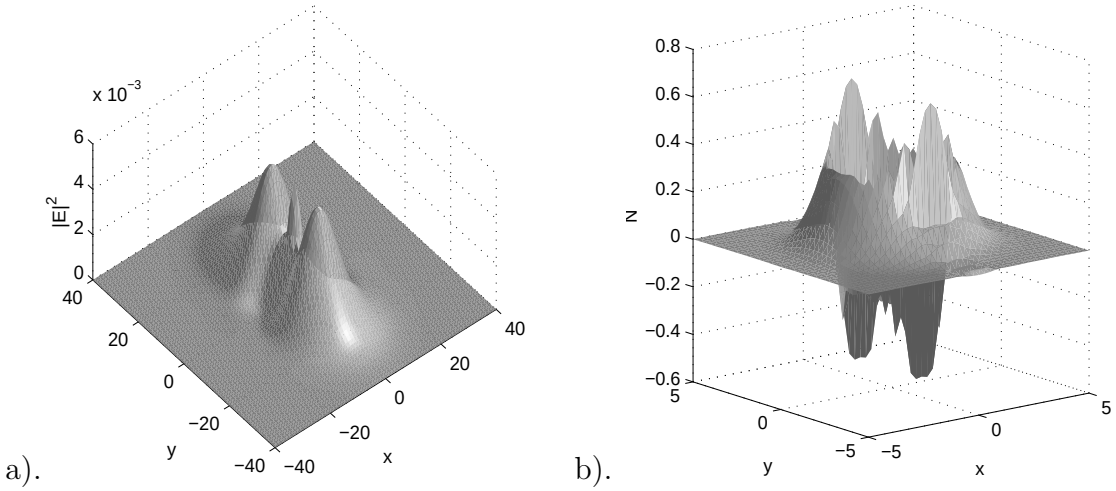

Figure 4.6: Numerical solutions in Example 4. Surface-plot at time $t = 2.0$: a). Electric field $|E(x, y, 2.0)|^2$, b). Ion density $N(x, y, 2.0)$.

We solve the problem on the interval [-128,128], i.e., a = -128 and b = 128 with mesh size $h = \frac{1}{4}$ and time step $k = 0.005$. We take p = 10. Figure 4.8 shows the evolution of the dispersive wave field $|E|^2$ for case 1, Figure 4.9 shows the evolutions of the dispersive wave field $|E|^2$ and the acoustic (nondispersive) field N for case 2, Figure 4.10 for case 3 and Figure 4.11 for case 4.

Case 1 corresponds to a soliton-soliton collision when the ratio ν/λ is small, i.e., the generalized ZS (3.1), (3.2) is close to the NLS equation. As is seen, the collision seems quite elastic (cf. Figure 4.8). Case 2 and case 3 correspond to the fusion of the colliding subsonic solitons into the new soliton in the system (3.1), (3.2) at the different velocities. At very small values of V, the collision results in the direct fusion of the colliding solitons into a new solitonlike state, its amplitude and width are almost constant in time (cf. Figure 4.9). With the growth of V, the appearing soliton demonstrates irregular oscillations in its amplitude and size; the oscillations are accompanied by a conspicuous emission of the acoustic waves (cf. Figure 4.10). Case 4 corresponds to the collision of two transonic solitons. Note that the emission of the sound waves is inconspicuous at this value of V (cf. Figure 4.11).

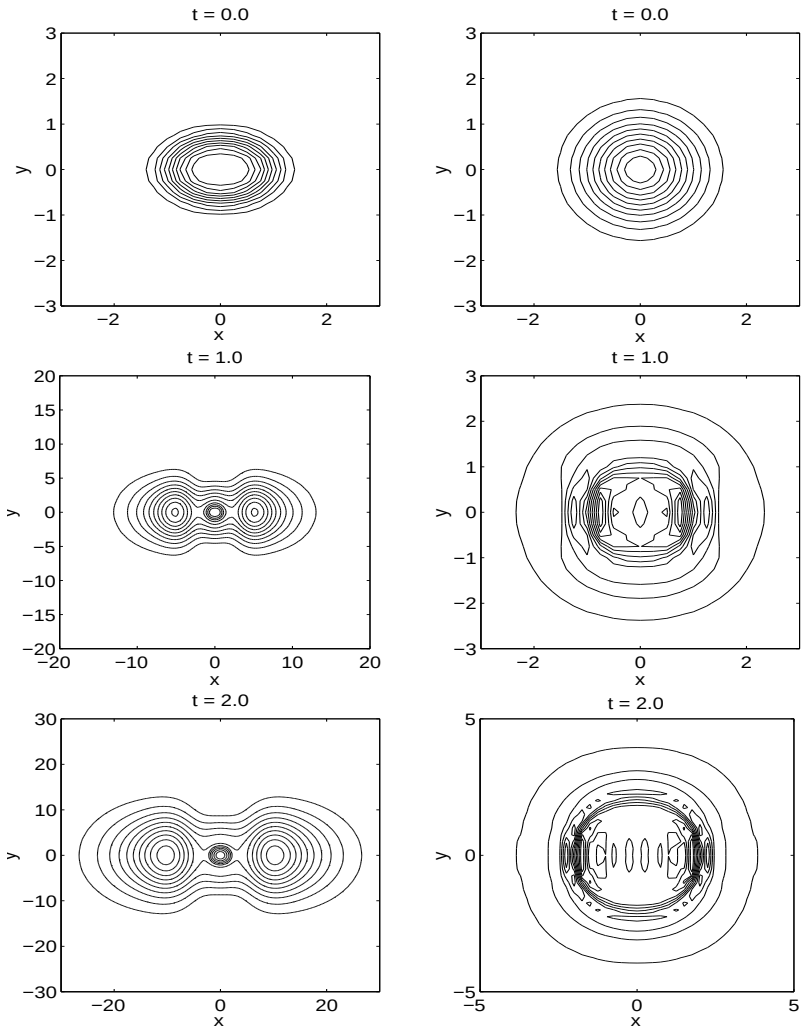

Figure 4.7: Contour-plots at different times. Left: Electric field $|E|^2$; Right: ion density N.

From Figures 4.8-4.11, we can see that the time-splitting spectral method can really be applied to solve soliton-soliton collisions of generalized Zakharov system. Furthermore, the DSC-RK4 can also achieve similar results.

4.2.5 Solutions of the damped Zakharov system

In this subsection we present numerical tests of the TSSP for solving the generalized ZS in 2d with a damping term. In our computations, the initial condition and

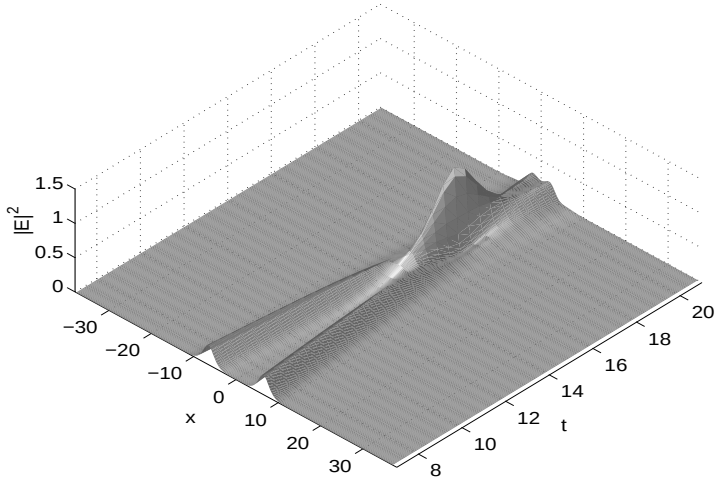

Figure 4.8: Evolution of the wave field $|E|^2$ in Example 5 for case 1.

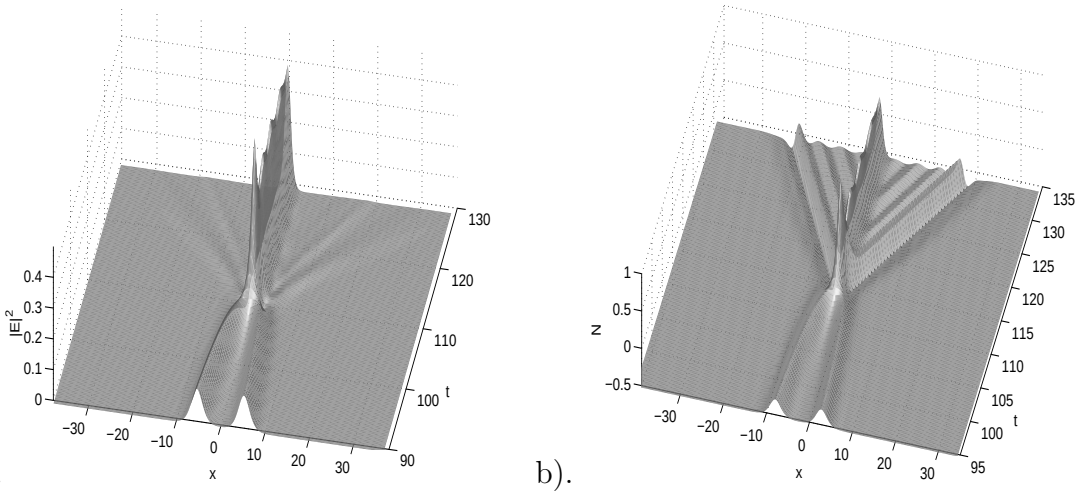

Figure 4.9: Numerical solutions in Example 5 for case 2. a). Evolution of the wave field $|E|^2$; b). Evolution of the acoustic field N.

parameters α, λ, ε, ν are always chosen such that the initial Hamiltonian $H(0) < 0$.

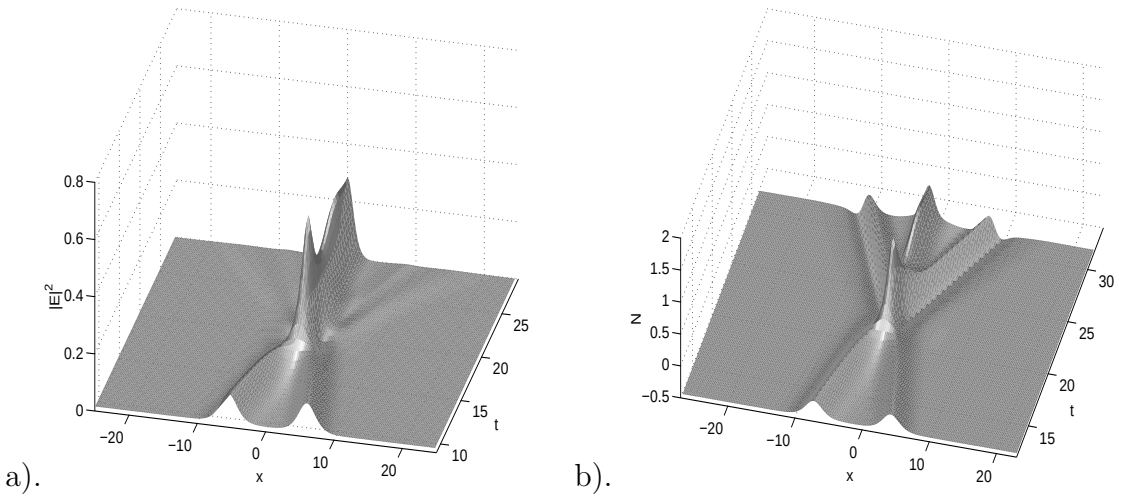

Figure 4.10: Numerical solutions in Example 5 for case 3. a). Evolution of the wave field $|E|^2$; b). Evolution of the acoustic field N.

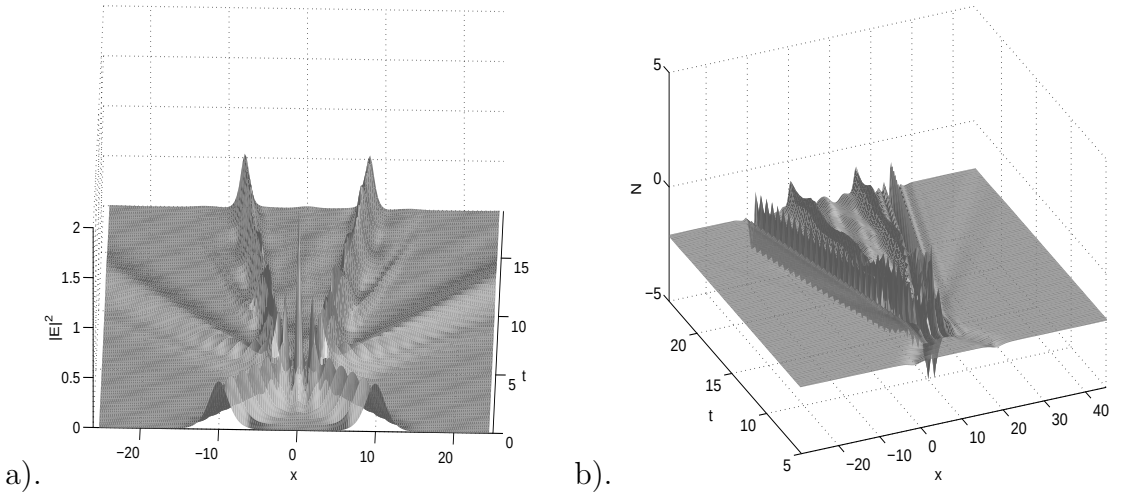

Figure 4.11: Numerical solutions in Example 5 for case 4. a). Evolution of the wave field $|E|^2$; b). Evolution of the acoustic field N.

Example 6 A 2d damped problem of the generalized ZS. We choose $d = 2$ in (1.1)-(1.3) and present computations for three cases:

$$\text{Case 1:} \quad \alpha = 20, \quad \lambda = 0, \quad \varepsilon = 1, \quad \nu = -1;$$

$$\text{Case 2:} \quad \alpha = 1, \quad \lambda = 20, \quad \varepsilon = 1, \quad \nu = -1;$$

$$\text{Case 3:} \quad \alpha = 1, \quad \lambda = 0, \quad \varepsilon = 0.1, \quad \nu = -20,$$

with different linear damping term $\gamma = 0.8$, $\gamma = 0.1$, $\gamma = 0$.

The initial condition is taken as

$$E(x, y, 0) = \frac{1}{\sqrt{\pi}}\, e^{-\frac{x^2+y^2}{2}},$$
$$N(x, y, 0) = \frac{\nu}{\pi}\, e^{-(x^2+y^2)}, \qquad N_t(x, y, 0) = 0.$$

It is easy to see the initial condition satisfies $N(x, y, 0) = \nu|E(x, y, 0)|^2$, so $\lambda > 0$ or $\alpha \cdot \nu < 0$ correspond to the focusing NLS, which is possible blow up.

We solve the problem on the rectangle $[-4, 4]^2$ with mesh size $h = \frac{1}{32}$ and time step $k = 0.001$ for cases 1 and 2 and the rectangle $[-10, 10]^2$ with mesh size $h = \frac{5}{64}$ and time step $k = 0.0001$ for case 3. Figures 4.12-4.14 show the surface plots of $|E|^2$ and N at different times with $\gamma = 0.8,\ 0.1$ and 0 for case 1, Figures 4.15-4.17 for case 2 and Figures 4.18-4.20 for case 3. Figure 4.21 shows $D(t)$, $H(t)$, $N(0, 0, t)$ and $|E(0, 0, t)|^2$ as functions of time with $\gamma = 0.8,\ 0.1$ and 0 for three cases.

From our numerical results we see that the time-splitting spectral method can still be applied to solve the 2d problem of the generalized ZS with a linear damping term. As we see in Figures 4.12-4.21, numerical results also confirm that the solutions will be blown up if the initial Hamiltonian $H(0) < 0$. Case 1 and Case 3 correspond to $\alpha \cdot \nu < 0$, the blowup is arrested if the damping parameter γ is bigger than a certain value. As shown in the following Figures, blowup is arrested for $\gamma = 0.8$ while the solutions blow up for $\gamma = 0.1$ and $\gamma = 0$. Results also show a very sharp spike with a peak value that increases when parameter ε decreases as can be seen from Figures. Case 2 corresponds to $\lambda > 0$, the blowup is arrested as well if the damping parameter γ is bigger than a certain value. When there is no blowup or blowup is arrested, the spectral order accuracy of TSSP can still be observed.

4.2.6 Solutions of the Zakharov system for multi-component plasma

In this subsection we present numerical test of the TSSP (3.81)-(3.82) for solving the ZS with two components appearing in [24, 25] in 1d.

Example 7 Soliton-soliton collisions in 1d of the ZS with multicomponent. We choose $d = 1$ in (2.49)-(2.51). We use the family of one-soliton solutions (2.78)-(2.80) to test our method TSSP. The initial data is chosen as

$$
\begin{aligned}
&E(x,0) = E_s(x+p,0,\eta_1,V_1,\varepsilon_1,\nu_1) + E_s(x-p,0,\eta_2,V_2,\varepsilon_1,\nu_1),\\
&N_1(x,0) = N_s(x+p,0,\eta_1,V_1,\varepsilon_1,\nu_1) + N_s(x-p,0,\eta_2,V_2,\varepsilon_1,\nu_1),\\
&\frac{\partial N_1}{\partial t}(x,0) = \frac{\partial N_s(x+p,0,\eta_1,V_1,\varepsilon_1,\nu_1)}{\partial t} + \frac{\partial N_s(x-p,0,\eta_2,V_2,\varepsilon_1,\nu_1)}{\partial t},\\
&N_2(x,0) = \nu_2|E_s(x+p,0,\eta_1,V_1,\varepsilon_1,\nu_1)|^2 + \nu_2|E_s(x-p,0,\eta_2,V_2,\varepsilon_1,\nu_1)|^2,\\
&\frac{\partial N_2}{\partial t}(x,0) = \nu_2\frac{\partial|E_s(x+p,0,\eta_1,V_1,\varepsilon_1,\nu_1)|^2}{\partial t} + \nu_2\frac{\partial|E_s(x-p,0,\eta_2,V_2,\varepsilon_1,\nu_1)|^2}{\partial t},
\end{aligned}
$$

where $x = \mp p$ are initial locations of the two solitons.

In all the numerical simulations reported in this example, we set $\lambda = 2\nu_2$, and $\Phi_0 = 0$. We only simulated the symmetric collisions, i.e., the collisions of solitons with equal amplitudes $\eta_1 = \eta_2 = \eta$ and opposite velocities $V_1 = -V_2 \equiv V$. Here, we present computations for four cases:

$$
\begin{aligned}
\text{Case 1:}\quad & \varepsilon_1 = 1.0,\ \ \nu_1 = 0.2,\ \ \eta = 0.3,\ \ V = 0.5;\\
& \varepsilon_2 = 0.1,\ \ \nu_2 = 1.0,\ \ \eta = 0.3,\ \ V = 0.5;\\
\text{Case 2:}\quad & \varepsilon_1 = 1.0,\ \ \nu_1 = 0.2,\ \ \eta = 0.3,\ \ V = 0.5;\\
& \varepsilon_2 = 1.0,\ \ \nu_2 = 1.0,\ \ \eta = 0.3,\ \ V = 0.5;\\
\text{Case 3:}\quad & \varepsilon_1 = 1.0,\ \ \nu_1 = 2.0,\ \ \eta = 0.3,\ \ V = 3.0;\\
& \varepsilon_2 = 0.1,\ \ \nu_2 = 1.0,\ \ \eta = 0.3,\ \ V = 3.0;\\
\text{Case 4:}\quad & \varepsilon_1 = 1.0,\ \ \nu_1 = 2.0,\ \ \eta = 0.3,\ \ V = 3.0;\\
& \varepsilon_2 = 1.0,\ \ \nu_2 = 1.0,\ \ \eta = 0.3,\ \ V = 3.0.
\end{aligned}
$$

We solve the problem on the interval [-128,128], i.e., a = -128 and b = 128 with mesh size $h = \frac{1}{4}$ and time step $k = 0.005$. We take p = 10. Figure 4.22 shows the evolution of the dispersive wave field $|E|^2$ for case 1-4.

Case 1 and Case 3 correspond to a soliton-soliton collision when $1/\varepsilon_2^2 \gg 1/\varepsilon_1^2$. That means the dispersive waves interact with two far different acoustic modes. Note that Figures 4.22-a, 4.22-c, 4.22-e, and compare them with Figure 4.8, Figure 4.11-a, 4.11-b, respectively. The numerical results confirm that, as was stated in Chapter 2, the generalized ZS (1.1)-(1.3) with $d = 1$, $\alpha = -2$ and $\gamma = 0$ can be obtained from ZS (2.49)-(2.51) with two different components. Case 2 and Case 4 correspond to soliton-soliton collision at the same scale, e.g., $1/\varepsilon_2^2 = 1/\varepsilon_1^2$. Again, we compare Figures 4.22-b, 4.22-d, 4.22-f with Figure 4.8, Figure 4.11-a, 4.11-b, respectively. We observe that ZS (2.49)-(2.51) can not reduce to one component at the same scale.

4.2.7 Dynamics of 3d vector Zakharov system

Example 8 Dynamics of 3d vector Zakharov system, i.e., we choose $d = 3$, $a = 2$ and $\varepsilon = 1$ in (3.86), (3.87). The initial conditions are taken as

$$E_j(x,y,z,0) = e^{2i(\lambda_1 x - \lambda_2 y + 2\lambda_3 z)}(\gamma_{1j}\gamma_{2j}\gamma_{3j})^{1/4}\frac{e^{-\frac{1}{2}(\gamma_{1j}x^2+\gamma_{2j}y^2+\gamma_{3j}z^2)}}{\sqrt{3}\pi^{3/4}}, \quad j = 1,2,3,$$
$$N(x,y,z,0) = e^{-2(x^2+y^2+z^2)},$$
$$N_t(x,y,z,0) \equiv 0;$$

with

$$\gamma_{11} = 1,\ \gamma_{21} = 2,\ \gamma_{31} = 4; \quad \gamma_{12} = 4,\ \gamma_{22} = 2,\ \gamma_{32} = 1; \quad \gamma_{13} = 2,\ \gamma_{23} = 4,\ \gamma_{33} = 1.$$

We solve the vector ZS for two different initial parameters:

I. Zero initial phase data, i.e. $\lambda_1 = \lambda_2 = \lambda_3 = 0$;

II. Nonzero initial phase data, i.e. $\lambda_1 = \lambda_2 = \lambda_3 = 1$.

From (3.86), (3.87), after a simple analysis, we get

$$\begin{aligned}\frac{d}{dt}\|E_j(t)\|^2 &= \frac{d}{dt}\int_{\mathbb{R}^d}|E_j(\mathbf{x},t)|^2\ d\mathbf{x}\\ &= 2(a-1)\ \mathrm{Im}\int_{\mathbb{R}^d}\frac{\partial E_j}{\partial x_j}\nabla\cdot\overline{\mathbf{E}}\ d\mathbf{x}, \qquad t\geq 0, \quad j=1,\cdots,d. \end{aligned} \tag{4.8}$$

Plugging the above initial data into (4.8) at $t=0$, we obtain for case I:

$$\left.\frac{d||E_1(t)||^2}{dt}\right|_{t=0} = \left.\frac{d||E_2(t)||^2}{dt}\right|_{t=0} = \left.\frac{d||E_3(t)||^2}{dt}\right|_{t=0} = 0 \tag{4.9}$$

and for case II:

$$\left.\frac{d||E_1(t)||^2}{dt}\right|_{t=0} > 0, \qquad \left.\frac{d||E_2(t)||^2}{dt}\right|_{t=0} > 0, \qquad \left.\frac{d||E_3(t)||^2}{dt}\right|_{t=0} < 0. \tag{4.10}$$

In the two cases, the wave energy for each component of the electron field are set the same.

We solve the problem in the box $[-16,16]^3$ with mesh size $h=\frac{1}{4}$ and the time step $k=0.001$. Figure 4.23 shows the time evolution of the total wave energy $||\mathbf{E}(t)||_{l^2}^2$, and the wave energy of the three components of the electric field $||E_1(t)||_{l^2}^2$, $||E_2(t)||_{l^2}^2$, $||E_3(t)||_{l^2}^2$ for the two cases.

From Figure 4.23, we can see that the total wave energy $||\mathbf{E}(t)||_{l^2}^2$ is conversed in the two cases. In case 1, the conservation of the wave energy of the third component of the electron filed is due to the symmetry of the initial data. The predication in (4.9) is confirmed (cf. 4.23a) and the wave energy of the first component increases after a short period, on the other hand the wave energy of the second component decreases in order to keep the conservation of the total wave energy. In case 2, the predication of (4.10) is confirmed (cf. 4.23b), and time evolution of the wave energy for the first two components forms almost the same pattern (increasing-decreasing-increasing) when the pattern for the third component is opposite due to conservation of the total wave energy. The wave energy fluctuates much larger in case 2 than that in case due to the nonzero initial phase in the electron field. Furthermore, the wave energy for each component almost does not change after some time. This implies that the electron does exchange from one component to another after some time.

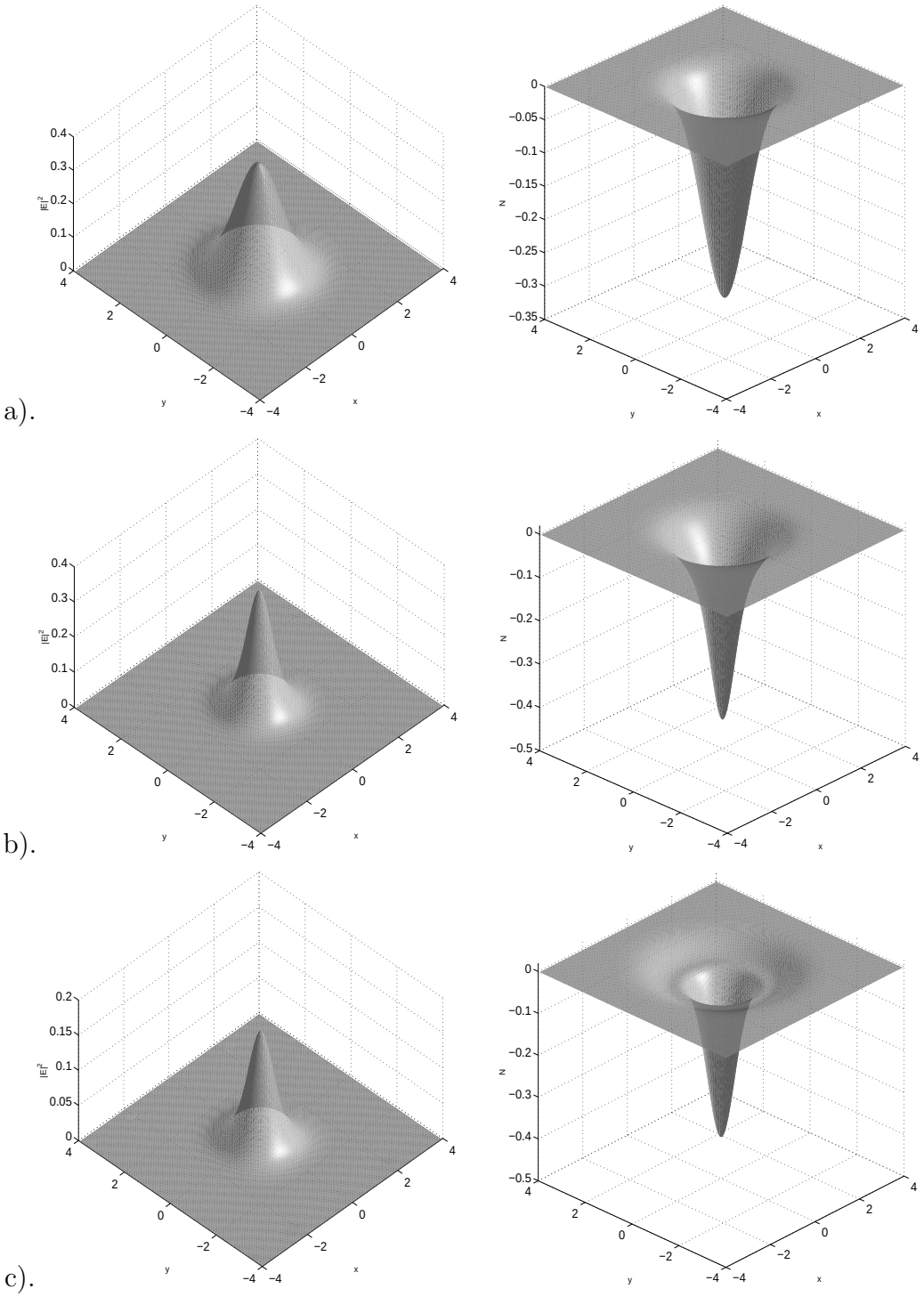

Figure 4.12: Numerical results in Example 6 for case 1. Surface-plot of the electric field $|E(x, y, t)|^2$ and ion density $N(x, y, t)$ with $\gamma = 0.8$ at different times: a). $t = 0$, b). $t = 0.5$, c). $t = 1.0$.

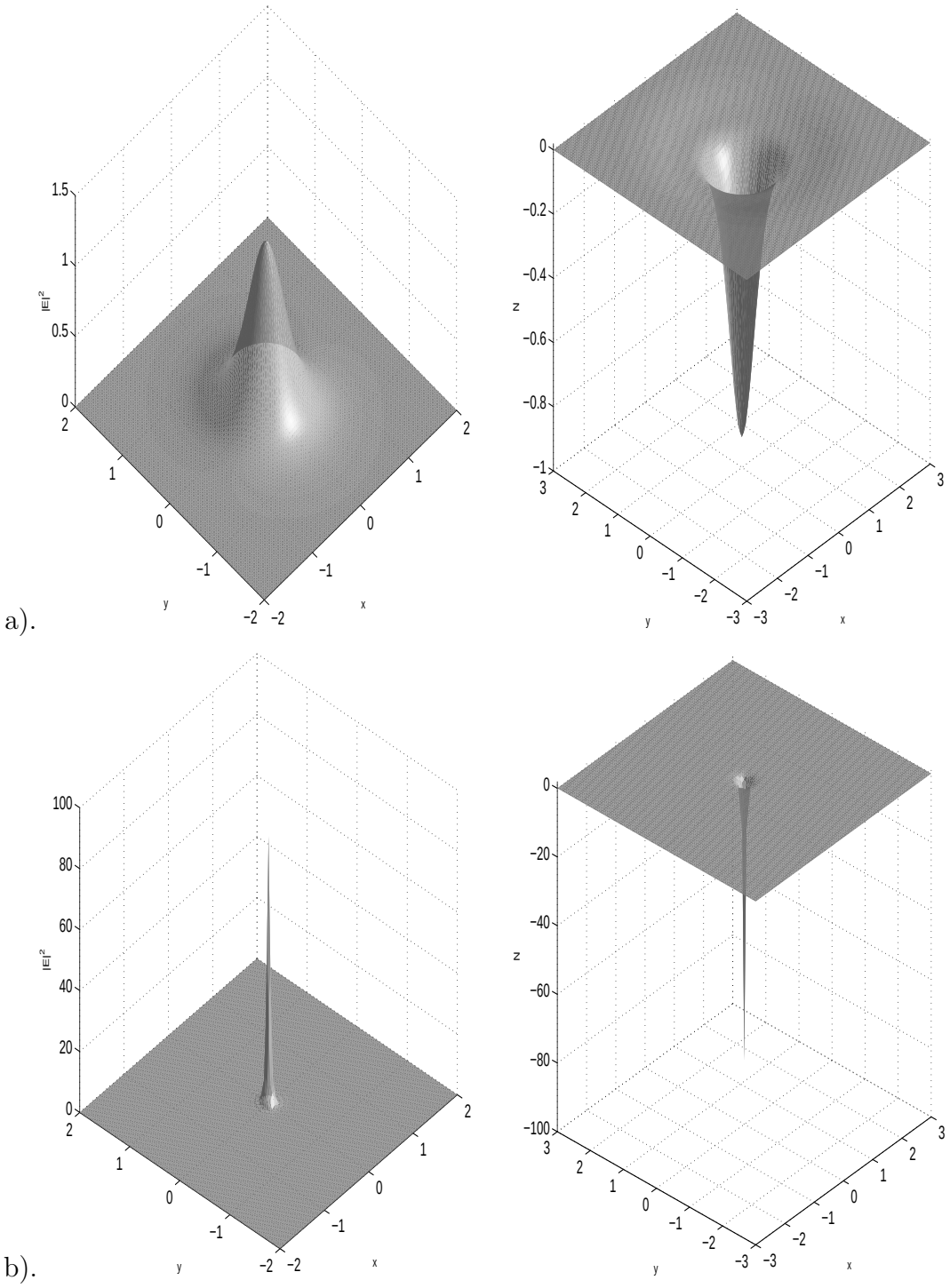

Figure 4.13: Numerical results in Example 6 for case 1. Surface-plot of the electric field $|E(x, y, t)|^2$ and ion density $N(x, y, t)$ with $\gamma = 0.1$ at different times: a). Before blow up (t=0.7), b). After blow up (t=1.333).

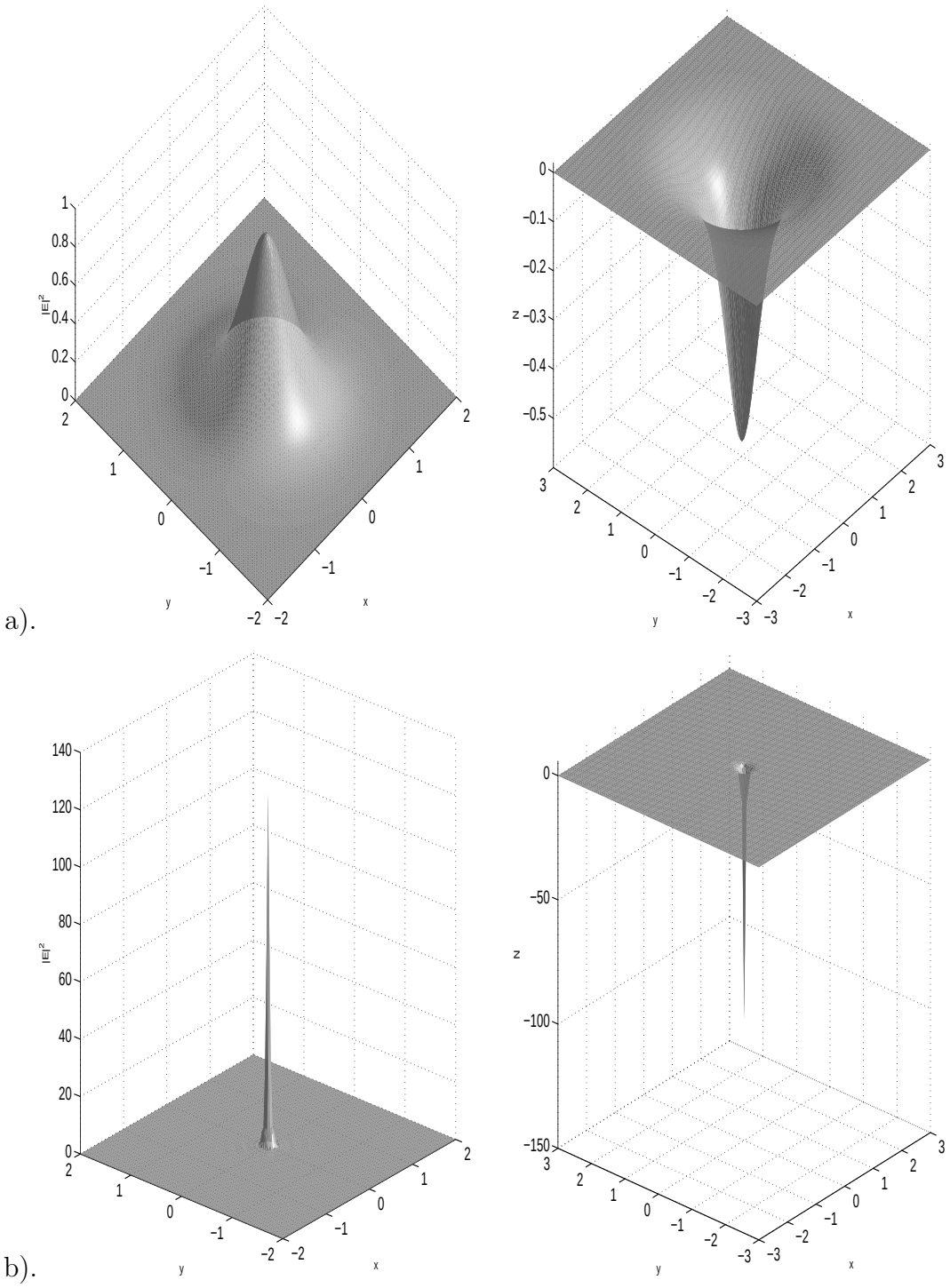

Figure 4.14: Numerical results in Example 6 for case 1. Surface-plot of the electric field $|E(x, y, t)|^2$ and ion density $N(x, y, t)$ with $\gamma = 0$ at different times: a). Before blow up (t=0.5), b). After blow up (t=1.177).

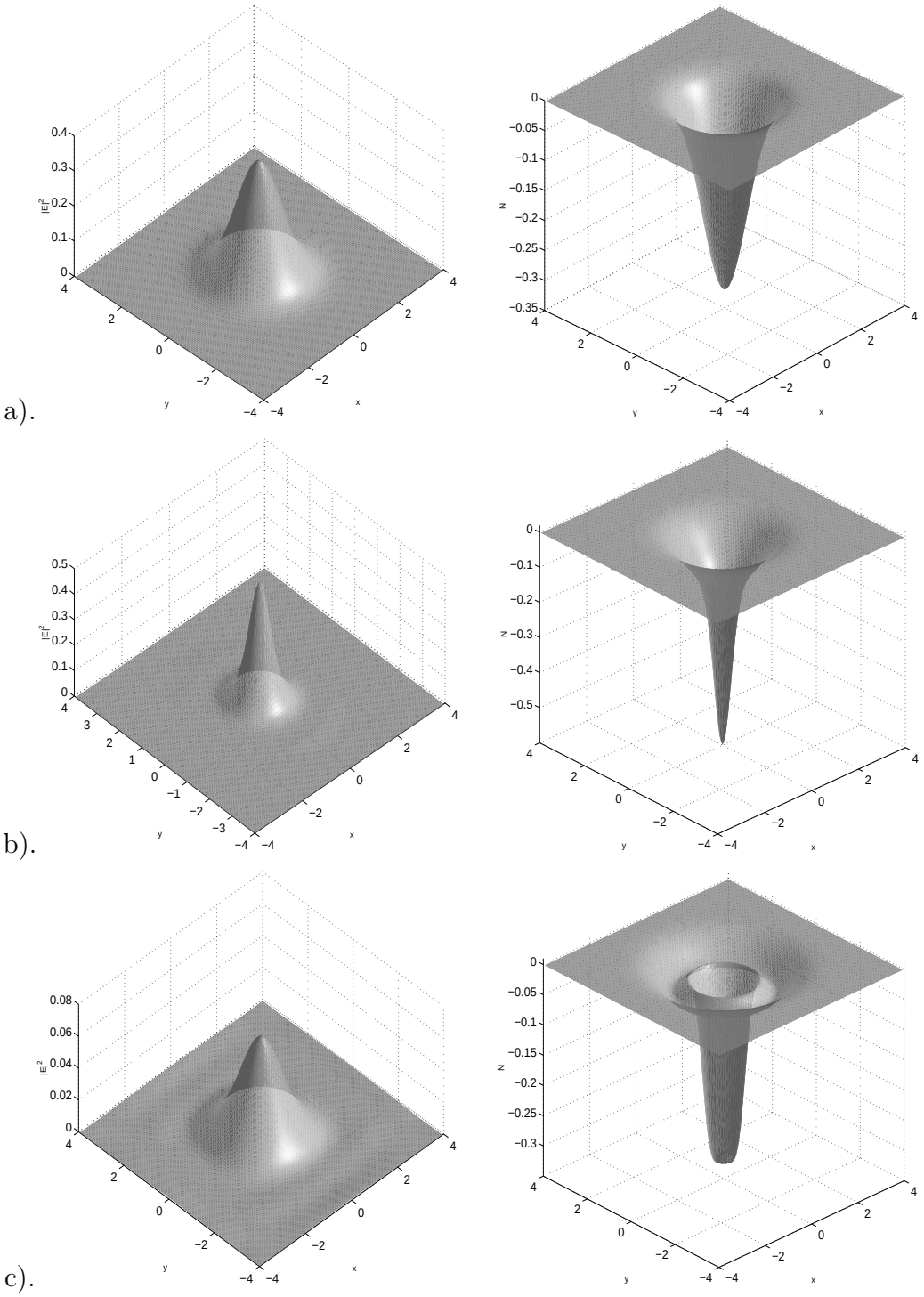

Figure 4.15: Numerical results in Example 6 for case 2. Surface-plot of the electric field $|E(x, y, t)|^2$ and ion density $N(x, y, t)$ with $\gamma = 0.8$ at different times: a). $t = 0$, b). $t = 0.5$, c). $t = 1.0$.

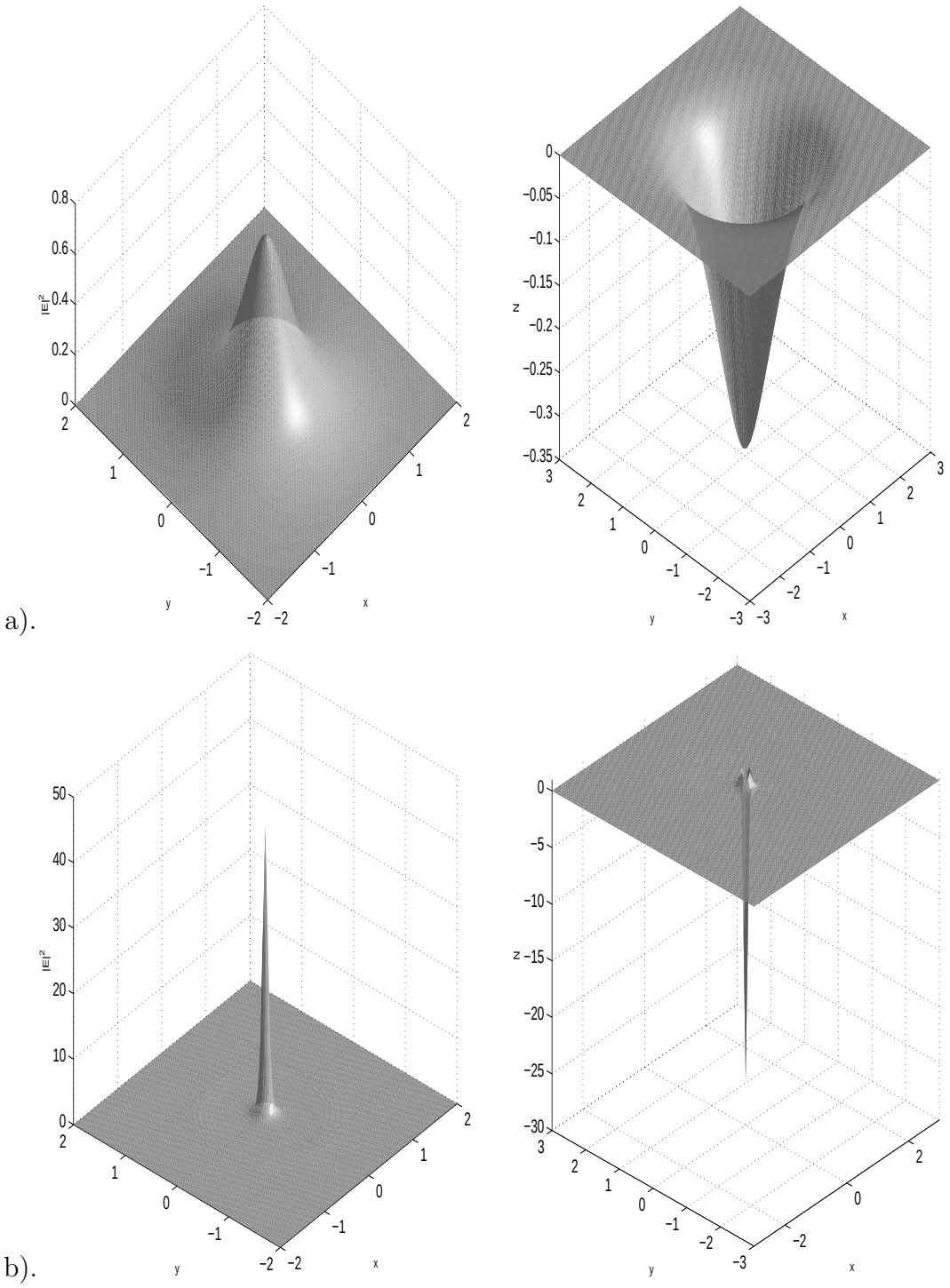

Figure 4.16: Numerical results in Example 6 for case 2. Surface-plot of the electric field $|E(x, y, t)|^2$ and ion density $N(x, y, t)$ with $\gamma = 0.1$ at different times: a). Before blow up (t=0.2), b). After blow up (t=0.473).

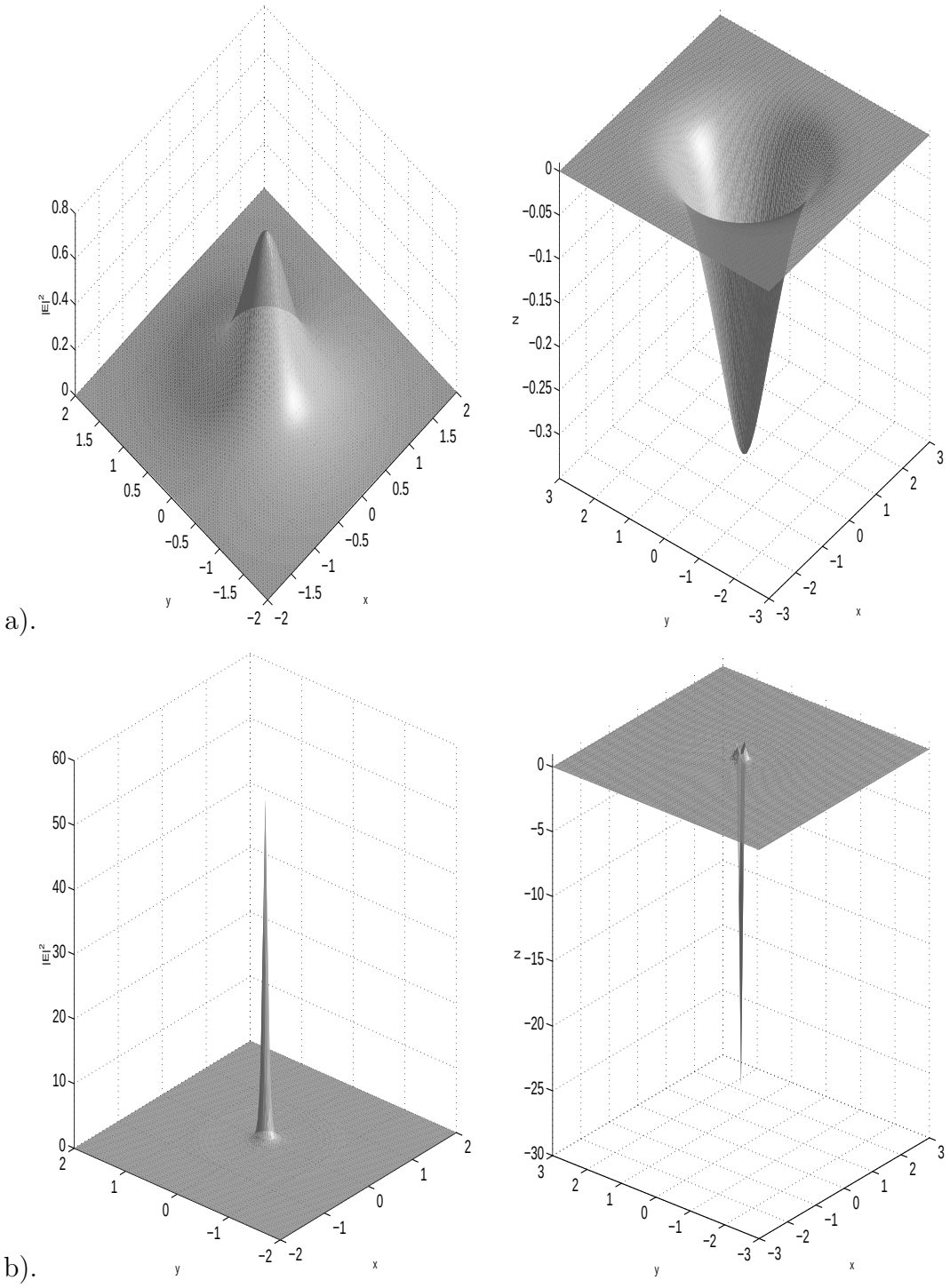

Figure 4.17: Numerical results in Example 6 for case 2. Surface-plot of the electric field $|E(x, y, t)|^2$ and ion density $N(x, y, t)$ with $\gamma = 0$ at different times: a). Before blow up (t=0.2), b). After blow up (t=0.442).

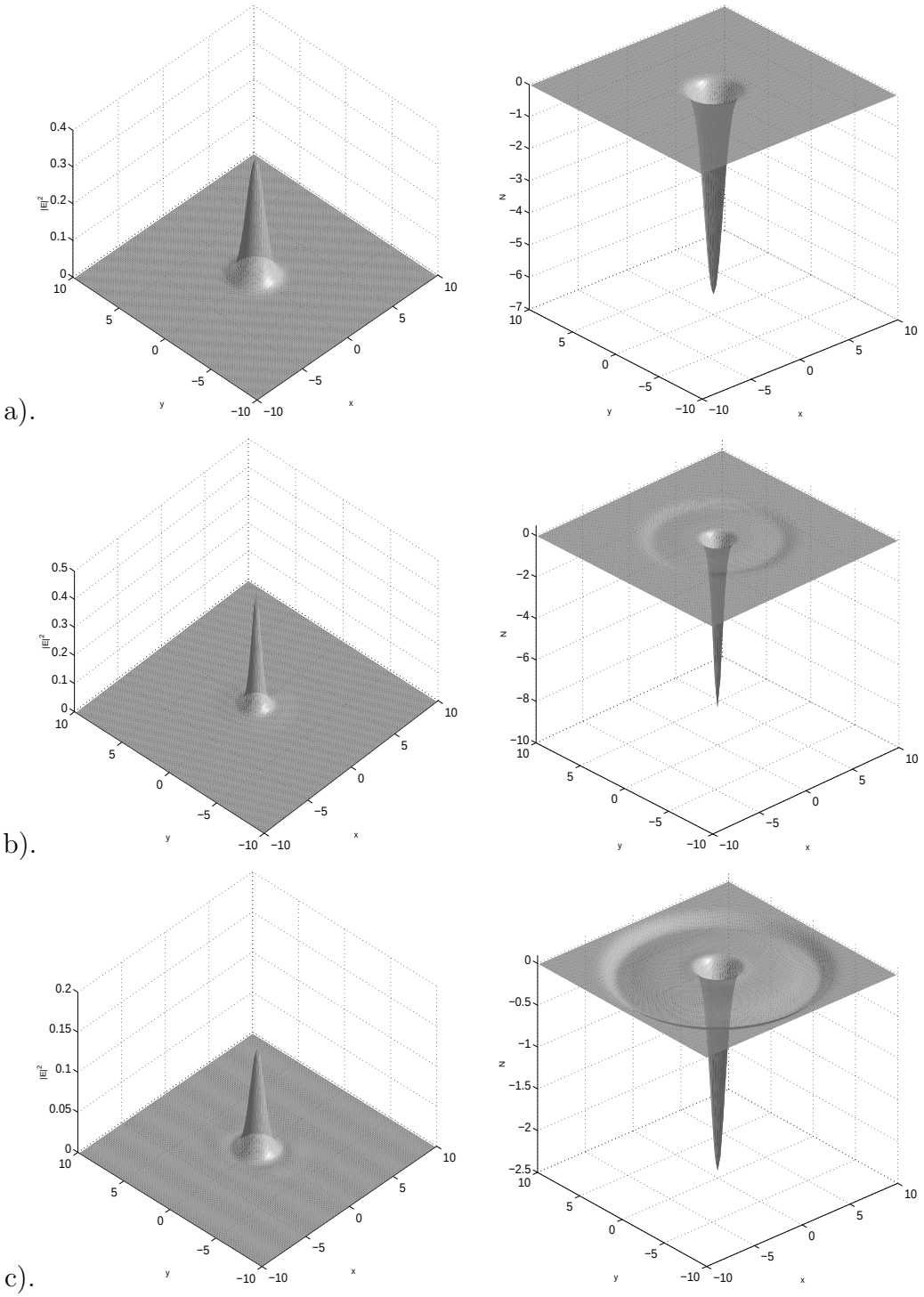

Figure 4.18: Numerical results in Example 6 for case 3. Surface-plot of the electric field $|E(x,y,t)|^2$ and ion density $N(x,y,t)$ with $\gamma = 0.8$ at different times: a). $t = 0$, b). $t = 0.5$, c). $t = 1.0$.

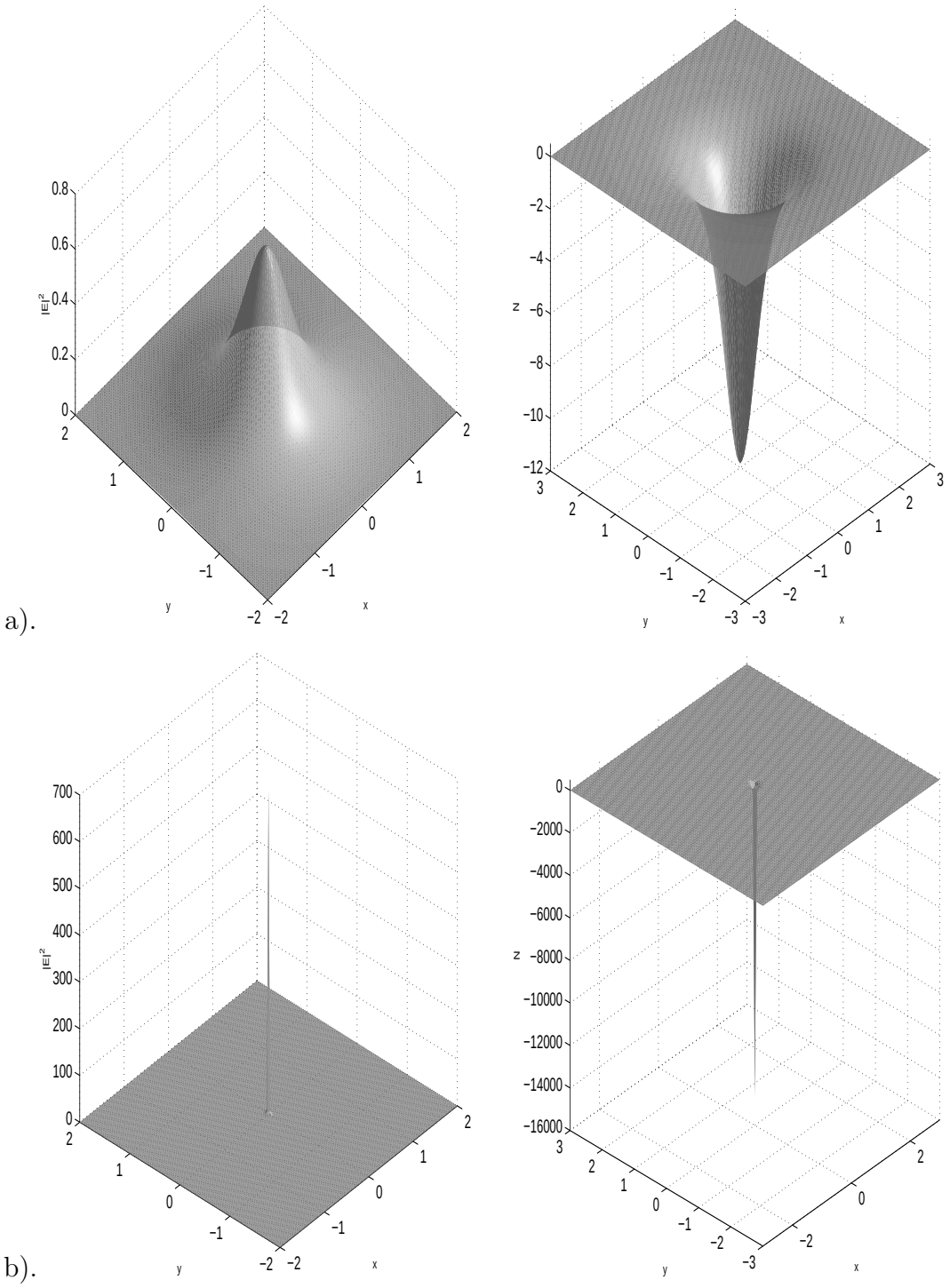

Figure 4.19: Numerical results in Example 6 for case 3. Surface-plot of the electric field $|E(x, y, t)|^2$ and ion density $N(x, y, t)$ with $\gamma = 0.1$ at different times: a). Before blow up (t=0.2), b). After blow up (t=0.4594).

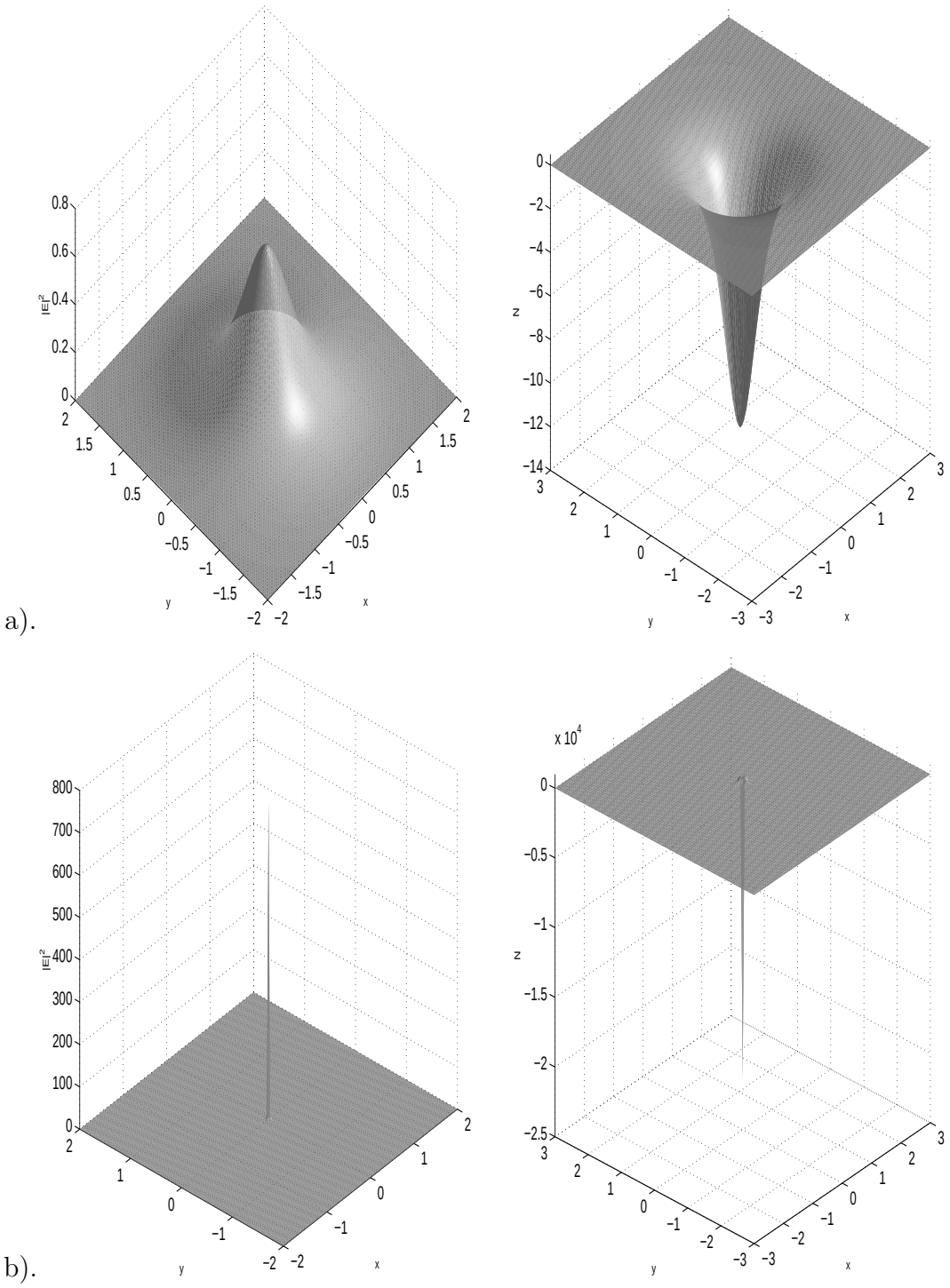

Figure 4.20: Numerical results in Example 6 for case 3. Surface-plot of the electric field $|E(x, y, t)|^2$ and ion density $N(x, y, t)$ with $\gamma = 0$ at different times: a). Before blow up (t=0.2), b). After blow up (t=0.4316).

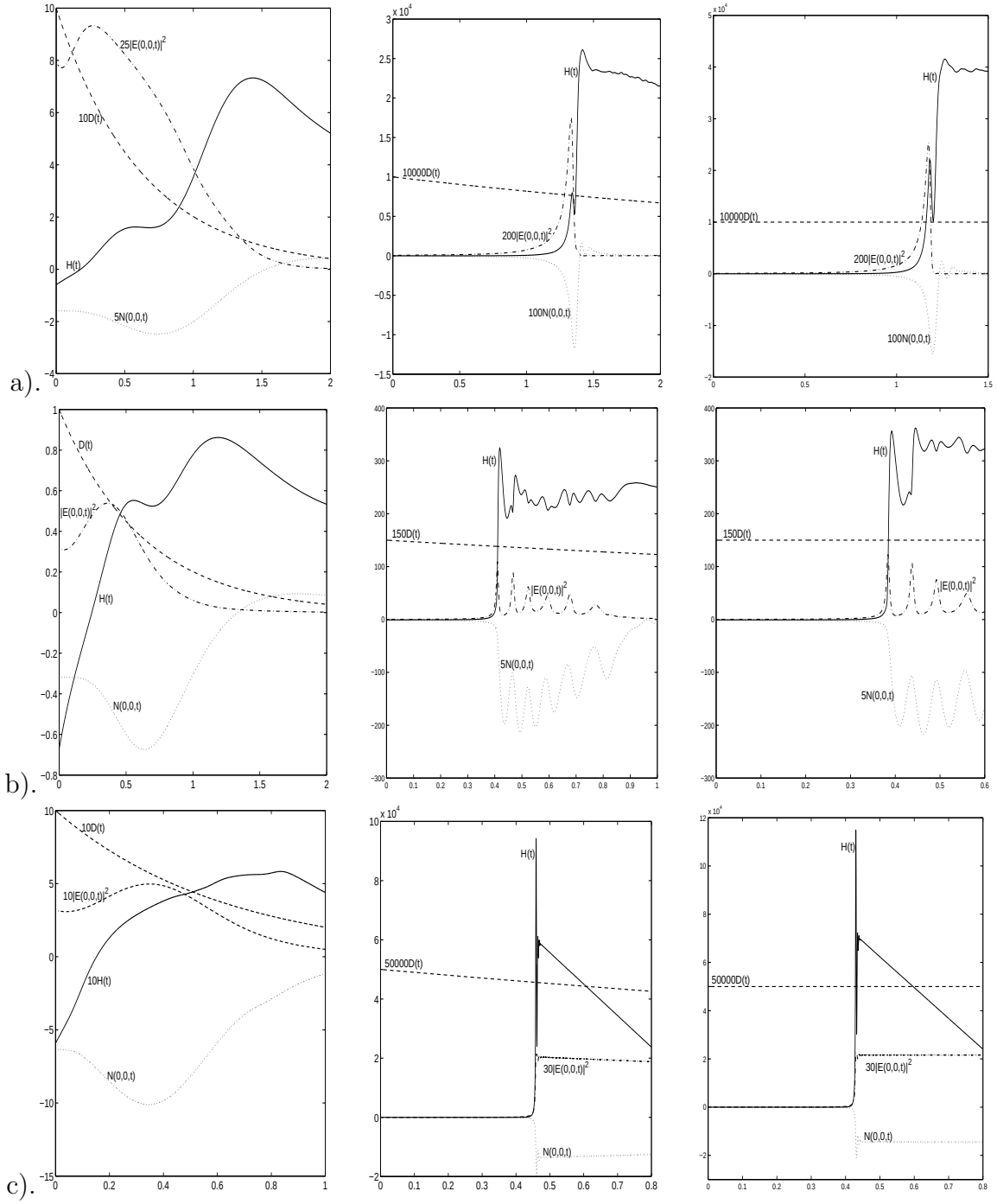

Figure 4.21: Numerical results in Example 6 for three cases: Energy, electric field and ion density as functions of time with $\gamma = 0.8$ (left: no blow up) , $\gamma = 0.1$ (center: blow up) and $\gamma = 0$ (right: blow up). a). Case 1, b). Case 2, c). Case 3.

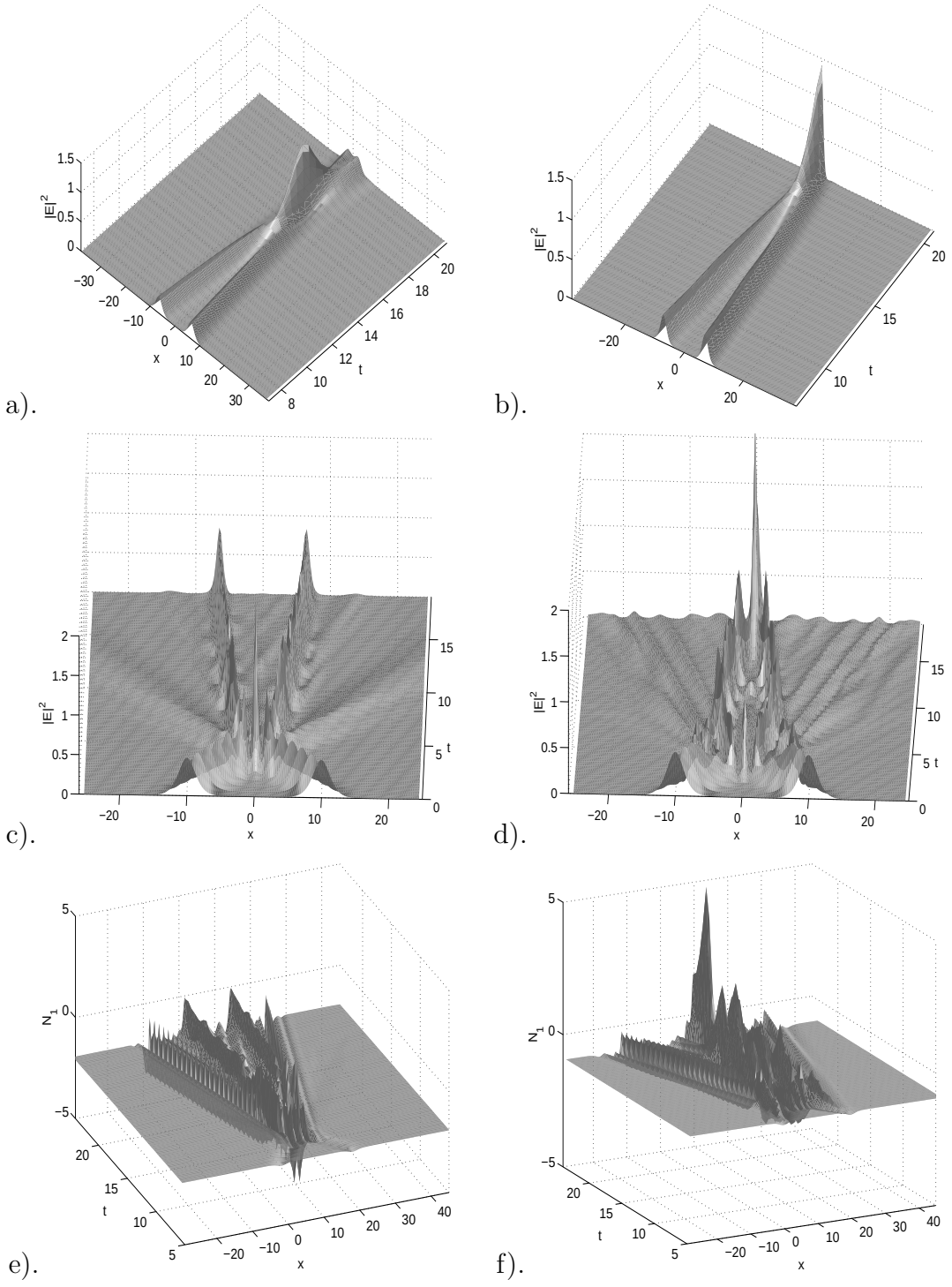

Figure 4.22: Evolution of the wave field $|E|^2$ and the acoustic field N_1 in Example 7. a). Case 1, b). Case 2, c)&e). Case 3, d)&f). Case 4.

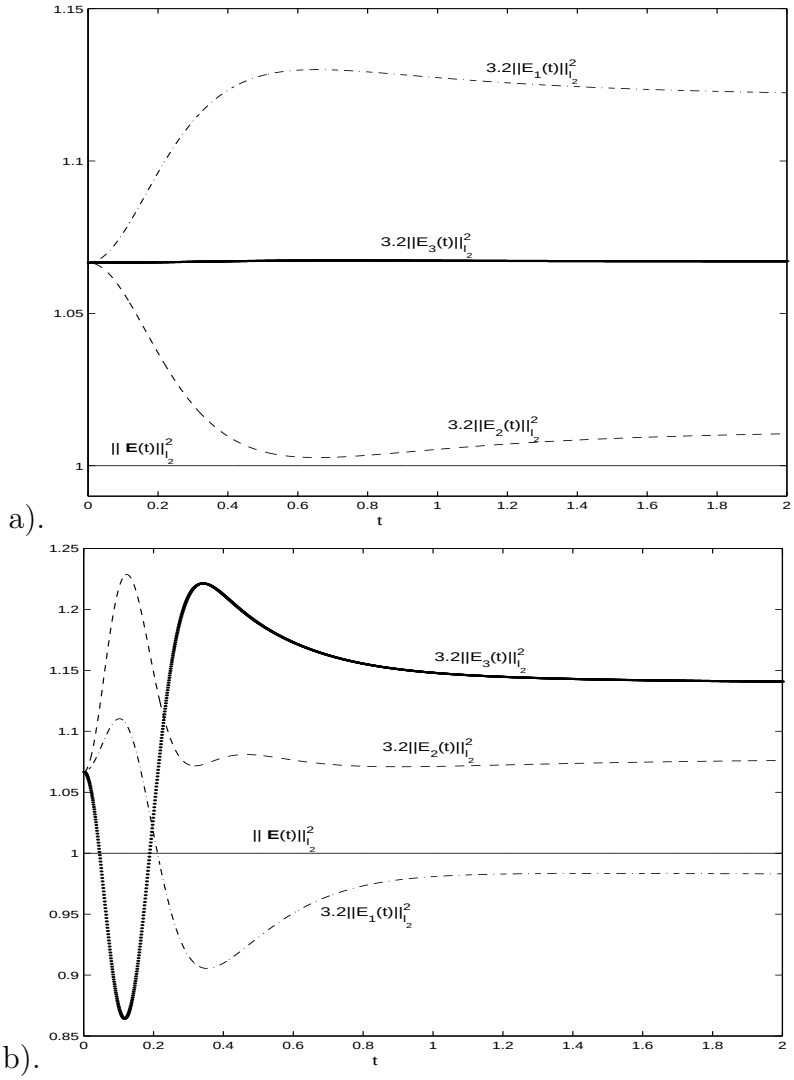

Figure 4.23: Evolution of the total wave energy $||\mathbf{E}(t)||_{l^2}^2$, and the wave energy of the three components of the electric field $||E_1(t)||_{l^2}^2$, $||E_2(t)||_{l^2}^2$, $||E_3(t)||_{l^2}^2$ in Example 8 for: a). Case I, b). Case II.

Chapter 5

Conclusion

We derived the Zakharov system (ZS) which governs the coupled dynamics of the electric-field amplitude and of the low-frequency density fluctuations of the ions and also analyzed its properties. We then presented two numerical methods: the time-splitting spectral method (TSSP) and discrete singular convolution method (DSC-RK4) for numerical discretization of the Zakharov system (ZS). We showed that the method of TSSP is explicit, easy to extend to high dimensions, easy to program, less memory requirement, weaker stability constraint, and time reversible and time transverse invariant if the generalized ZS is. Furthermore it keeps the same decay rate of wave energy in the generalized ZS, and gives exact results for plane-wave solutions of ZS. Numerical results for a solitary wave solution demonstrate that the method is of spectral-order accuracy in space and second-order accuracy in time as well as 'good' ε-resolution in the 'subsonic limit' regime, i.e. $0 < \varepsilon \ll 1$. The method is applied successfully to simulate soliton-soliton collisions of the ZS, a 2d problem as well as the generalized ZS with a damping term. Furthermore, extension of TSSP to standard vector ZS and ZS for multi-component plasma are presented. Numerical results demonstrate the efficiency and high accuracy of TSSP for these problems. As a local method, the DSC-RK4 can compete with the standard Fourier pseudospectral method (FPS-RK4) in terms of accuracy and stability. In addition, the number of grid points and boundary conditions are limited to the power of

2 and periodic in the TSSP, FPS-RK4 and WG-RK4 methods. There are no such limitations in the DSC-RK4 algorithm. Numerical results demonstrate the efficiency and high accuracy of the two proposed methods.

Bibliography

[1] M. Abramowitz and I.A. stegun, Handbook of mathematical functions, Dover, New York, (1972).

[2] K. Amaratunga and J. Williams, Wavelet-Galerkin solutions for the one-dimensional partial differential equations, Int. J. Numer. Methods Eng. 37, 2703 (1994).

[3] G. Bao, G.W. Wei and A.H. Zhou, Analysis of regularized Whittaker-Kotel'nikov-Shannon sampling expansion, preprint.

[4] W. Bao, F.F. Sun and G.W. Wei, Numerical methods for the generalized Zakharov system, J. Comput. Phys., Vol. 190, No. 1, pp. 201-228, 2003.

[5] W. Bao and F.F. Sun, Numerical simulation of the vector Zakharov system for multi-component plasma, preprint.

[6] W. Bao and F.F. Sun, Explicit unconditionally stable numerical methods for the generalized and vector Zakharov system, preprint.

[7] W. Bao, S. Jin and P.A. Markowich, On time-splitting spectral approximations for the Schrödinger equation in the semiclassical regime, J. Comput. Phys. 175, 487 (2002).

[8] W. Bao, D. Jaksch and P.A. Markowich, Numerical solution of the Gross-Pitaevskii equation for Bose-Einstein condensation, preprint.

[9] G. Beylkin, On the representation of operators in bases of compactly supported wavelets, SIAM J. Numerical Analysis 29 (6), 1716 (1992).

[10] J. Bourgain and J. Colliander, On wellposedness of the Zakharov system, Internat. Math. Res. Notices 11, 515 (1996).

[11] C. Canuto, M.Y. Hussaini, A. Quarteroni and T.A. Zhang, Spectral Methods in Fluid Dynamics (Springer-Verlag, New York. 1988).

[12] Q. Chang and H. Jiang, A conservative difference scheme for the Zakharov equations, J. Comput. Phys. 113, 309 (1994).

[13] Q. Chang, B. Guo and H. Jiang, Finite difference method for generalized Zakharov equations, Math. Comp. 64, 537 (1995).

[14] F.F. Chen, Introduction to plasma physics, Plenum, New York, (1994).

[15] J. Colliander, Wellposedness for Zakharov systems with generalized nonlinearity, J. Diff. Eqs. 148, 351 (1998).

[16] I. Daubechies, Orthonormal bases of compactly supported wavelets, Comm. Pure and Appl. Math. 41, 909 (1988).

[17] A.S. Davydov, Phys. Scr. 20, 387 (1979).

[18] B. Fornberg and T.A. Driscoll, A fast spectral algorithm for nonlinear wave equations with linear dispersion, J. Comput. Phys. 155, 456 (1999).

[19] R. Glassey, Approximate solutions to the Zakharov equations via finite differences, J. Comput. Phys. 100, 377 (1992).

[20] R. Glassey, Convergence of an energy-preserving scheme for the Zakharov equations in one space dimension, Math. Comp. 58, 83 (1992).

[21] D. Gottlieb and S.A. Orszag, Numerical analysis of spectral methods (Soc. for Industr. & Appl. Math., Philadelphia, 1977).

[22] I.S. Gradshteyn and I.M. Ryzhik, Table of integrals, series, and products, Academic Press, New York, (1980).

[23] S. Guan, C.-H. Lai and G.W. Wei, Bessel-Fourier analysis of patterns in a circular domain, Physica D. 151, 83 (2001).

[24] H. Hadouaj, B. A. Malomed and G.A. Maugin, Soliton-soliton collisions in a generalized Zakharov system, Phys. Rev. A 44, 3932 (1991).

[25] H. Hadouaj, B. A. Malomed and G.A. Maugin, Dynamics of a soliton in a generalized Zakharov system with dissipation, Phys. Rev. A 44, 3925 (1991).

[26] P.J. Hansen and D.R. Nicholson, Amer. J. Phys. 47, 769 (1979).

[27] R.H. Hardin and F.D. Tappert, Applications of the split-step Fourier method to the numerical solution of nonlinear and variable coefficient wave equations, SIAM Rev. Chronicle 15, 423 (1973).

[28] E.A. Kuznetsov, The collapse of electromagnetic waves in plasmas, Sov.Phys. JETP 39, 1003 (1974).

[29] P.K. Newton, Wave interactions in the singular Zakharov system, J. Math. Phys. 32 (2), 431 (1991).

[30] D.R. Nicholson, Introduction to plasma theory, Wiley (reprint edition 1992 by Krieger) (1983).

[31] G.L. Payne, D.R. Nicholson, and R.M. Downie, Numerical solution of the Zakharov equations, J. Comput. Phys. 50, 482 (1983).

[32] S. Qian and J.Weiss, Wavelets and the numerical solution of partial differential equations, J. Comp. Phys. 106(1), 155 (1993).

[33] R.D. Richtmyer and K.W. Morton, Difference methods for initial- value problems, New York (1967).

[34] A.M. Rubenchik, R.Z. Sagdeev and V.E. Zakharov, Collapse versus cavitons, Comments Plasma Phys. Controlled Fusion, 9, 183 (1985).

[35] L. Stenflo, Phys. Scr. 33, 156 (1986).

[36] B.F. Sanders, N.K. Katoposes and J.P. Boyd, Spectral modeling of nonlinear dispersive waves, J. Hydraulic. Eng. ASCE 124, 2 (1998).

[37] E.I. Schulman and Dokl.Akad. Nauk SSSR 259, 579 (1981) [Sov. Phys. Dokl. 26, 691 (1981)].

[38] L. Schwartz Théore des Distributions (Paris: Hermann), 1951.

[39] G. Strang, On the construction and comparison of differential schemes, SIAM J. Numer. Anal. 5, 506 (1968).

[40] C. Sulem and P.L. Sulem, Regularity properties for the equations of Langmuir turbulence, C. R. Acad. Sci. Paris Sér. A Math. 289, 173 (1979).

[41] C. Sulem and P.L. Sulem, The nonlinear Schrödinger equation, (Springer 1999).

[42] T.R. Taha and M.J. Ablowitz, Analytical and numerical aspects of certain nonlinear evolution equations, II. Numerical, nonlinear Schrödinger equation, J. Comput. Phys. 55, 203 (1984).

[43] T.R. Taha and M.J. Ablowitz, Analytical and numerical aspects of certain nonlinear evolution equations, III. Numerical, Korteweg-de Vries equation, J. Comput. Phys. 55, 231 (1984).

[44] S.G. Thornhill and D. ter Haar, Langmuir turbulence and modulational instability, Phys. Reports 43, 43 (1978).

[45] G.W. Wei, Discrete singular convolution for the Fokker-Planck equation, J. Chem. Phys. 110, 8930 (1999).

[46] G.W. Wei, A unified approach for solving the Fokker-Planck equation, J. Phys. A. 33, 4935 (2000).

[47] G.W. Wei, Solving quantum eigenvalue problems by discrete singular convolution, J. Phys. B. 33, 343 (2000).

[48] G.W. Wei, Vibration analysis by discrete singular convolution, J. Sound Vibration. 244, 535 (2001).

[49] G.W. Wei, A new algorithm for solving some mechanical problems, Comput. Methods Appl. Mech. Engrg. 190, 2017 (2001).

[50] G.W. Wei, Quasi-wavelets and quasi interpolating wavelets, Chem. Phys. Lett. 296, 215 (1998).

[51] S.Y. Yang, Y.C. Zhou and G.W. Wei, Comparison of the discrete singular convolution algorithm and the Fourier pseudospectral method for solving partial differential equations, Comput. Phys. Commun, 143, 113 (2002).

[52] V.E. Zakharov, Zh. Eksp. Teor. Fiz. 62, 1745 (1972) [Sov. Phys. JETP 35, 908 (1972)].

[53] V.E. Zakharov, Collapse and self-focusing of Langmuir waves, Handbook of plasma physics, (M.N. Rosenbluth and R.Z. sagdeev, eds.), vol.2, (A.A. Galeev and R.N. Sudan, eds.), 81, Elsevier.